

MOTION CODING STRATEGIES IN THE RETINA

by

Stuart Trenholm

Submitted in partial fulfilment of the requirements
for the degree of Doctor of Philosophy

at

Dalhousie University
Halifax, Nova Scotia
February 2013

© Copyright by Stuart Trenholm, 2013

DALHOUSIE UNIVERSITY

DEPARTMENT OF MEDICAL NEUROSCIENCE

The undersigned hereby certify that they have read and recommend to the Faculty of Graduate Studies for acceptance a thesis entitled “MOTION CODING STRATEGIES IN THE RETINA” by Stuart Trenholm in partial fulfilment of the requirements for the degree of Doctor of Philosophy.

Dated: February 25, 2013

External Examiner: _____

Research
Co-Supervisors: _____

Examining Committee: _____

Departmental Representative: _____

DALHOUSIE UNIVERSITY

DATE: February 25, 2013

AUTHOR: Stuart Trenholm

TITLE: MOTION CODING STRATEGIES IN THE RETINA

DEPARTMENT OR SCHOOL: Department of Medical Neuroscience

DEGREE: PhD CONVOCATION: May YEAR: 2013

Permission is herewith granted to Dalhousie University to circulate and to have copied for non-commercial purposes, at its discretion, the above title upon the request of individuals or institutions. I understand that my thesis will be electronically available to the public.

The author reserves other publication rights, and neither the thesis nor extensive extracts from it may be printed or otherwise reproduced without the author's written permission.

The author attests that permission has been obtained for the use of any copyrighted material appearing in the thesis (other than the brief excerpts requiring only proper acknowledgement in scholarly writing), and that all such use is clearly acknowledged.

Signature of Author

Table of Contents

List of Tables.....	vii
List of Figures.....	viii
Abstract.....	x
List of Abbreviations and Symbols Used.....	xi
Acknowledgements.....	xiii
Chapter 1: Introduction.....	1
The Retina.....	1
Directionally Selective Ganglion Cells.....	3
Electrical Coupling in the Retina.....	5
Chapter 2: Parallel Mechanisms Encode Direction in the Retina.....	6
Abstract.....	6
Publication Information.....	6
Introduction.....	7
Results.....	9
A Genetically Labeled Population of ON-OFF Retinal Ganglion Cells that Exhibit Asymmetric Dendritic Arbors.....	9
Asymmetric Dendritic Arbors of Hb9::eGFP DSGCs Align with the Preferred Direction.....	12
The Inhibitory DS Circuitry Aligns with Dendritic Asymmetries Along the Dorsal-Ventral Axis.....	15
Directional Selectivity in GFP ⁺ Ganglion Cells Does Not Critically Depend on the Classic Inhibitory Circuitry.....	17
Directional Selectivity in the Absence of Inhibition Arises in Ganglion Cells.....	20
Interactions Between Pre- and Postsynaptic DS Mechanisms in Symmetrical Ganglion Cells.....	23
Discussion.....	26
An Entire Population of ON-OFF DSGCs with Asymmetric Dendritic Arbors.... Nonlinearities Within Asymmetric Dendritic Arbors Confer Centrifugal Preferences.....	27
Parallel Mechanisms Underlie DS Coding.....	29
Conclusion.....	31
Methods.....	31

Animals.....	31
Retinal Preparation.....	31
Whole-Cell Patch-Clamp Recordings.....	32
Light Stimulus.....	32
Targeting, Imaging, and Reconstructing GFP ⁺ Ganglion Cells.....	33
Analysis of Physiological Data.....	33
Morphological Analysis.....	34
Computational Model of Inhibition Independent DS in GFP ⁺ Ganglion Cells.....	34
Supplementary Material.....	35
Computational Model of DS in Asymmetric Dendritic Trees.....	39
Chapter 3: Lag Normalization in an Electrically Coupled Neural Network.....	44
Abstract.....	44
Publication Information.....	44
Introduction.....	44
Results.....	45
Anticipation of Moving Stimuli.....	45
Lag Normalization.....	45
Ganglion Cells Prime the Responses of Their Electrically Coupled Neighbours...	48
Lag Normalization Requires Gap Junctions Between DSGCs.....	51
Discussion.....	53
Methods.....	54
Physiological Recordings.....	54
Light Stimulus.....	55
Analysis of Physiological Data.....	55
Model of DSGC Network.....	56
Supplementary Material.....	60
Chapter 4: Dynamic Modulation of Gap Junction-Mediated Anticipatory Signals in a Network of Directionally Selective Retinal Neurons	64
Abstract.....	64
Publication Information.....	64

Introduction.....	65
Results.....	67
Reciprocal Gap Junction Coupling in Superior Coding DSGCs.....	67
Coupling is Weak and Symmetrical Along the Preferred-Null Axis.....	71
Excitatory Subthreshold Receptive Fields of Coupled DSGCs.....	73
Gap Junction-Mediated Priming of DSGC Responses.....	74
Lateral Priming Signals Rectify During Responses to Moving Stimuli.....	77
Postsynaptic Gain Control Underlies Rectification.....	80
Discussion.....	84
Dendrodendritic Electrical Coupling in Superior Coding ON-OFF DSGCs.....	84
Composite Receptive Field Structure of Coupled DSGCs.....	85
Priming by Gap Junction-Mediated Lateral Excitation.....	86
Rectification of Lateral Excitatory Signals in Coupled DSGCs.....	87
Conclusion.....	88
Methods.....	89
Wholemound Retinal Preparation.....	89
Physiological Recordings.....	90
Light Stimulus.....	90
Data Analysis.....	91
Supplementary Material.....	92
Chapter 5: Discussion.....	99
Motion Coding Strategies in the Retina.....	99
Classical Directional Selectivity.....	99
Non-Classical DS.....	101
Anticipation.....	102
Conclusion.....	103
Appendix: Copyright Permissions.....	104
References.....	107

List of Tables

Supplementary Table 2.1 – Biophysical parameters for the different regions of the asymmetric DSGC model.....	41
---	----

List of Figures

Figure 1.1 – Schematic of the retina.....	2
Figure 1.2 – Multiple types of ganglion cells in mouse retina.....	4
Figure 2.1 – A single, asymmetric ON-OFF ganglion cell is labelled in the Hb9::eGFP retina.....	11
Figure 2.2 – Asymmetric dendritic morphology correlates with directional preferences.....	14
Figure 2.3 – Inhibitory DS circuitry aligns along the dorsal-ventral axis.....	16
Figure 2.4 – Directionally selective responses persist in the presence of GABA _{A,C} receptor antagonists.....	18
Figure 2.5 – Inhibition-independent directional selectivity is apparent only at slower velocities.....	19
Figure 2.6 – Directional selectivity in the presence of inhibitory blockers appears to arise from nonlinear properties of ganglion cells.....	22
Figure 2.7 – Interactions between the inhibitory circuit and dendritic DS mechanisms revealed in symmetrical DSGCs.....	25
Figure 3.1 – Lag normalization in the electrically-coupled population of upward coding ON-OFF DSGCs.....	47
Figure 3.2 – Gap junctions between upward coding DSGCs mediate lateral excitation.....	50
Figure 3.3 – Serial interactions between multiple electrically-coupled DSGCs are required for lag normalization.....	52
Figure 4.1 – Superior coding Hb9::eGFP directionally selective ganglion cells are homologously tracer coupled and exhibit coupled spikelets.....	70
Figure 4.2 – Reciprocal coupling between ON-OFF DSGCs is symmetrical and weak.....	72
Figure 4.3 – Coupled DSGCs have extensive excitatory subthreshold receptive fields..	74
Figure 4.4 – Lateral electrical signals boost weak light-evoked responses.....	75
Figure 4.5 – Moving stimuli evoke responses outside of the classical receptive field of coupled DSGCs.....	77
Figure 4.6 – Gap junctions between ON-OFF DSGCs do not exhibit voltage-dependent inactivation.....	80
Figure 4.7 – Offset inhibition does not drive skewed responses.....	82
Figure 4.8 – Post-synaptic gain control is important for terminating responses.....	83

Supplementary Figure 2.1 – A number of morphological features in the Hb9 ⁺ DSGCs are remarkably homogenous.....	35
Supplementary Figure 2.2 – Asymmetric DSGCs pointing in the preferred direction exist in the population of Hb9 ⁺ DSGCs.....	36
Supplementary Figure 2.3 – Conductance measurements.....	37
Supplementary Figure 2.4 – Inhibition in GFP ⁺ ON-OFF DSGCs is mediated by GABAergic receptors.....	38
Supplementary Figure 2.5 – Excitatory currents recorded at -60 mV and +40 mV have similar kinetics.....	39
Supplementary Figure 2.6 – Linear and non-linear modeling of directional selectivity in an asymmetric ganglion cell.....	42
Supplementary Figure 3.1 – Responses to negative contrast stimuli are lag normalized.....	60
Supplementary Figure 3.2 – Coupled and uncoupled ON-OFF DSGCs show similar velocity tuning.....	61
Supplementary Figure 3.3 – Spiking responses in a coupled DSGC are consistent over many trials and are not biased by filtering.....	62
Supplementary Figure 3.4 – Lag normalization in non-DS retinal ganglion cells.....	63
Supplementary Figure 4.1 – Superior coding DSGCs exhibit depolarization induced feedback spikelets in wt retina.....	92
Supplementary Figure 4.2 – Depolarization induced feedback spikelets do not exhibit a reversal potential.....	93
Supplementary Figure 4.3 – Gap junctions lower input resistance.....	94
Supplementary Figure 4.4 – Subthreshold receptive fields are excitatory.....	95
Supplementary Figure 4.5 – Responses to moving stimuli are more sustained than to static stimuli.....	96
Supplementary Figure 4.6 – Spatially offset inhibition.....	97
Supplementary Figure 4.7 – Coupling between ON-OFF DSGCs appears to be dendrodendritic.....	98

Abstract

Early experimental work suggested that the retina's main role was to detect changes in brightness and contrast, namely working as a light detector, and that most of the complex computations in the visual system happened upstream in the brain. In reality, there is a growing wealth of literature indicating that the retina itself processes multiple channels of visual information (contrast, motion, orientation, etc.), making it much more complex than it originally appeared. For instance, there now appear to be over 20 types of retinal ganglion cells. To this end, the work in this thesis will focus on the identification and characterization of a single type of retinal ganglion cell in the mouse retina. In the first section of my results, I will show that this cell type, identified as the only GFP⁺ ganglion cell in the transgenic Hb9::eGFP retina, is a directionally selective ganglion cell (DSGC), that preferentially responds to objects moving upward through the visual field. This cell has a pronounced morphological asymmetry that helps it to synergistically (along with asymmetric inhibition) generate directionally selective responses. In the second results section, I will describe a novel phenomenon exhibited by Hb9⁺ DSGCs: Thanks to gap junction mediated signals, Hb9⁺ cells are able to anticipate moving stimuli and correct for lags that are inherent in visual signals generated by photoreceptors. In the third results section I will elucidate the mechanisms for the gap junction mediated anticipatory signals outlined in the second results section. Together, these results provide a significant advancement in our understanding of how the retina processes moving stimuli and provide a compelling example of how chemical and electrical synapses interact to allow for exquisite signal multiplexing.

List of Abbreviations and Symbols Used

18 β GA	18 β -Glycyrrhetic Acid
A	Amp
AI	asymmetry index
AMPA	α -amino-3-hydroxy-5-methyl-4-isoxazolepropionic acid
AU	arbitrary units
BC	bipolar cell
C	Coulomb
Ca ²⁺	calcium
C1, C2	cell 1, cell 2
CC	coupling coefficient
Curare	D-tubocurare
D	dorsal
Da	Dalton
DS	directional selectivity or directionally selective
DSGC	directionally selective ganglion cell
DSI	directional selectivity index
E _{Cl}	reversal potential for chloride
EPSC	excitatory postsynaptic current
GABA	γ -aminobutyric acid
G _e	excitatory conductance
GC	ganglion cell
GCL	ganglion cell layer
G _i	inhibitory conductance
eGFP	enhanced green fluorescent protein
Hb9	homeobox 9
Hz	Hertz
I	current
ILM	inner limiting membrane
INL	inner nuclear layer
IPL	innerplexiform layer
IPSC	inhibitory postsynaptic current
K ⁺	potassium
K _{dr}	delayed rectifier potassium channel
K _A	A-type potassium channel
K _{IH}	hyperpolarization activated potassium channel
LGN	lateral geniculate nucleus
Min	minutes
Mnx1	motor neuron and pancreas homeobox 1
ms	milliseconds
N	nasal or null
Na ⁺	sodium
Na _v	voltage gated Na ⁺ channel

NMDA	N-methyl-D-aspartate
OLM	outer limiting membrane
ONL	outer nuclear layer
OPL	outer plexiform layer
P, Pref	preferred
Prs	photoreceptor layer
PSP	postsynaptic potential
PTX	picrotoxin
RF	receptive field
RGC	retinal ganglion cell
R_m	input resistance
RPE	retina pigment epithelium
s	seconds
S	Siemens
SC	superior colliculus
SD	standard deviation
s.e.m.	standard error of the mean
SI	skew index
sK_{Ca}	small conductance calcium activated potassium channel
T	temporal
t_d	apparent time delay
TPMPA	(1,2,5,6-Tetrahydropyridin-4-yl)methylphosphinic acid
TTX	tetrodotoxin
V	ventral or Volt
VC	voltage clamp
V_{rest}	resting membrane potential

Acknowledgements

Dr. Gautam Awatramani. Your relentless pursuit of new results and your commitment to my success led me to many interesting and worthwhile findings and has become a part of my own work ethic. Thank you very much for helping me set a strong foundation for a future in science.

Dr. William Baldridge. Your kindness and guidance have been very much appreciated throughout the years. Also, moving our lab across the country was much easier thanks to your efforts. It would have been much more difficult to remain a Dalhousie student abroad, and arrange my defence at a distance, had it not been for your tireless assistance.

Drs. Kazue Semba, Stefan Krueger, Robert Brownstone. Thank you for your support and advice during my committee meetings, comprehensive exam and defence.

Dr. Alberto Pereda, for serving as my external examiner.

Collaborators. Thanks to **Dr. Robert Smith** for your continued support in modelling our experimental results, to **Drs. David Schwab** and **Vijay Balasubramanian** for helping us to better understand lag normalization, and to **Jiawei Zhang** and **Dr. Tim Lewis** for teaching me a thing or two about computational modelling.

Miscellaneous. Thanks to **Dr. Bryan Daniels** for letting me listen to music (or at least not complaining about it) and letting me harass him with questions, to **Alexander Goroshkov** for teaching me the ways of 2-Photon microscopy, to **Dr. Steven Barnes** for being the only one around at odd hours in the evening to talk about science with, **Dr. Robert Chow** for all your help throughout the years, **Dr. Kerry Delaney** for useful discussions, to **Alex Hoggarth** and **Amanda McLaughlin** for bringing youthful enthusiasm to the lab and for genotyping mice, to **Kyle Johnson** for being much better at computer programming than me, to **Priyanka Singh, Belinda Dunn** and **Zhiwei Shi** for maintaining mouse colonies, to **Neasa Bheilbigh** and **Marika Forsythe** for help in morphological reconstructions, to animal care facilities at both Dalhousie and UVic for your help such that everything ran smoothly, and to the computational neuroscience summer school at the University of Ottawa for introducing me to computational modelling.

Family. I would like to thank my parents, Bruce and Marlene, for their unwavering love, generosity and support throughout graduate school. I thank my loving and beautiful wife Leah for her support and cheerful spirit. Finally, I thank my brother and sister-in-law, Matthew and Justine, for keeping me well stocked in high-quality single malts throughout my studies.

Chapter 1: Introduction

The Retina

In the 4th century BC, the Greek philosopher and mathematician Archytas proposed that vision arose from an invisible fire emitted from the eyes that revealed the shapes and colours of encountered objects. Remarkably, the modern understanding of vision is no less impressive. In our current understanding, vision arises in the retina, the thin neural tissue that lines the back of the eye. From there, visual signals pass via the optic nerve to the brain, where further processing takes place.

The retina is a highly structured neural tissue that comprises 5 neuronal cell types that interact in 2 distinct synaptic layers (**Figure 1.1**). Vision starts when rod and cone photoreceptors convert light energy into electrochemical signals. Photoreceptor signals are transmitted to the rest of the retina through glutamate release at synaptic connections with bipolar cells in the outer plexiform layer. Bipolar cells split the visual signal into ON (increase in brightness) and OFF (decrease in brightness) channels, via disparate expression of sign-reversing metabotropic glutamate receptors and sign-conserving ionotropic glutamate receptors, respectively. Bipolar cells are interneurons that convey photoreceptor signals to ganglion cells via glutamatergic synapses in the inner plexiform layer. Ganglion cells in turn send visual signals out of the eye, via bursts of action potentials, along the optic nerve. In addition to this vertical retinal pathway, retinal signals are highly modified in each synaptic layer, with horizontal cells modulating signals in the outer plexiform layer and amacrine cells modulating signals in the inner plexiform layer.

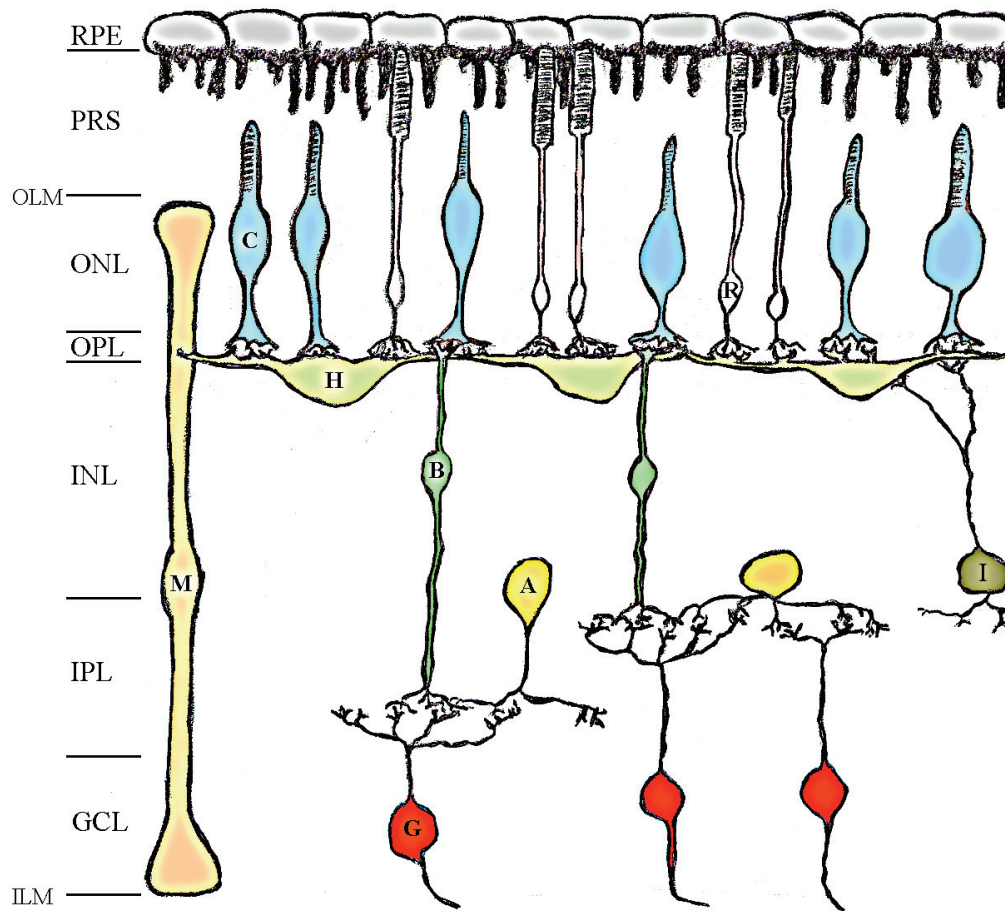


Figure 1.1. Schematic of the retina. RPE, retinal pigmented epithelium; PRS, photoreceptor layer; ONL, outer nuclear layer; OPL, outer plexiform layer; INL, inner nuclear layer; IPL, inner plexiform layer; GCL, ganglion cell layer; OLM, outer limiting membrane; ILM, inner limiting membrane; C, cone; R, rod; H, horizontal cell; B, bipolar cell; A, amacrine cell; I, interplexiform cell; M, Muller cell; G, ganglion cell. (Adapted from and used with permission from Dr. Bryan Daniels).

Directionally Selective Ganglion Cells

In the mouse retina, there are 20⁺ types of ganglion cells (Volgyi et al., 2009). These cells can be broadly broken down into ON, OFF and ON-OFF subtypes based on their light responses (**Figure 1.2A**) and their dendritic stratifications. Another common way to distinguish ganglion cells is to define their light responses as either sustained or transient (**Figure 1.2A**). Of special importance for the work presented in this thesis, certain ganglion cells can also be categorized based on their directionally selective (DS) light responses, such that they respond robustly to stimuli moving in a particular direction (the preferred direction) while stimuli moving in the opposite (or null) direction generate little to no response (**Figure 1.2B,C**). In the mouse retina there are at least 8 types of DS ganglion cells (DSGCs) that make up ~10% of the ganglion cell population (Kim et al., 2008, Auferkorte et al., 2012): 3 ON DSGCs, 4 ON-OFF DSGCs and 1 OFF DSGC. Both ON and ON-OFF DSGCs were first described in the rabbit retina (Barlow and Hill, 1963, Barlow et al., 1964, Barlow and Levick, 1965), while OFF DSGCs were only described more recently in mouse retina (Kim et al., 2008). The mechanistic details about how DS responses are generated in the retina will be described in Chapter 2.

ON-OFF DSGCs, which will be the focus of this thesis, were first described nearly 50 years ago (Barlow and Hill, 1963) and the four subtypes of these cells code the four cardinal directions: up, down, left and right (Oyster and Barlow, 1967). In the mouse retina, these cells have recently been shown to project to subcortical visual pathways (Huberman et al., 2009, Kay et al., 2011) and are therefore likely to be important for driving DS responses in visual cortex (Hubel and Wiesel, 1959), though to date this has not been shown. In contrast to ON-OFF DSGCs, ON DSGCs code direction in only 3 different visual axes: inferior, superior-temporal and superior-dorsal (Oyster and Barlow, 1967), and project to accessory optic system (Oyster et al., 1980) where they appear to be important for driving reflexes including the optokinetic response (Oyster et al., 1972, Yoshida et al., 2001). OFF DSGCs are restricted to coding a single visual axis (superior) and appear to primarily project to superior colliculus (Kim et al., 2008). One remarkable feature of these OFF DSGCs is that the entire population bears remarkably asymmetric dendritic trees that seem to *point* in the preferred direction (Kim et al., 2008). In Chapter 2, I will describe the identification and characterization of a population of superior coding

ON-OFF DSGCs with asymmetric dendritic morphology and I will provide evidence that this structural asymmetry promotes DS responses.

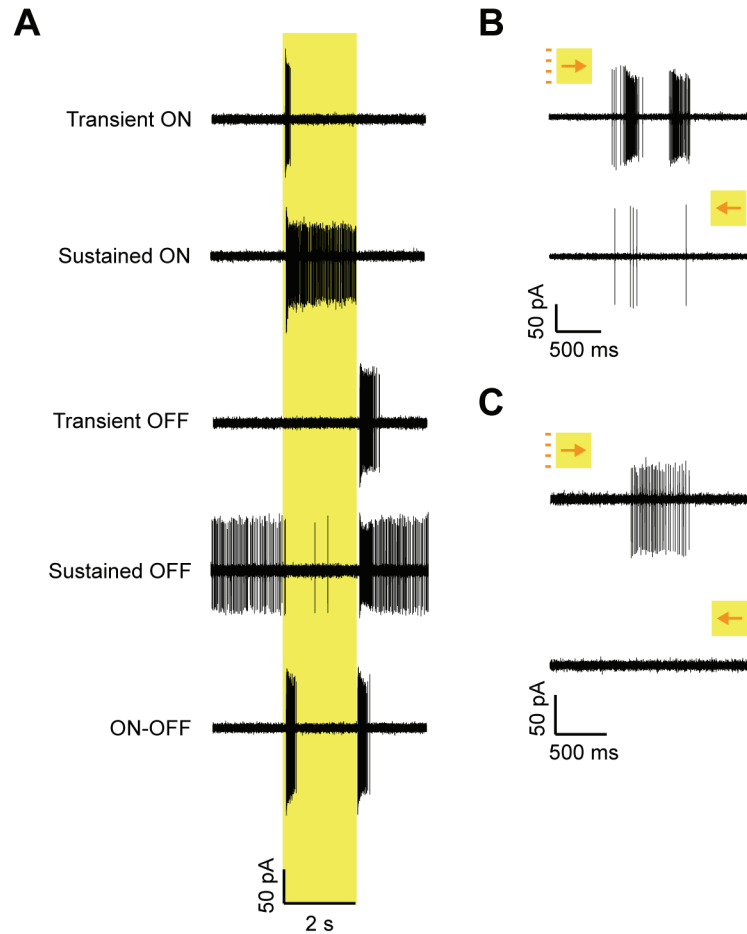


Figure 1.2. Multiple types of ganglion cells in mouse retina. **A**, Shows the spiking light responses of five different types of ganglion cells in mouse retina. The yellow bar indicates a 300 μm diameter spot (96% positive contrast) flashed for 2 seconds. **B**, Plots the spiking response of an ON-OFF DSGC to stimuli (300x300 μm bar) moving at 600 μm/s in the preferred (*top*) and null (*bottom*) directions. **C**, Plots the spiking response of an ON DSGC to the same stimuli moving at 300 μm/s in the preferred (*top*) and null (*bottom*) directions.

Electrical Coupling in the Retina

The history of gap junction signalling is a long and winding road. From the early hypothesizing of Golgi, to its subsequent disregard by Cajal and others, to its first concrete demonstration in the 1950s (Furshpan and Potter, 1957), gap junction have only recently been substantiated as common and important signalling substrates in vertebrate nervous systems (Pereda et al., 2012). Gap junctions are connexin containing channels that are coextensive across the membranes of two adjacent cells (for a review, see Bennett and Zukin, 2004, Connors and Long, 2004). Each hemichannel or connexon (i.e. the gap junction channel components belonging to a single cell) is a connexin hexamer. There are roughly 20 connexin isoforms in the murine genome, with the numbering system indicating the molecular weight of each connexin (ex. connexin 45 has a molecular weight of approximately 45 kDa). Each connexin subtype confers slightly different properties in expression systems, and many can form heteromeric gap junctions (i.e. a gap junction comprised of hemichannels made from different connexin subtypes), but little is known about how different connexin subtypes affect neural signalling.

The adult mammalian retina is an extensively electrically coupled tissue, with gap junctions being present between many neurons in all neural layers (Bloomfield and Volgyi, 2009). While gap junctions in the outer retina are important for controlling receptive field sizes (Bloomfield and Volgyi, 2009), in the inner retina, where it is important to conserve spatial information, gap junctions do not modulate receptive field size (Hu et al., 2010). As such, roles for electrical coupling in the inner retina remain poorly defined. In Chapter 3, I will describe a novel phenomenon discovered in electrically coupled ON-OFF DSGCs that enables them to anticipate moving stimuli and correct for delays inherent in phototransduction. In Chapter 4, I will examine how electrical and chemical inputs dynamically interact in electrically coupled ON-OFF DSGCs, allowing them to anticipate moving stimuli.

Chapter 2: Parallel Mechanisms Encode Direction in the Retina

Abstract

In the retina, presynaptic inhibitory mechanisms that shape directionally selective (DS) responses in output ganglion cells are well established. However, the nature of inhibition-independent forms of directional selectivity remains poorly defined. Here, we describe a genetically specified set of ON-OFF DS ganglion cells (DSGCs) that code superior motion. This entire population of DSGCs exhibits asymmetric dendritic arborizations that orientate toward the preferred direction. We demonstrate that morphological asymmetries along with nonlinear dendritic conductances generate a centrifugal (soma-to-dendrite) preference that does not critically depend upon, but works in parallel with the GABAergic circuitry. We also show that in symmetrical DSGCs, such dendritic DS mechanisms are aligned with, or are in opposition to, the inhibitory DS circuitry in distinct dendritic subfields where they differentially interact to promote or weaken directional preferences. Thus, pre- and postsynaptic DS mechanisms interact uniquely in distinct ganglion cell populations, enabling efficient DS coding under diverse conditions.

Publication Information

This chapter has previously been published as: **Trenholm S**, Johnson K, Li X, Smith RG, Awatramani GB. Parallel mechanisms encode direction in the retina. *Neuron*. 2011, 71:683-94. All experiments were performed and analyzed by ST and were designed by ST and GBA. KJ wrote analysis programs in Matlab and helped with anatomical analyses. The computational model was developed XL, RGS and GBA. The paper was written by ST and GBA.

Introduction

Directionally selective ganglion cells (DSGCs) of the retina respond vigorously to visual stimuli moving in a preferred but not a null direction. Barlow and Levick (1965) postulated that directionally selective (DS) responses arose from lateral asymmetries within the inhibitory circuitry. Over the years, results from numerous studies have provided conflicting evidence for and against a critical role for inhibition in DS computations, leaving this issue unresolved.

Support for inhibitory circuit mechanisms came from early pharmacological analysis that revealed a critical role for GABA_A receptors in mediating directional selectivity (Wyatt and Day, 1976, Caldwell et al., 1978), a finding that is now well substantiated (for review see Taylor and Vaney, 2003, Demb, 2007). Subsequently, inhibitory currents preferentially evoked by null-direction stimuli were directly measured using patch-clamp techniques (Taylor et al., 2000). Mounting evidence suggests the cholinergic/GABAergic starburst amacrine cells (SACs) as the likely source of asymmetric inhibition to DSGCs. The radial dendrites of SACs exhibit a centrifugal directional preference (Euler et al., 2002), which arises through a combination of intrinsic mechanisms (Tukker et al., 2004, Hausselt et al., 2007) and network interactions (Fried et al., 2005, Lee et al., 2010). Direct stimulation of individual SACs with patch electrodes or optical neuromodulators revealed that SACs with somata located on the null side of a DSGC (i.e., the side at which null direction stimulus approaches) provide stronger GABAergic inhibition compared to those on the preferred side (Fried et al., 2002, 2005, Lee et al., 2010, Wei et al., 2011, Yonehara et al., 2011). Serial block-face electron microscopic analysis further revealed an exquisite specificity in the alignment between synaptically connected SAC and DSGC processes, indicating that these connections were optimized for preferential activation during null direction stimulus motion (Briggman et al., 2011). Moreover, targeted ablation of SACs abolishes DS responses in ganglion cells (Yoshida et al., 2001). Together, these findings suggest that SACs are the leading substrate for DS computations in the retina.

In contrast to inhibitory circuit mechanisms, previous studies in a variety of species have reported that DS responses persisted when GABA_A receptors were blocked (Bulthoff and Bulthoff, 1987, Ogmen, 1991, Smith et al., 1996, Grzywacz et al., 1997,

Ackert et al., 2009). Much less is known about mechanisms that could generate directional selectivity in the retina independent of inhibitory circuits. One possibility is that nonlinear conductances could generate directional selectivity within the dendrites of DSGCs, as appears to happen in SACs (Hausselt et al., 2007). However, in rabbit ON-OFF DSGCs, nonlinear conductances were found to amplify DS responses but not generate them (Oesch et al., 2005).

In other parts of the CNS, dendritic morphology is known to contribute to DS coding (Rall, 1964, Livingstone, 1998, London and Hausser, 2005, Branco et al., 2010). However, it is unclear whether dendritic shape significantly influences DS coding in the retina. First, DS can be faithfully computed by symmetrical ganglion cells (Amthor et al., 1989, Oyster et al., 1993, Yang and Masland, 1994), obviating the need for morphological specializations. Second, DS can be computed within a small region of the receptive field, again suggesting that the shape of the DSGC is not important (Barlow and Levick, 1965). Third, although DSGC dendrites were often found to be highly asymmetric, these appeared randomly orientated, suggesting that morphological differences would only add noise to the population signal (Yang and Masland, 1994, Huberman et al., 2009). Finally, even in the newly described OFF DSGC which does exhibit systematic dendritic asymmetries that correlate with directional preferences, the DS responses appear to arise from spatially offset lateral inhibition (Kim et al., 2008). Thus, to date there is little evidence to support a role for ganglion cell dendritic morphology in DS processing.

When considering mechanisms underlying directional selectivity, most studies failed to fully appreciate the diversity of DSGC populations. The mouse retina includes at least eight subtypes (four types of ON-OFF, three ON, and one OFF) that have distinct molecular, morphological, and physiological characteristics. If different types of DSGCs utilize distinct computational mechanisms, pooling results from random cell types could potentially lead to ambiguous results. To this end, here we define the properties of a genetically specified population of ON-OFF DSGCs in which the preferred direction is strongly correlated with asymmetries in dendritic arborizations. We demonstrate that in addition to the conventional inhibitory circuitry, a parallel dendritic mechanism contributes to the formation of DS responses. This dendritic mechanism aligns with, but

does not rely critically upon, GABAergic inhibition. Furthermore, we show that in symmetrical DSGCs, these different DS mechanisms work in parallel or in opposition within distinct dendritic subfields, to strengthen or weaken DS responses, respectively. Thus, in the retina, multiple mechanisms appear to encode DS responses.

Results

A Genetically Labeled Population of ON-OFF Retinal Ganglion Cells that Exhibit Asymmetric Dendritic Arbors

During a screen carried out to detect genetic markers expressed in the retina, we identified the Hb9::eGFP transgenic mouse line (Arber et al., 1999) that exhibited a sparse neuronal labeling pattern in the ganglion cell layer (~80 cells/mm²; n = 6 retinas; **Figure 2.1A**). Axonal labeling indicated that GFP was expressed in ganglion cells. Two-photon imaging of the live retina revealed that GFP⁺ cells were ON-OFF ganglion cells, as their dendrites ramified in discrete strata in both the ON and OFF layers of the inner plexiform layer (**Figure 2.1B,C**). No other types of ganglion, amacrine or bipolar cells were labeled in this mouse line, making it ideally suited for the study of ON-OFF ganglion cells.

Next, individual GFP⁺ ganglion cells were loaded with Alexa 594 using a patch electrode (**Figure 2.1C**) and their dendritic arborizations in both ON and OFF layers were traced offline. Examples of these reconstructions illustrate the homogeneity in morphological characteristics (**Figure 2.1D, 2.2A**). GFP⁺ ganglion cells were found to bear similar morphological characteristics as those described previously for bistratified DSGCs (Sun et al., 2002, Coombs et al., 2006). The one notable difference compared to previous descriptions, however, was that the dendritic arborizations in both the ON and OFF subfields of every GFP⁺ ganglion cell were found to be highly asymmetric (**Figure 2.1D,E**). The degree of polarization was quantified as an asymmetry index (AI; 0 indicating perfect symmetry while values closer to 1 indicate stronger asymmetry; see Methods). On average, AIs for the entire population of GFP⁺ ganglion cells measured

were 0.82 ± 0.03 for the ON dendrites and 0.75 ± 0.03 for the OFF dendrites ($n = 42$; **Figure 2.1E**). In addition, dendritic trees of all cells orientated towards the ventral pole (**Figure 2.1D; 2.2C**). Although asymmetric dendritic trees in ON-OFF DSGCs have been commonly observed (Amthor et al., 1989, Oyster et al., 1993, Yang and Masland, 1994), our finding that the entire population of DSGCs was asymmetric and pointed in the same direction was unexpected.

GFP⁺ ganglion cells were also relatively homogenous in a number of other features compared to previous descriptions of ON-OFF DSGCs. For example, the size of their dendritic fields showed little variance when compared to those of ON-OFF ganglion cells previously described (**Supplementary Figure 2.1**; Sun et al., 2002). Consistent with previous observations in the murine retina, the dendritic field diameter did not depend on the distance from the optic disk. In addition, soma size, total dendritic length, number of branches, branch order and number of primary dendrites were also relatively constant (**Supplementary Figure 2.1**). Together, these data suggest that a single subset of ON-OFF DSGCs is labeled in the Hb9::eGFP mouse retina.

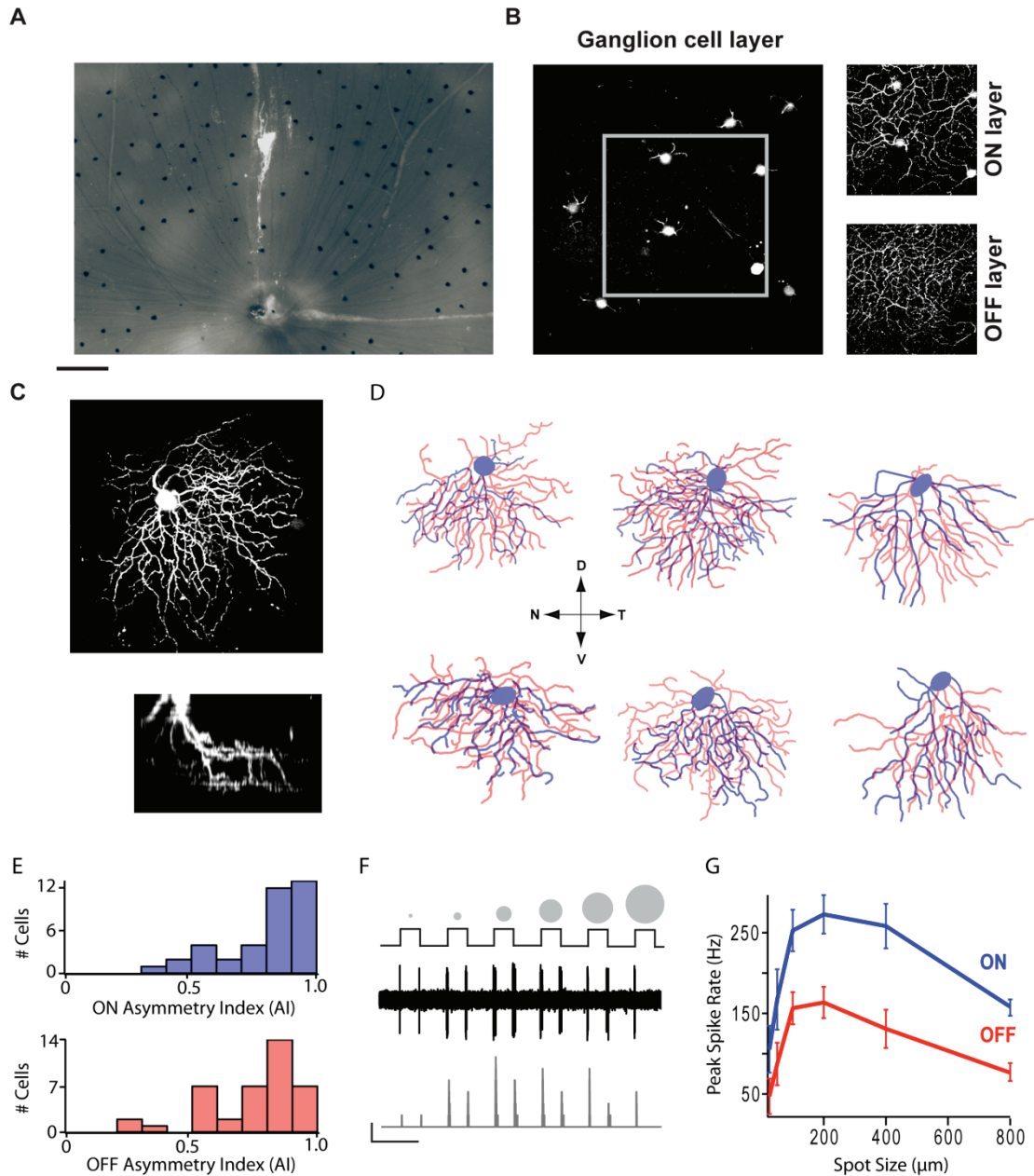


Figure 2.1. Systematic dendritic asymmetries within an entire population of genetically specified ON-OFF directional selective ganglion cells. **A**, Photomicrograph of the Hb9::eGFP whole-mount retina showing a mosaic of GFP⁺ ganglion cells with their axons streaming towards the optic disc. **B**, Two-photon image of GFP labeling in the ganglion cells in the living retina showing their dendrites in the ON and OFF strata of the inner plexiform layer. **C**, An image stack of an individual Alexa 594 loaded GFP⁺ ganglion cell. The lower image is rotated 90° to show the stratification of the ON and OFF dendrites. **D**, Reconstructions of six GFP⁺ ganglion cells (from stacks similar to ones shown in (C)). ON dendrites are labeled in blue; OFF dendrites are labeled in red

(the coloring scheme is maintained in subsequent figures; see also **Supplementary Figure 2.1** for detailed morphological analysis). **E**, Histograms representing the asymmetry index for ON and OFF dendrites calculated for 42 GFP⁺ DSGCs. AI values fall between 0 and 1, with 1 indicating perfect asymmetry and 0 indicating perfect symmetry. **F**, The response of a GFP⁺ ganglion cell to bright spots of increasing size (25-800 μm) centered over its receptive field. The middle trace shows the raw spiking data (*black*). The bottom traces is plot of the spike rate (binned over 25 ms; grey). Scale bars: 50 Hz and 5 s. **H**, The average spike rate ($n = 11$) for both the ON and OFF responses to spots are plotted. Scale bar: 160 μm (**A**), 55 μm (**B**), 50 μm (**C top**), 50 μm and 20 μm (for x and y scales, respectively, **C bottom**), 40 μm (**D**).

Asymmetric Dendritic Arbors of Hb9::eGFP DSGCs Align with the Preferred Direction

We next used two-photon targeted patch-clamp techniques to examine the physiological responses of GFP⁺ ganglion cells. In response to spots of light of increasing size centered over the receptive field, robust responses were observed at the onset and offset of the stimulus, confirming that GFP⁺ cells received ON and OFF inputs (**Figure 2.1F**). The optimum spot stimulus was 100 to 200 μm in diameter, similar to the dendritic field size ($192.8 \pm 2.7 \mu\text{m}$; $n = 42$; **Figure 2.1G**, **Supplementary Figure 2.1**).

When we presented moving stimuli (a 400 μm spot moving in 8 directions at 1000 $\mu\text{m/s}$), DSGCs responded to the leading (ON) and trailing (OFF) edges of the spot with a burst of spikes (**Figure 2.2B**). Stimuli moving in the centrifugal (soma to dendrite) direction evoked the maximal response, while those moving in the centripetal direction (dendrite to soma) evoked weaker responses (**Figure 2.2B**). The direction of preferred response was consistent from cell to cell and always pointed towards the ventral pole, parallel to the dendritic tree (**Figure 2.2B-D**). The DS index (DSI; see Methods) for ON and OFF responses were 0.45 ± 0.03 and 0.52 ± 0.03 respectively ($n = 42$; note DSI ranges from 0 to 1, with larger values indicating stronger DS). Plotting the angle of the DSI against that of the AI for ON and OFF responses/dendritic trees (**Figure 2.2E**) yielded striking correlations with slopes of 0.96 ($R^2 = 0.92$) and 0.97 ($R^2 = 0.94$), respectively. These findings contrast with previous reports that found ON-OFF DSGC dendrites to be either symmetric or asymmetric but randomly oriented with respect to the

preferred direction (Yang and Masland, 1994; Huberman et al., 2009; but see Kim et al., 2008 for OFF DSGCs). The strong correlation between morphological and functional asymmetries observed here suggests that dendrites play a role in computing DS.

While our results clearly demonstrate that GFP⁺ cells in the Hb9::eGFP retina belong to a unique set of polarized DSGCs that code superior motion, it is not clear if asymmetries are present in ganglion cells that code other directions. To test this possibility, we next recorded from GFP⁻ DSGCs in the Hb9::eGFP retina (**Supplementary Figure 2.2**). In a random sample of 14 cells, we found that 4 displayed asymmetry comparable to the GFP⁺ cells. In these cells, asymmetry appeared to be oriented in the same direction as the preferred responses (**Supplementary Figure 2.2**). In the general population, however, only a weak correlation between the orientation of dendrites and response preference was observed for ON but not for OFF dendrites ($R^2 = 0.20$ and 0.03 for ON and OFF, respectively; **Supplementary Figure 2.2**). Without knowing whether asymmetric cells belong to a specific population of DSGCs or if they are part of a population with varying morphologies, it is difficult to establish the functional significance of these findings. Hence, the identification of a genetic marker that labeled a specific population of asymmetrical DSGCs in this study was pivotal in establishing the functional relevance of morphological specializations.

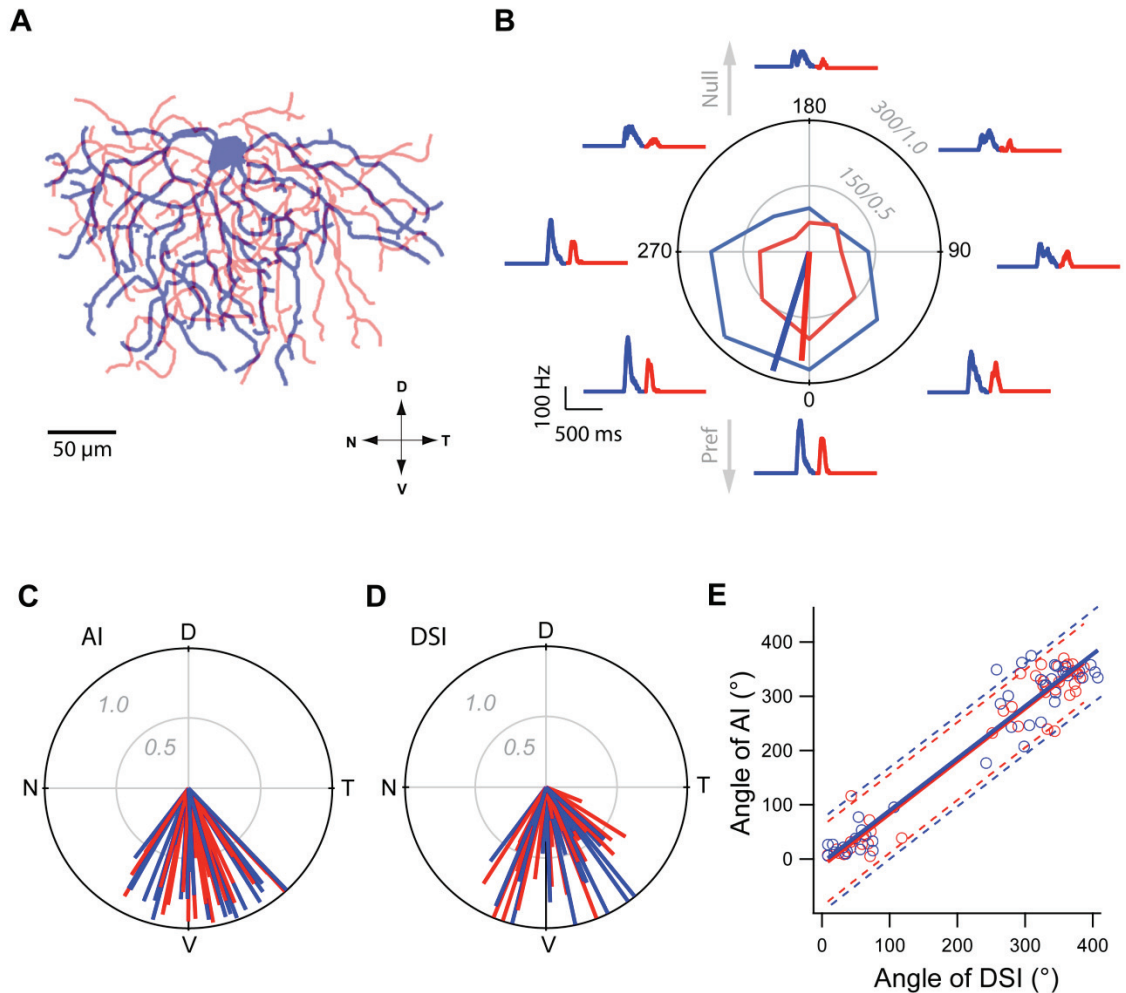


Figure 2.2 – Asymmetric dendritic morphology correlates with directional preferences. **A**, A reconstruction of a GFP⁺ DSGC showing that the majority of dendrites project towards the temporal pole. **B**, Polar plot representing the peak ON (leading edge) and OFF (trailing edge) spike rates evoked by a 400 μm spot moved in 8 directions over the receptive field of a GFP⁺ DSGC. Radial axis of the polar plot represents spike rate/DSI. DSI values range from 0 to 1, with larger values indicating more asymmetric responses. Spike rate histograms surround the polar plot (ON and OFF responses are depicted in blue and red, respectively, here and in the rest of the figures) for each of the 8 stimulus directions. **C**, A polar plot of asymmetry index (AI) vectors for GFP⁺ DSGCs. **D**, A polar plot of the directional selectivity index (DSI) vectors for GFP⁺ DSGCs. **E**, The angle of AI and DSI for individual cells are plotted against each other ($R^2 = 0.92, 0.94$ for ON and OFF, respectively; $n = 42$). Dotted lines represent 90% prediction bands for ON (blue) and OFF (red) DSI/AI correlations (see **Supplementary Figure 2.2** for Hb9⁻ DSGCs).

The Inhibitory DS Circuitry Aligns with Dendritic Asymmetries Along the Dorsal-Ventral Axis

To understand the mechanisms that generate DS in this asymmetrical population of cells, we first investigated whether they received inputs from the classic inhibitory DS circuitry. To do so, currents evoked by moving stimuli were measured using whole-cell voltage clamp techniques, while holding the membrane at different potentials (**Supplementary Figure 2.3**). The total conductance was split into its inhibitory and excitatory components based on their reversal potentials set at 0 mV and -60 mV, respectively (**Supplementary Figure 2.3**; Taylor and Vaney, 2002).

This analysis revealed that inhibitory conductances evoked by null direction stimuli were significantly larger than those evoked by preferred direction stimuli (Null: 12.6 ± 2.0 nS and 6.8 ± 2.1 nS for ON and OFF responses, respectively; Pref: 2.8 ± 0.8 nS and 1.4 ± 0.3 nS for ON and OFF responses, respectively; $P < 0.001$; Mann-Whitney Rank Sum Test; $n = 8$; **Figure 2.3A,C**). These data are consistent with the spiking responses measured in these cells that indicated a significantly weaker response for null direction stimuli. In contrast, excitatory conductances sometimes trended towards being larger for preferred direction stimuli (**Figure 2.3B**). However, on average this difference was not statistically significant (Pref: 4.8 ± 0.5 nS for 3.5 ± 0.8 nS, for ON and OFF responses, respectively; Null: 4.4 ± 0.9 nS and 2.8 ± 1.0 nS for ON and OFF responses, respectively; $P > 0.1$; Mann-Whitney Rank Sum Test; $n = 8$; **Figure 2.3B,D**). Consistent with previous reports (Taylor and Vaney, 2002), the asymmetry of inhibitory inputs was significantly stronger than that observed for excitatory inputs (**Figure 2.3E**; G_i DSI : -0.65 ± 0.07 and -0.57 ± 0.05 for ON and OFF responses, respectively; G_e DSI: 0.09 ± 0.06 and 0.19 ± 0.09 for ON and OFF responses, respectively). Thus, Hb9⁺ DSGCs appear to be driven by patterns of inhibitory and excitatory synaptic conductances that are typically associated with DS computations. Importantly, the inhibitory DS circuitry is aligned along the dorsal-ventral axis, parallel to the asymmetric dendritic arbors.

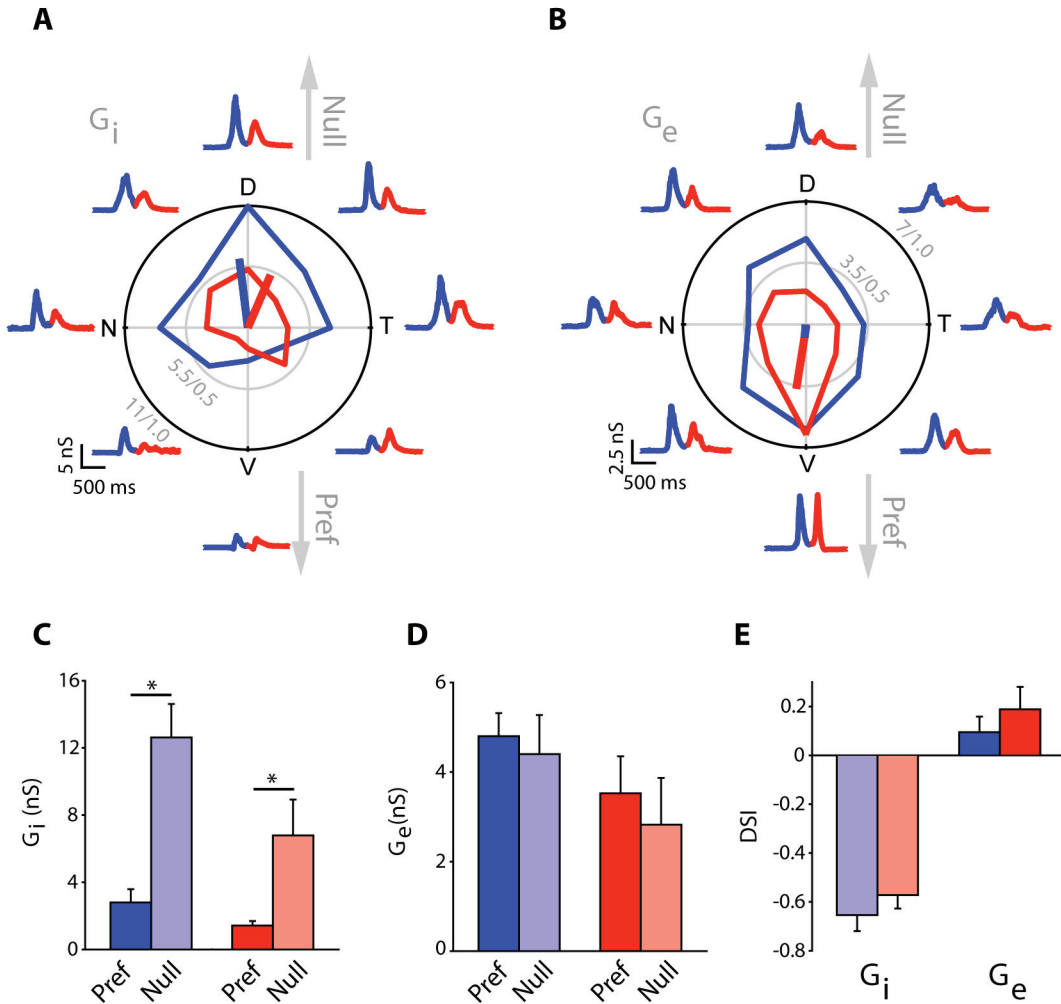


Figure 2.3. Inhibitory DS circuitry aligns along the dorsal-ventral axis. **A**, A polar plot of the peak inhibitory conductances (G_i) measured in a whole-cell voltage clamp recording from an $Hb9^+$ DSGC. Traces around the plot illustrate the inhibitory conductances measured in the corresponding directions (see **Supplementary Figure 2.3** for conductance analysis). **B**, A polar plot of the peak excitatory conductances (G_e) in the same $Hb9^+$ DSGC shown in (**A**). Traces around the plot illustrate the excitatory conductances measured in the corresponding directions. **C**, The average inhibitory conductances measured in the null and preferred directions ($n = 8$; * indicates $P < 0.001$) for ON and OFF responses. **D**, The average excitatory conductances evoked in the null and preferred directions ($n = 8$; $P > 0.1$) for ON and OFF responses. **E**, Average DSI values for G_i and G_e for ON (blue) and OFF (red) responses.

Directional Selectivity in GFP⁺ Ganglion Cells Does Not Critically Depend on the Classic Inhibitory Circuitry

Although the presence of asymmetric inhibition suggests that conventional mechanisms generate DS responses in Hb9⁺ cells, they do not preclude the existence of additional mechanisms suggested by their morphology. To test the functional significance of asymmetric dendritic morphology of ON-OFF DSGCs, we next studied their response properties before and after blocking the conventional inhibitory DS circuit using a cocktail of antagonists (100 μ M picrotoxin, 50 μ M TPMPA and 50 μ M D-tubocurarine to antagonize GABA_{A,C} and nicotinic receptors, respectively). This cocktail is expected to block the output of starburst amacrine cells and other GABAergic amacrine cells known to generate DS (Fried et al., 2002, Taylor and Vaney, 2003, Demb, 2007). Indeed, we found this cocktail effectively blocked all inhibitory currents in these cells (**Supplementary Figure 2.4**).

Figure 2.4A illustrates the responses to slow-moving spots (200 μ m/s) measured in control conditions, illustrating the preferred direction toward the ventral pole. Remarkably, responses in this cell remained DS after the cocktail of antagonists was applied (**Figure 2.4B**). Although less robust than control DS responses, spike rates in the preferred direction were more than double those evoked in the null direction (**Figure 2.4C**; control DSI: 0.64 ± 0.07 and 0.63 ± 0.09 for ON and OFF responses, respectively; DSI in blockers: 0.40 ± 0.06 and 0.35 ± 0.04 for ON and OFF responses, respectively; $P < 0.05$ for both ON and OFF; $n = 11$). In addition, the direction of the preferred response was always maintained (**Figure 2.4D**; average deviation of the preferred direction was $-20 \pm 10^\circ$ compared to control for ON responses and $-1 \pm 17^\circ$ for OFF responses; $P > 0.2$, Moore's paired-sample test). Together, these results demonstrate a form of directional selectivity that does not critically rely upon, but is in alignment with, the classic inhibitory DS circuitry.

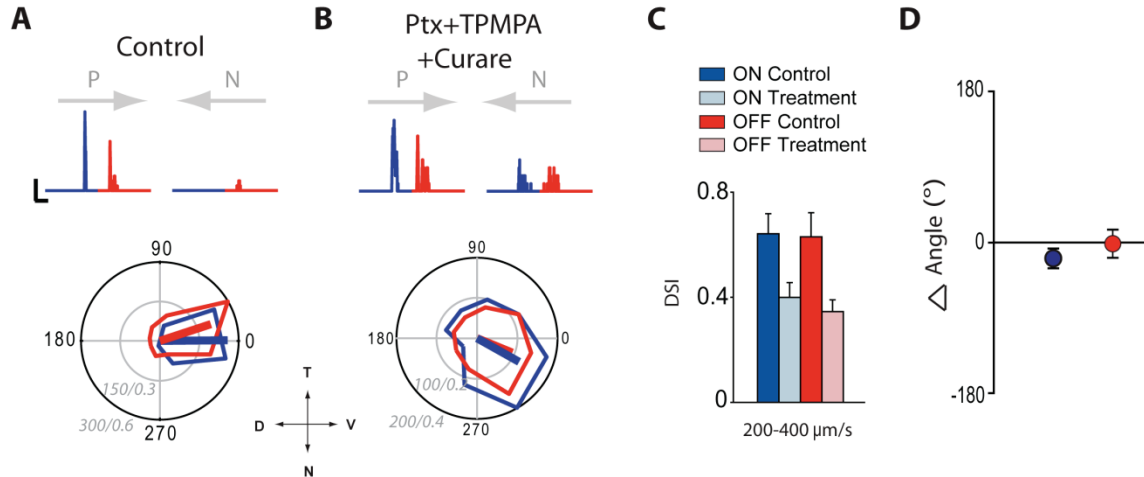


Figure 2.4. Directionally selective responses persist in the presence of GABA_{A,C} receptor antagonists. **A**, Control directionally selective response. The top traces are spike rate histograms for ON and OFF responses. In this and all subsequent figures, the grey arrows above responses indicate the preferred (P) and null (N) directions. Below is a polar plot of the peak spike rate. Scale bar for spike rate histograms: 100Hz, 1s. **B**, Responses in the same cell shown in (A) in the added presence of drugs (picrotoxin, TPMPA and D-tubocurarine; also see **Supplementary Figure 2.4**). Scale bar for spike rate histograms: 50Hz, 1s. The radial scale bar of the polar plots of (A) and (B) represent Hz/DSI. The stimuli speed for (A) and (B) is 200 μ m/s. **C**, Average DSI for both ON (blue) and OFF (red) responses (n = 11). **D**, Average change in the preferred direction in control vs. drugs for both ON (blue) and OFF (red) responses ($P > 0.2$, Moore's paired-sample test).

The DS responses observed in the presence of GABA_A receptor blockers were surprising considering the abundant literature supporting a critical role for inhibition in mediating DS (Wyatt and Day, 1976, Caldwell et al., 1978, Taylor and Vaney, 2002). Even in previous studies where DS was detectable under saturating concentrations of inhibitory blockers, it was relatively mild (Smith et al., 1996, Grzywacz et al., 1997). As we had performed our initial experiments at relatively slow stimulus speeds, we next tested the effects of varying speed on DSI, in an attempt to reconcile our findings with previous work.

In control conditions, increasing the stimulus speed resulted in an increased spike rate for null and preferred stimuli and led to a mild decrease in DSI at the high range of

speeds tested (100 to 2400 $\mu\text{m/s}$; **Figure 2.5A**). Application of the cocktail of antagonists augmented spiking responses for both preferred and null directions, though null direction responses tended to show much greater augmentation, confirming that inhibitory circuit mechanisms usually suppressed these responses (data not shown). In the presence of blockers, at the slower speeds, null direction responses always remained lower than those elicited in the preferred direction and consequently, responses remained DS (**Figure 2.5B**). However, as the stimulus speed was increased, DSI declined. By 1000 $\mu\text{m/s}$, DS was weak and only detected in a few cells, but on average was not statistically significant (ON DSI: 0.50 ± 0.08 in control compared to 0.05 ± 0.02 in blockers; $P < 0.005$; OFF DSI: 0.57 ± 0.07 compared to 0.06 ± 0.09 in blockers; $P < 0.005$; $n = 11$). At speeds higher than 1000 $\mu\text{m/s}$, DS responses were never observed. As higher ranges of speeds are typically used to stimulate DS responses in most studies, these findings suggest one possible reason why DS was not observed previously in the presence of blockers.

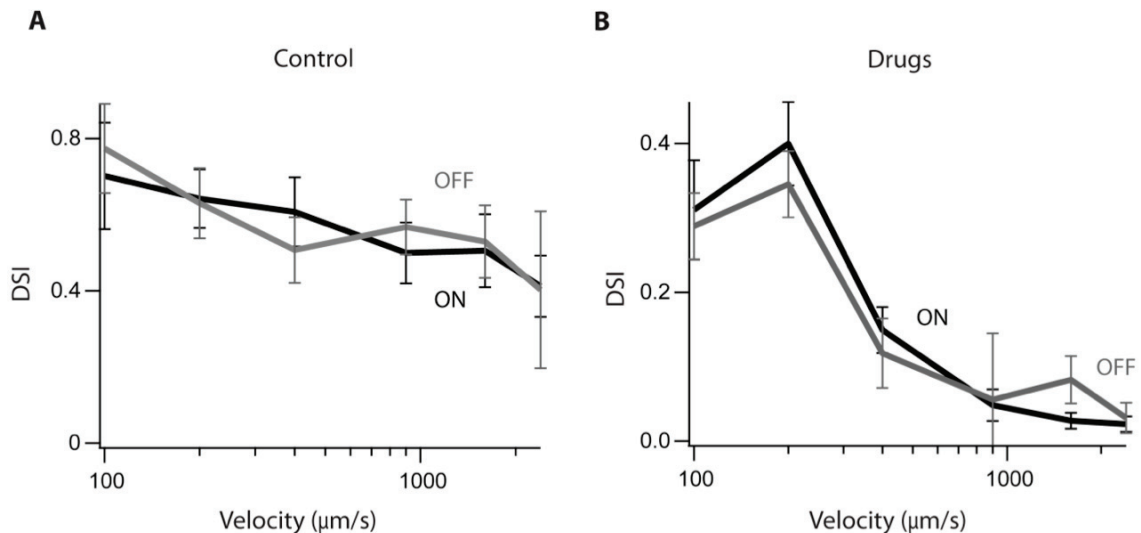


Figure 2.5. Inhibition-independent directional selectivity is apparent only at slower velocities. Average DSI for ON (*black*) and OFF (*gray*) responses as a function of stimulus velocity in (A) control conditions and (B) in the presence of drugs (picrotoxin, TPMPA and D-tubocurarine; $n = 6$). Data have been presented as mean \pm s.e.m.

Directional Selectivity in the Absence of Inhibition Arises in Ganglion Cells

To distinguish whether DS in the presence of inhibitory blockers arose pre- or postsynaptically, the properties of ganglion cell light-evoked synaptic inputs were analyzed using whole-cell voltage-clamp techniques. In these experiments, after measuring spikes in cell-attached mode in the presence of blockers (**Figure 2.6A**), the same cell was patched with an electrode containing intracellular solution. After break-in, the DSGC was dialyzed with QX314 and Cs⁺ and repeatedly injected with brief depolarizing pulses (-60 mV to 0 mV) until Na⁺ currents and a large fraction of voltage-gated K⁺ currents were blocked. Under these conditions, moving spots elicited large inward currents in both the null and preferred directions ($V_{\text{HOLD}} = -60$ mV; **Figure 2.6B**). When the cell was held ~0 mV, the inhibitory inputs that are usually associated with stimulating these cells (see **Figure 2.3A**, **Supplementary Figure 2.3**) were not apparent, confirming that they were effectively blocked with the cocktail of antagonist (also see **Supplementary Figure 2.4**). At +40 mV, light evoked outward going currents. Importantly, the temporal characteristics of currents measured at -60 and +40 mV were similar (**Supplementary Figure 2.5**), indicating that they were not contaminated by voltage-dependent conductances, and thus provided a reliable readout of bipolar cell output. Reversal of the excitatory currents also indicated that gap junctions did not significantly contribute to the DS responses (Ackert et al., 2009).

Under conditions in which inhibitory receptors and active postsynaptic conductances were blocked, preferred and null-direction stimuli evoked excitatory currents that were similar in size. The amplitude of the peak currents were not significantly different whether measured at -60 mV (Pref: -228 ± 30 pA and -136 ± 24 pA, for ON and OFF, respectively; Null: -206 ± 30 pA and -131 ± 18 pA for ON and OFF, respectively; $P > 0.6$; $n = 6$) or +40 mV (Pref: 353 ± 64 pA and 214 ± 44 pA, for ON and OFF, respectively; Null: 373 ± 67 pA and 216 ± 40 pA for ON and OFF, respectively; $P > 0.6$; $n = 6$). Similarly, the total charge of the response was similar in magnitude in the null and preferred directions, indicating that moving spots stimulated an equal number of inputs in both directions (-60 mV ON, -113 ± 18 nC for Pref compared to -126 ± 21 nC for Null; -60 mV OFF, -54 ± 13 nC for Pref compared to -66 ± 16 nC for Null; +40 mV ON, 227 ± 52 nC for Pref compared to 265 ± 54 nC for Null; +40 mV

OFF, 124 ± 26 nC for Pref compared to 141 ± 29 nC for Null; $P > 0.5$; $n = 6$). The symmetry in input strength contrasts with the asymmetry in the spiking responses and suggests that non-linearities within the ganglion cell must contribute to direction discrimination.

To test whether asymmetric dendritic trees could confer intrinsic DS properties to ganglion cells, we constructed a computational model based on the morphology of GFP⁺ DSGCs (**Supplementary Figure 2.6**). Interestingly, the addition of voltage-gated Na⁺ channels to dendrites (Oesch et al., 2005) was required to produce DS with a similar preferred direction as measured experimentally (**Supplementary Figure 2.6**). Thus, non-linear conductances and asymmetric dendritic trees appear to be essential requirements for the formation of DS in the absence of inhibition.

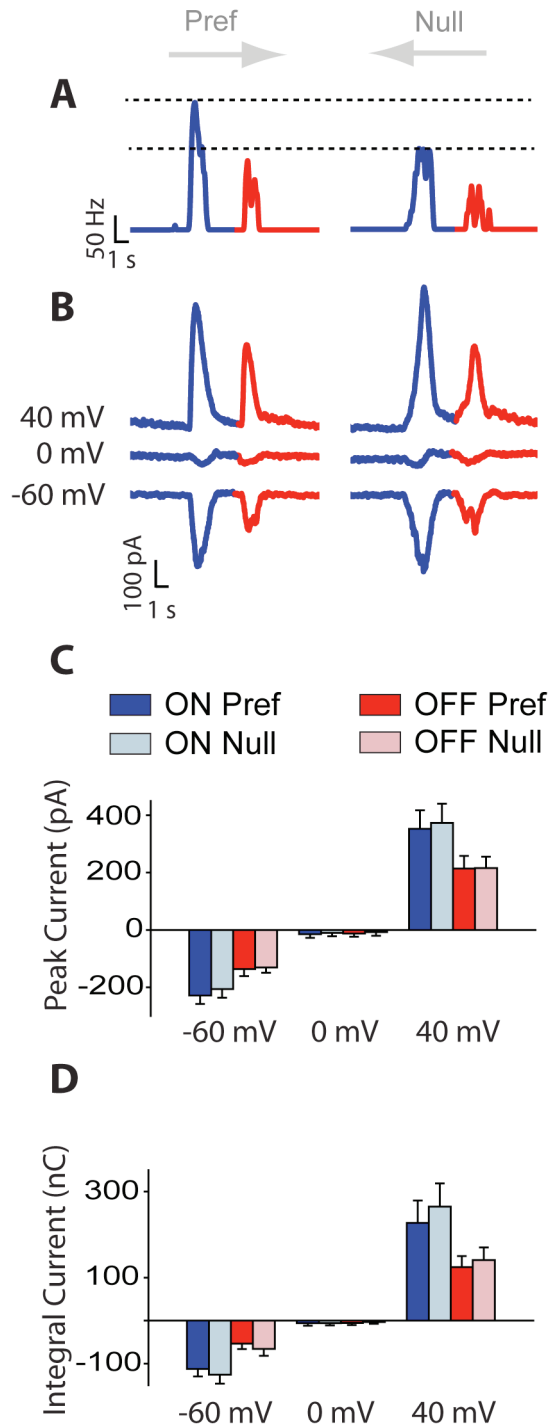


Figure 2.6. Directional selectivity in the presence of inhibitory blockers appears to arise from nonlinear properties of ganglion cells. **A**, Spike rate histograms of responses measured in the preferred (Pref) and the null directions in the added presence of drugs (picrotoxin, TPMPA and D-tubocurarine). **B**, Voltage-clamp recordings of excitatory currents measured in the continued presence of drugs, from the same cell shown in (**A**). Responses were measured at three different holding potentials as indicated.

These currents did not appear to be contaminated by voltage-dependent conductances (see **Supplementary Figure 2.5**). **C,D**, The average peak amplitude (**C**) and total charge (**D**) of excitatory currents measured in preferred and null directions. There are no statistical differences between any preferred null pairs ($P > 0.5$; $n = 6$). Data have been presented as mean \pm s.e.m.

Interactions Between Pre- and Postsynaptic DS Mechanisms in Symmetrical Ganglion Cells

If active conductances in dendrites contribute strongly to the formation of centrifugal preferences in asymmetric DSGCs, then it might be predicted that these would also affect processing in symmetric DSGCs. Indeed, such centrifugal dendritic preferences are predicted to hold regardless of DSGC morphology (Schachter et al., 2010). However, it might be expected that in symmetrical cells, the influence of dendrites pointing in opposite directions would cancel each other out, limiting their functional role. To test the impact of dendritic processing in symmetric DSGCs, we measured DS responses in different regions within the receptive fields of symmetric GFP⁻ DSGCs, in an attempt to isolate local dendritic contributions. For these experiments, moving stimuli (400 $\mu\text{m/s}$) were presented within a circular area (200 μm in diameter) in different parts of the DSGC receptive field (**Figure 2.7A,B**).

Strong DS responses were evoked when stimuli were presented within the null side of the receptive field (the side of the cell first stimulated by null direction moving stimuli; **Figure 2.7A,C**; DSI 0.76 ± 0.11 and 0.69 ± 0.08 for ON and OFF, respectively; $n = 6$). In this region, like in the Hb9⁺ ganglion cells, inhibitory-circuit and dendritic DS mechanisms are expected to work in synergy. However, when stimuli were presented on the preferred side, DS was significantly reduced or absent (**Figure 2.7B,C**; DSI 0.03 ± 0.22 and 0.13 ± 0.15 for ON and OFF, respectively; $n = 6$). The absence of DS cannot be explained by lack of inputs from SACs, since these appear to be evenly distributed throughout the dendritic tree (Briggman et al., 2011). However, a non-discriminatory zone (NDZ) in a region on the preferred side has previously been described in rabbit DSGCs (Barlow and Levick, 1965, He et al., 1999). We hypothesized that in this region

of the dendritic field, inhibitory-circuit and dendritic DS mechanisms work in opposition, resulting in the formation of a non-directional zone.

To test the hypothesis that heterogeneous interactions between multiple DS mechanisms occur in different parts of the DSGC receptive field, we next measured responses in the presence of the cocktail of inhibitory antagonists. When moving stimuli were presented on the null side, consistent with previous results in the Hb9⁺ cells, DS persisted (**Figure 2.7A,D**; DSI, 0.47 ± 0.11 and 0.28 ± 0.18 for ON and OFF respectively), though was significantly reduced compared to control ($P < 0.05$). Application of inhibitory blockers tended to increase spike rates more in the null direction, suggesting inhibitory circuits were functional within the tested subfield. When stimuli were centered over the receptive field, DS was reduced drastically (data not shown; ON DSI, 0.14 ± 0.06 ; OFF DSI 0.20 ± 0.05). In this case, the influence of dendritic DS would be expected to be negligible since dendrites on opposing sides of the soma would nullify each other. When the stimuli was centered over the preferred side, a centrifugal dendritic preference was revealed in a region that had been the non-discriminating in control conditions (**Figure 2.7B,D**; ON DSI, -0.42 ± 0.12 ; OFF DSI -0.20 ± 0.08). The direction of this preference was centrifugal, as expected from a dendritic DS mechanism, but opposite to the preferred direction of the cell measured in control. It is important to note that the rate of null direction spikes was strongly enhanced (ON: 82 ± 17 Hz for control compared to 213 ± 67 Hz for drugs; OFF: 68 ± 17 Hz for control compared to 153 ± 20 Hz for drugs; $P < 0.05$; $n = 6$) indicating that even within this region that had been non-directional in control conditions, presynaptic circuits provide null-direction inhibition. Thus, it appears that over the null side of the DSGC receptive field, inhibitory circuit-dependent and dendritic mechanisms act in synergy, while over the preferred side they act in opposition, consistent with previous predictions (Schachter et al., 2010).

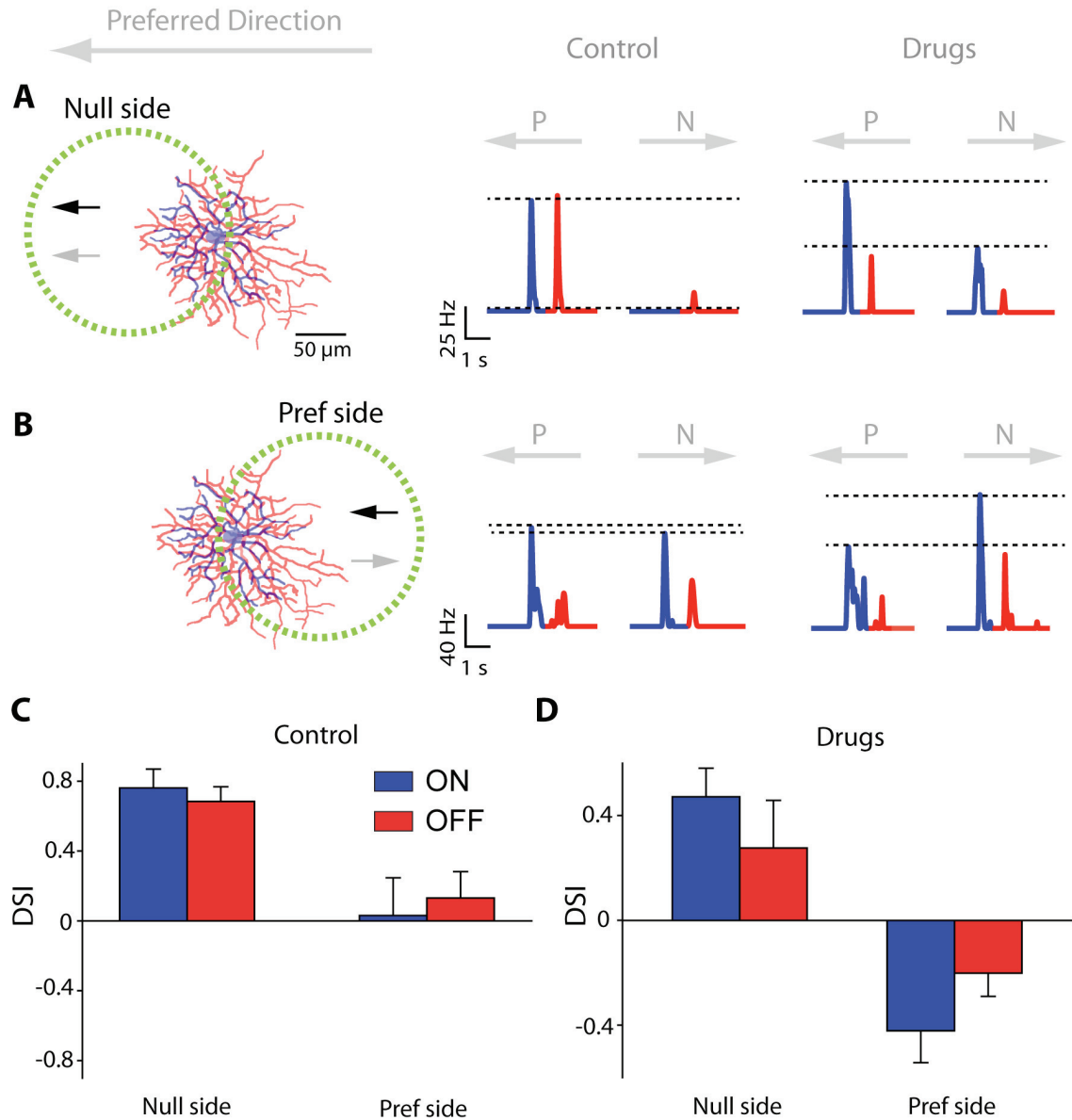


Figure 2.7. Interactions between the inhibitory circuit and dendritic DS mechanisms revealed in symmetrical DSGCs. **A**, Symmetrical DSGCs were stimulated within an area on the null side of the cell (*left*). Moving stimuli were presented within the area indicated by the dotted yellow circle (200 μm diameter). Spike rate histograms for preferred and null directions are shown in control (*middle*) and in the presence of drugs (*right*). **B**, Same as in (**A**), but stimuli were presented in an area located on the preferred (Pref) side of the cell (called the NDZ) delineated by the dotted circle. **C,D**, The average DSI for responses evoked in the null and preferred side in control (**C**) and in the added presence of drugs (**D**). Within the dotted circles, the black arrows indicate the direction of DS responses expected from circuit mechanism, whereas the gray arrows point in the direction of DS responses expected from dendritic mechanisms. Data have been presented as mean \pm s.e.m.

Discussion

Most models of directional selectivity in the mammalian retina involve lateral asymmetries within the inhibitory circuitry, likely arising from SACs. Here, we demonstrate that for a select population of ganglion cells, directional selectivity persists when classical inhibitory DS circuitry is blocked, suggesting the existence of a parallel DS mechanism. We explored the cellular basis for this form of directional selectivity and its contribution to shaping responses in asymmetrical and symmetrical ganglion cells.

An Entire Population of ON-OFF DSGCs with Asymmetric Dendritic Arbors

The morphology of DSGCs in many species is known to be variable, ranging from highly asymmetrical to completely symmetrical (Amthor et al., 1989, Oyster et al., 1993, Yang and Masland, 1994). However, it is not clear whether these differences in dendritic shapes arise randomly in development or correspond to a morphological specialization. Here, we present evidence demonstrating systematic dendritic asymmetries in an entire mosaic of ON-OFF DSGCs. Ganglion cells labeled in the Hb9::eGFP retina exhibit highly asymmetric dendritic trees orientated towards the ventral pole of the retina. Every GFP⁺ cell tested (n = 42) showed dendritic asymmetries. GFP⁺ cells were also relatively uniform in a number of other morphological characteristics compared to the general population of ON-OFF DSGCs (Sun et al., 2002, Coombs et al., 2006). In addition, every GFP⁺ cell was found to code superior motion. Together, the relatively uniform morphological and physiological characteristics of GFP⁺ ganglion cells in the Hb9::eGFP retina indicate that they belong to a single subset of ON-OFF DSGCs. Thus, the molecular specification of distinct DSGC populations exhibiting dendritic asymmetries highlights the importance of dendritic processing in DS coding, a property that has previously been hard to assess with random samplings from mixed populations of DSGCs (**Supplementary Figure 2.2**).

The asymmetric morphological characteristics of the Hb9⁺ cells contrast with the recently identified subset of ON-OFF DSGCs that code posterior motion, specified by the dopamine receptor 4 promoter (DRD4). DRD4⁺ cells are roughly the same size as Hb9⁺ cells, but do not bear any systematic dendritic asymmetries (Huberman et al., 2009).

However, we found that even in a small sample of posterior coding DSGCs ($n = 7$), examples of cells that exhibited dendritic asymmetries parallel to the preferred direction were apparent. Aside from the direction of their dendritic orientation, these asymmetrical cells appeared morphologically similar to $Hb9^+$ cells (**Supplementary Figure 2.2**). This observation raises the possibility that multiple populations of DSGCs might code a single direction in the murine retina. Indeed, in mouse retina there is a large overlap in the dendritic field coverage between neighboring $DRD4^+$ DSGCs (Huberman et al., 2009), which contrasts the territorial organization of DSGCs in rabbit retina (Vaney, 1994). In addition, the density of $DRD4^+$ DSGCs was found to be roughly 3 times what we report here for the $Hb9^+$ DSGCs. A more thorough characterization of $DRD4^+$ cells and/or new genetic markers will reveal whether more than one population of DSGCs encodes a single direction of motion.

Nonlinearities Within Asymmetric Dendritic Arbors Confer Centrifugal Preferences

Considering that conventional inhibitory mechanisms were manifest in the $Hb9^+$ ganglion cells, it was interesting to find that DS responses persisted in a cocktail of antagonists that block GABA receptors. These results clearly demonstrate the existence of an additional DS mechanism that does not critically rely on inhibition. From a theoretical point of view, the minimum requirements for direction discrimination are 1) an asymmetry and 2) a non-linear interaction between inputs (Borst and Egelhaaf, 1989). Our experimental findings indicate that non-linearities within asymmetric dendritic trees of DSGCs can confer inhibition-independent DS. The evidence for this is summarized below.

Under inhibitory receptor blockade, although DS is apparent in the spiking responses of DSGCs, the excitatory synaptic inputs measured under voltage-clamp were of equal strength in the preferred and null-directions. This finding suggests that non-linearities within $Hb9^+$ ganglion cells convert the temporal sequence of inputs distributed over their asymmetric dendritic trees into a DS output. Interestingly, SACs also have the intrinsic ability to respond preferentially to centrifugal motion (Euler et al., 2002),

suggesting a common dendritic mechanism might underlie direction coding in both cell types.

Insights into the how dendrites compute DS are offered by a computational model (**Supplementary Figure 2.6**). This model demonstrates that for the passive case, null and preferred responses produce little or mild reverse (centripetal) DS at the soma (Livingstone, 1998, Branco et al., 2010), consistent with results from our voltage-clamp experiments. However, the model also allows us to estimate responses at the distal dendrites. Interestingly, for stimuli that produce mild centripetal DS at the soma, distal dendrites were found to express a strong preference for centrifugal motion. This occurred because during centrifugal motion, signals activated near the soma appear delayed at the periphery and thus coincide with local signals at the dendritic tips, summing effectively. On the other hand, during centripetal motion proximal and distal inputs are activated out of phase and thus, at the dendrite, sum poorly (Rall, 1964, Tukker et al., 2004, Hausselt et al., 2007). Furthermore, the relatively high input resistance at the distal dendrites compared to the proximal dendrites amplifies the differential responses, thereby promoting dendritic spike initiation during preferred motion. Indeed, these simulations of centrifugal preferences in the distal dendrites are supported by Ca^{2+} imaging studies from SACs (Euler et al., 2002), but remain to be validated in DSGCs.

How are centrifugal preferences of dendrites transferred to the soma? Following Hausselt et al. (2007), we found that addition of non-linear conductances (in this case voltage-gated Na^+ channels; see Oesch et al., 2005) to asymmetric dendrites of DSGCs resulted in an amplification of distal PSPs which effectively reversed and amplified DS preference at the soma (**Supplementary Figures 2.6**). Such non-linearities resulted in the formation of dendritic spikes which propagated to the soma where they evoked somatic action potentials with high probability (Oesch et al., 2005; Schachter et al., 2010), thus creating a robust centrifugal preference at the soma (**Supplementary Figure 2.6**). Thus, active non-linear conductances in the asymmetric dendrites appear to be a critical requirement for inhibition-independent DS. Although this relatively simple computational model reproduces our basic experimental findings, the mechanistic details remain to be tested.

Parallel Mechanisms Underlie DS Coding

We hypothesize that multiple DS mechanisms work together to shape response properties of Hb9⁺ ganglion cells. Moving stimuli evoked a characteristic pattern of inhibitory and excitatory synaptic conductances in Hb9⁺ DSGCs, similar to those described for other types of DSGCs (Taylor and Vaney, 2002). First, inhibitory conductances were significantly larger in the null compared to the preferred direction. Second, null-direction inhibition coincided with or preceded excitation, while preferred-direction inhibition was delayed with respect to excitation. Thus, conventional circuit mechanisms appear to contribute to shaping DS responses in Hb9⁺ ganglion cells. Interestingly, these circuit mechanisms are aligned with the asymmetric dendritic arbors, along the dorsal-ventral axis. Moreover, DS persisted under inhibitory receptor blockade and the directional preferences of Hb9⁺ cells were not significantly altered under these conditions. Together, these results reveal a novel DS mechanism that does not critically rely on inhibition but that is in alignment with conventional DS circuitry.

In asymmetric DSGCs, inhibitory and dendritic mechanisms appear to work in a complementary fashion, to generate similar directional preferences. A critical feature of DSGCs is that they respond poorly to null direction stimuli. During null direction movements, dendritic mechanisms result in weak responses (because of sub-optimal summation), making them more susceptible to being “vetoed” by inhibitory mechanisms, which are stronger in this direction. Thus, the combination of inhibitory and dendritic mechanisms allows for DS cells to produce little or no response to null motion. In the preferred direction, the dendritic mechanism results in an optimal summation of inputs, which when combined with weak delayed inhibition, result in a robust spiking response. Therefore, as in the case of SACs (Euler et al., 2002, Hausselt et al., 2007), the dendritic mechanism is not merely a supplementary mechanism for DS, but an essential one.

The relative weighting of inhibitory circuit and dendritic mechanisms is perhaps best exemplified when considering the response elicited within the non-discriminatory zone (NDZ) located on the preferred side of symmetrical DSGCs, where these two mechanisms appear to be in opposition. Here, inhibitory circuit mechanisms appear to favour centripetal preferences, while the dendritic DS mechanisms favour centrifugal

preferences (**Figure 2.7**). Interestingly, in the null direction, inhibition is not strong enough to suppress responses evoked in dendrites that are oriented so as to provide an optimal response (note: inhibitory contacts appear uniformly distributed throughout the dendritic field, Briggman et al., 2011). In the preferred direction, although inhibition is weak, the dendritic mechanisms do not favour the generation of strong responses. Thus, the opposing circuit and dendritic DS mechanisms both appear to strongly influence responses of ganglion cells leading to the formation of the NDZ (Schachter et al., 2010), first described many years ago (Barlow and Levick, 1965, He et al., 1999).

While our results show that both inhibitory and dendritic mechanism can generate DS responses in Hb9⁺ ganglion cells, assessing their relative contributions to DS under diverse speeds remains a challenge. In the presence of inhibitory blockers, DS is only apparent at the slower range of speeds. At speeds greater than 1000 $\mu\text{m/s}$ DS was essentially abolished under these conditions as previously noted (Wyatt and Day, 1976, Caldwell et al., 1978). However, blocking inhibition is also known to strongly affect the spatio-temporal characteristics of excitation, thereby affecting dendritic DS mechanisms, raising the possibility that dendritic mechanisms may operate differently in control conditions. Indeed, theoretical modeling studies suggest that dendritic mechanisms are tuned towards generating maximal DS responses at significantly higher speeds (1000-2000 $\mu\text{m/s}$; Tukker et al., 2004). In addition, under control conditions, responses in the NDZ remain non-directional at faster speeds (data not shown; Barlow and Levick, 1965, He et al., 1999), consistent with idea that dendritic and inhibitory mechanisms continue to oppose each other during faster movements (Schachter et al., 2010). Our results prompt an in-depth investigation into how multiple DS mechanisms interact under diverse conditions.

Conclusion

Our results demonstrate new insights into how neural circuit mechanisms interlace with the computational subunit properties of dendrites. In the retina, directional selectivity in SACs and a variety of DSGCs appears to be generated using a similar strategy, utilizing inhibitory circuit mechanisms in conjunction with active dendritic properties. The asymmetries in dendritic arborizations in Hb9⁺ DSGCs appear to represent a striking morphological adaptation that the retina has developed to avoid the NDZ by truncating their dendritic trees on the preferred side. Overall, when combined with asymmetric inhibition, asymmetric dendritic trees provide the most robust directional selectivity with the smallest arbour. Future investigations will reveal functional consequences of such adaptations.

Methods

Animals

Hb9::eGFP⁺ transgenic mice were kindly provided by Dr. Robert Brownstone (Dalhousie University) and maintained on a 12 hr light/dark cycle.

Retinal Preparation

All procedures were performed in accordance with the CACR and approved by Dalhousie University's Animal Care Committee. Briefly, mice were anaesthetized and decapitated. Eyes were removed and placed in warm Ringer's solution. Retinas were isolated and a small incision was made on the dorsal side of the retina to identify the orientation. The isolated retina was then placed down on a 0.22 μm membrane filter (Millipore, Bedford, MA, USA) with a pre-cut window that enabled transmitted light to reach the retina and for the preparation to be viewed under infrared illumination with the aid of a Spot RT3 CCD camera (Diagnostic Instruments, Inc., Sterling Heights, MI, USA) attached to an upright Olympus BX51 WI fluorescent microscope, equipped with either a 40 or 60 X water-immersion lens (Olympus Canada Inc., Markham, Ontario, Canada). The preparation was continually bathed with control Ringer's solution

containing (in mM): 110 NaCl, 2.5 KCl, 1 CaCl₂, 1.6 MgCl₂, 10 dextrose, and 22 NaHCO₃ that was bubbled with carbogen (95% O₂; 5 % CO₂; pH 7.4). All experiments were performed near physiological temperatures (35-36 °C). All reagents were purchased from Sigma-Aldrich Canada Ltd. (Oakville, Ont. CA) unless otherwise noted.

Whole-Cell Patch-Clamp Recordings

Extracellular recordings were made using 5–10 MΩ electrodes filled with Ringer's solution. Voltage-clamp whole-cell recordings were made using 4–6 MΩ electrodes containing: 112.5 mM CsCH₃SO₃, 1 mM MgCl₂, 10 mM EGTA, 10 mM HEPES, 4 mM ATP Mg₂, 0.5 mM GTP Na₃, and 0.2 mM Alexa 594 (Invitrogen, Burlington, Ontario, Canada). The pH was adjusted to 7.4 with CsOH. The reversal potential for chloride (E_{Cl}) was calculated to be ~-60 mV. The voltage-clamp recordings were made with a MultiClamp 700B amplifier (Molecular Devices, Sunnyvale, CA, USA). Signals were digitized at 10 kHz (National Instruments A/D board) and acquired using custom software written in the LabVIEW environment. Junction potentials (~10 mV) were left uncorrected and series resistance (~25 MΩ) was corrected offline.

Light Stimulus

Stimuli were generated with a DLP projector (Texas Instruments; refresh rate 75 HZ) controlled with custom software written by Dr. David Balya (Friedrich Meischer Institute, Switzerland). Neutral density filters were used to control the stimulus energy. The intensity of stimuli used was 0.5×10^{10} photons·s⁻¹·cm⁻² (sampled at 500 nm) as measured with a calibrated spectrophotometer (USB2000; Ocean Optics, Dunedin, FL). Light stimuli projected from below the specimen, were focused on the outer segments of the photoreceptors with the help of the sub-stage condenser. Flash responses were obtained using a series of spot sizes (25-800 μm). Directional selectivity was tested by moving a 400 μm spots presented at positive contrast only (50% to max). Spots were presented at different speeds over the cell in 8 different directions, equally divided over 360°. For experiments utilizing a cocktail of pharmacological blockers, a 200-400 μm

diameter mask was used to limit light stimulation to the cell of interest, and also to allow for comparison between Hb9⁺ cells and sub-fields of symmetrical Hb9⁻ cells.

Targeting, Imaging, and Reconstructing GFP⁺ Ganglion Cells

GFP⁺ ganglion cells were targeted using two-photon laser-scanning microscopy at 950 nm, to avoid bleaching photoreceptors (Euler et al., 2002). To facilitate targeting ganglion cells, two-photon fluorescent images were overlaid on the IR image acquired through the CCD camera. During physiological recordings, cells were dialyzed with 20–25 mM Alexa 594. Ganglion cells were imaged at 850 nm after physiological recordings were complete. Alexa 594-filled DSGCs were reconstructed from image stacks using manual or semiautomatic filament-tracing routines in Neuromantic (<http://www.reading.ac.uk/neuromantic/>) and Amira (Visage Imaging, San Diego, CA, USA). Retraced neurons were analyzed in MATLAB. The angle for the dendritic AI was computed by summing vectors representing each dendrite. The magnitude of AI was calculated by summing the length of all the dendrites on the preferred (PL) and null (NL) sides of the soma and calculating $AI = (PL - NL)/(PL + NL)$.

Analysis of Physiological Data

Spiking responses were accumulated as peristimulus time histograms (spike rates were binned over 25–50 ms), and the peak firing rate was analyzed in MATLAB. A DSI was calculated as: $DSI = (PR - NR)/(PR + NR)$, where PR and NR are the maximal spike rate evoked in preferred and null directions, respectively. The angle of the DSI was calculated as the vector sum of the peak spike rate for all eight stimulus directions. All spike data represent averages of two to four trials. Conductance analysis was performed as described by Taylor and Vaney (2002). Comparisons between two groups were made with t tests or the Moore's test (an equivalent for circular statistics). Paired t tests or Mann-Whitney U rank sum test was used to determine statistical significance when comparing responses before and after drug application. Data are presented as mean \pm s.e.m.

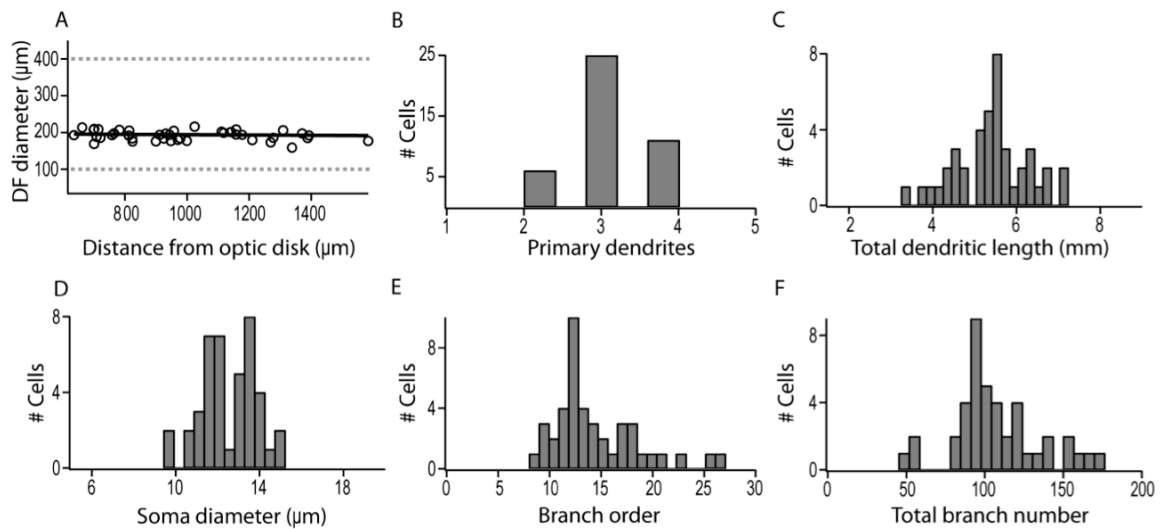
Morphological analysis

Cell diameter was calculated by measuring the area of a convex polygon obtained by linking the peripheral dendritic tips. The area was then converted to diameter by assuming a circular dendritic field. Branch order was defined as the maximum number of branches made by any one dendrite of the cell, with the primary dendrite being order 1.

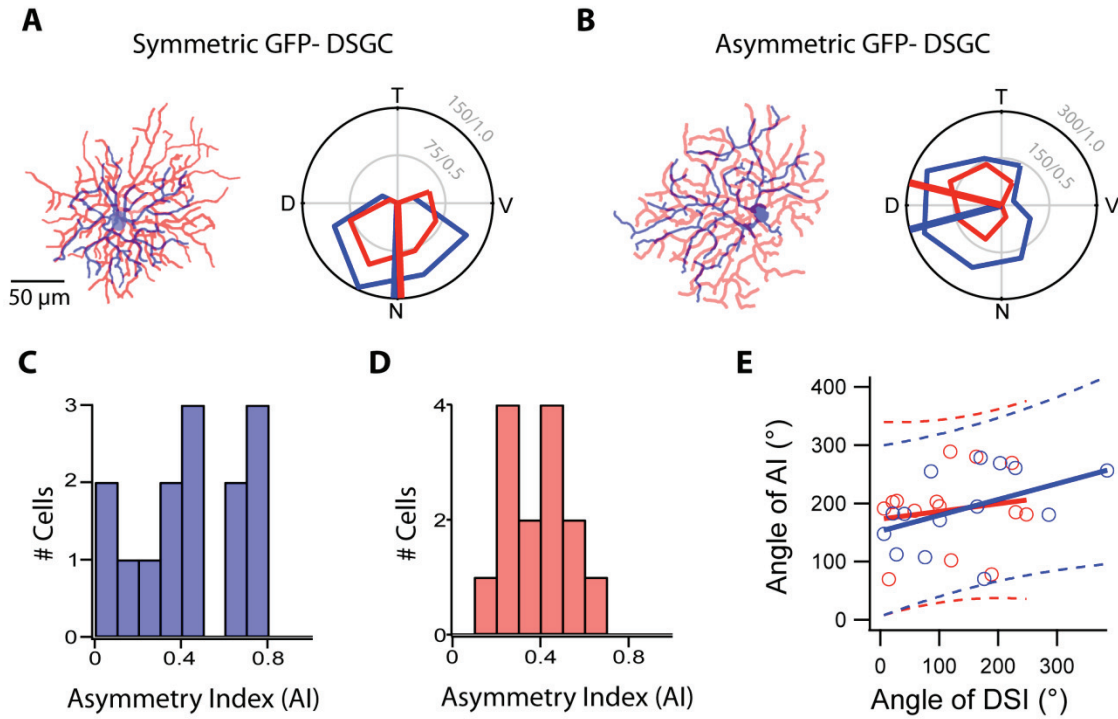
Computational model of inhibition independent DS in GFP⁺ ganglion cells

Simulations were performed in the Neuron-C simulator as previously described (Schachter et al., 2010). In brief, the morphology of a reconstructed GFP⁺ DSGC was imported into the simulator. Semi-random arrays of presynaptic cells were constructed automatically by the simulator with a regularity (mean/SD) of 6–10. Synapses were connected between presynaptic cells and the closest dendrite of a DSGC if they were within a threshold distance (typically 10 μm). We set the compartment size small enough (≤ 0.03 lambda) so that each synapse from a presynaptic array of cells was connected to a different compartment, preserving spatial acuity. We performed several types of simulations to calibrate our model to the physiological data (**Supplementary Figure 2.6**). Passive and active properties are listed in **Supplementary Table 2.1**. Our modeling condition here did not include inhibition on most runs.

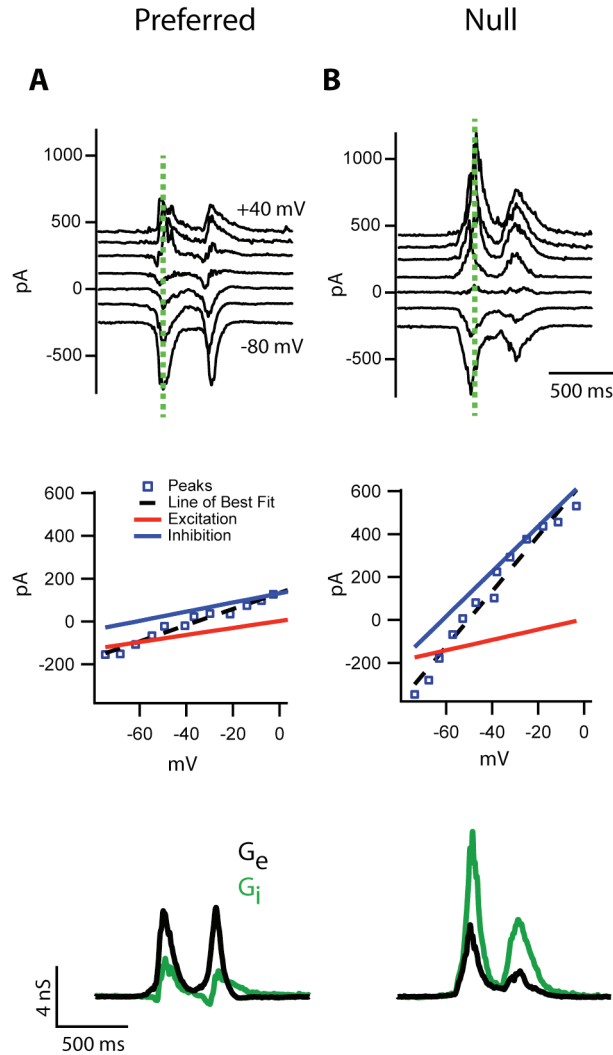
Supplementary Material



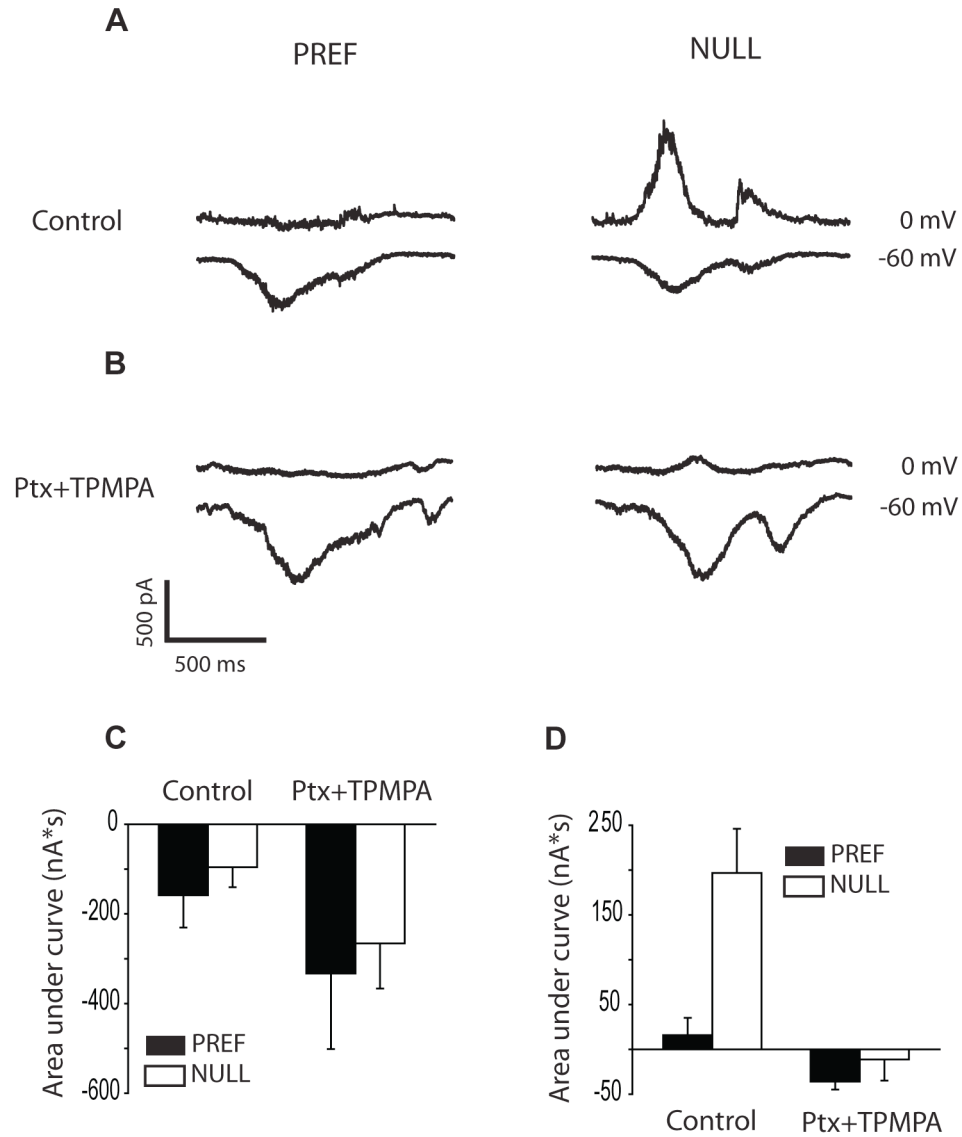
Supplementary Figure 2.1. A number of morphological features in the Hb9⁺ DSGCs are remarkably homogenous. **A**, Dendritic field diameter for Hb9⁺ ganglion cells. The dotted lines indicate the range of dendritic field diameters for ON-OFF ganglion cells found by Sun et al., (2002). **B-F**, Other morphological analyses as indicated (n = 42).



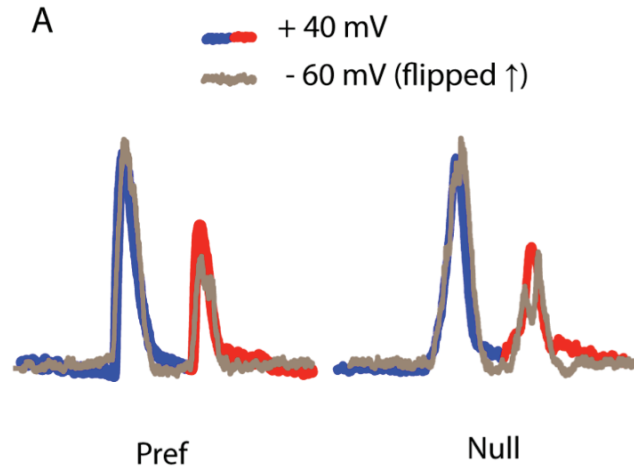
Supplementary Figure 2.2. Asymmetric DSGCs pointing in the preferred direction exist in the population of Hb9⁻ DSGCs. **A**, An example of an Hb9⁻ DSGC with fairly symmetrical morphology. **B**, An example of an asymmetric Hb9⁻ DSGC coding posterior motion, whose asymmetry correlates with its preferred direction, similar to Hb9⁺ cells. Asymmetry indices for ON (**C**) and OFF (**D**) dendritic layers of Hb9⁻ cells. **E**, The direction of AI plotted against the direction of DSI for Hb9⁻ cells, showing a weak correlation between morphology and directional preferences.



Supplementary Figure 2.3. Conductance measurements. **A**, Top panels: Responses to stimuli moving in the preferred direction recorded in an Hb9⁺ DSGC, using whole-cell patch-clamp techniques. Responses were recorded at a series of holding potentials (-80 to +40 mV, 10 mV steps). Middle panel illustrates the current-voltage relationship of the light-evoked responses. The blue squares represent the current measured at each voltage step measured at the time point indicated by the dotted green lines in top panel. The total conductance is estimated by the line of best fit (dotted black line). The total conductance is split into an inhibitory conductance that reverses at -60 mV (blue) and an excitatory component that reverses at 0 mV (red line). Holding potentials were corrected for series resistance and junction potentials. Bottom row: Excitatory (G_e) and inhibitory (G_i) conductances computed at all time points from currents measured in the top panel. **B**, The same analysis of the null direction.



Supplementary Figure 2.4. Inhibition in GFP⁺ ON-OFF DSGCs is mediated by GABAergic receptors. **A**, Inhibitory (measured at 0 mV) and excitatory currents (measured at -60 mV) evoked by a 400 μ m spots moving in the preferred (PREF) and null (NULL) directions, using whole-cell voltage clamp techniques. **B**, Responses in the same cell measured after application of GABA_{A,C} receptor antagonists (100 μ M picrotoxin and 50 μ M TPMPA). The average response before and after the application of drugs measured at a holding potential of -60 mV (**C**) and 0 mV (**D**) is shown (n = 3).



Supplementary Figure 2.5. Excitatory currents recorded at -60 mV and +40 mV have similar kinetics. A, The currents shown in **Figure 2.6** are shown here with the -60 mV trace flipped over the horizontal axis (shown in *grey*), and normalized in height to the ON (*blue*) responses for the +40 mV trace for comparison. Note the similar rise and decay kinetics in both preferred and null directions. These findings suggest that non-linear voltage-gated channels do not contribute to the EPSCs. Thus, these responses represent a reliable measure of bipolar cell output.

Computational Model of DS in Asymmetric Dendritic Trees

To test whether asymmetric dendritic trees could confer intrinsic DS properties to ganglion cells, we constructed a linear computational model (Methods) based on the morphology of GFP⁺ DSGCs. We evaluated whether biophysical mechanisms that are known to confer centrifugal preferences in the dendrites of SACs were also applicable to DS processing in ganglion cells.

First, the computational model was calibrated with biophysical parameters to match our recordings (**Supplementary Table 2.1**, **Supplementary Figure 2.6**), while omitting inhibition. Starting with a linear model, we calibrated the synaptic input currents and the input resistance to approximately match those of a real DSGC when its voltage-gated channels were blocked. Next, we added a complement of voltage-gated channels similar to those from (Schachter et al., 2010; **Supplementary Table 2.1**). These

endowed the model with the ability to initiate full-blown action potentials in its dendritic tree, similar to the ON-OFF DSGC (Oesch et al., 2005). We then calibrated the spike shape according to a phase plot (dV/dt vs. V). The somatic spikes of the model, being driven by full-blown dendritic spikes, were faster and larger than those in the real recordings. We achieved an approximate match by adding to the model a simulation of an electrode that contained a 0.1 ms time constant. Then we injected different currents into the model and calibrated the spike frequencies obtained by adjusting the densities and voltage-offsets of the voltage-gated channels. With these ganglion cell parameters set, we next tested the effects of simulating moving stimuli.

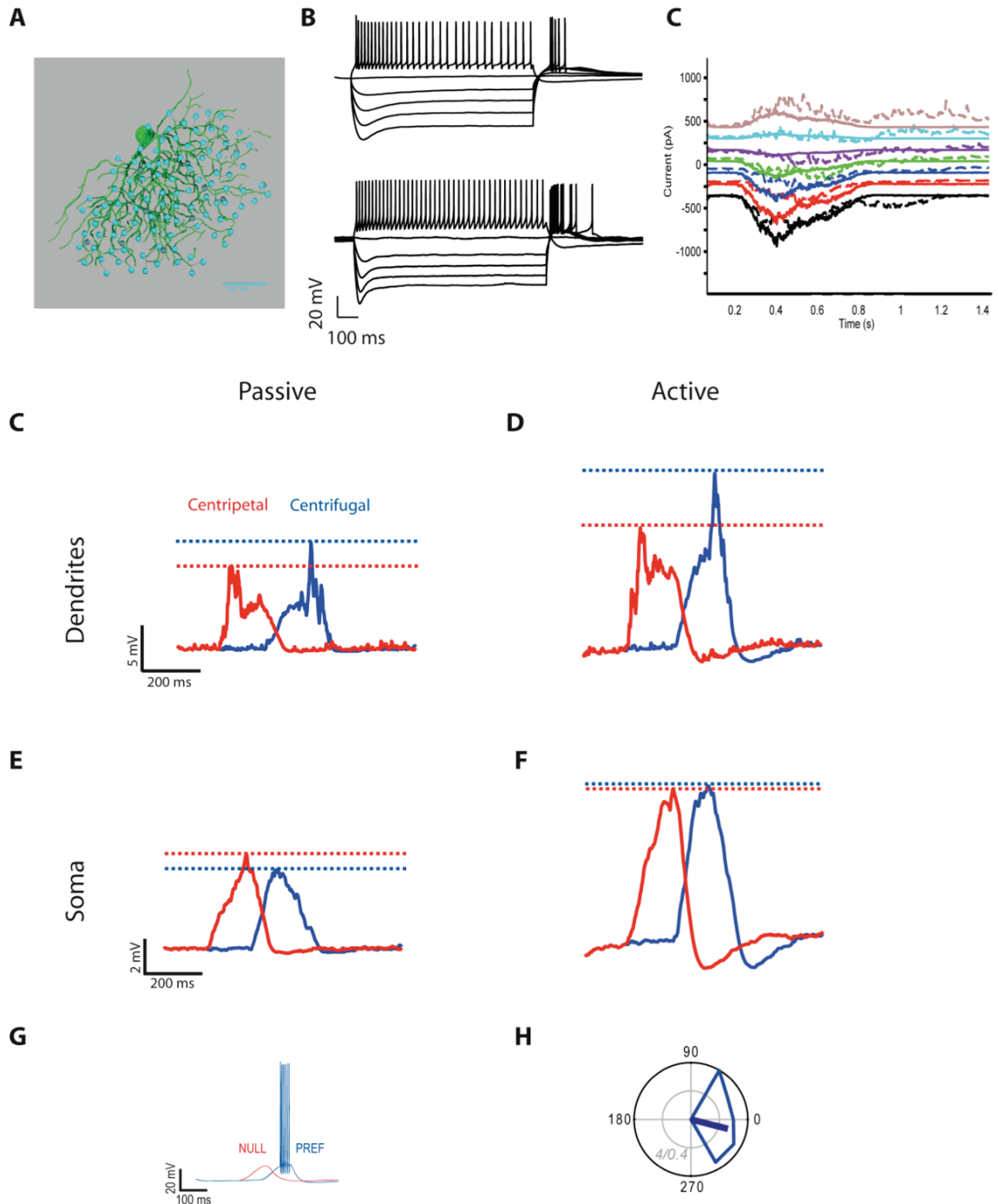
Consistent with previous work, in the linear model, centrifugal motion generated larger post-synaptic potentials (PSPs) at the dendritic tips compared with centripetal motion (Tukker et al., 2004). This occurred because in centrifugal motion, the somatic PSP summed with the dendritic PSP, whereas in centripetal motion, the dendritic PSP rose quickly but without summation from an underlying somatic PSP. In contrast, in the linear model, the somatic PSPs were larger for centripetal motion (Rall, 1964, London and Hausser, 2005, Branco et al., 2010). These two results are consistent because an asymmetry in one part of a linear model will always be balanced by an opposite asymmetry elsewhere. While the linear model predicted intrinsic centrifugal preferences of dendrites, it did not reproduce the centrifugal preferences of somatic spiking we measured experimentally (**Figure 2.2**). Thus, a simple linear model does not account for our experimental results.

The directional preference we observed in the dendrites of DSGCs was consistent with centrifugal preferences reported for the starburst amacrine cells. In the case of the SAC, however, non-linear conductances in distal dendrites cause a reversal of somatic preferences (Hausselt et al., 2007). Since non-linear Na^+ conductances are thought to be present in distal dendrites of rabbit DSGCs, where they appear to initiate dendritic spikes (Oesch et al., 2005), we next tested whether adding such non-linearities could affect the somatic response preference. We found that a low density ($< 10 \text{ mS/cm}^2$) of dendritic voltage-gated Na^+ channels added to the asymmetric DSGC model generated non-linear amplification of distal PSPs, which in turn led to a centrifugal preference for somatic

PSPs. A higher density of Na⁺ channels led to dendritic spikes, which propagated to the soma and triggered with high probability full-blown action potentials at the soma. Thus, under these conditions the strong centrifugal preference observed in the distal dendrites is also apparent at the soma. Thus, non-linear conductances in the dendritic tree of asymmetric DSGCs appear to be the essential requirements for the formation of inhibition-independent centrifugal responses.

	dendrite	soma	hillock	thin segment	axon
Na _v 1.2	0	0	0	0	50e-3
Na _v 1.6	35e-3	4e-3	4e-3	120e-3	0
K _{dr}	15e-3	15e-3	15e-3	20e-3	10e-3
K _A	35e-3	35e-3	35e-3	0	0
K _{IH}	0	0.09e-3	0	0.8e-3	0
sK _{Ca1}	0.12e-3	0.12e-3	0.12e-3	0	0
sK _{Ca2}	0.05e-3	0.05e-3	0.05e-3	0	0
Ca	1.4e-5	1.4e-5	1.4e-5	0	0
Ca-pump	2e-7	1e-7	1e-7	0	0
R _m	35e3	1e4	1e4	1e4	1e4

Supplementary Table 2.1. Biophysical parameters for the different regions of the asymmetric DSGC model. The values for the voltage gated channels and Calcium pump (Ca-pump) represent the channel densities in S/cm², and R_m is in Ohm-cm².



Supplementary Figure 2.6. Linear and non-linear modeling of directional selectivity in an asymmetric ganglion cell. **A**, Reconstruction of a GFP⁺ DSGC used for modeling. The light blue spheres represent excitatory synaptic inputs, and the dark blue spheres represent inhibitory inputs used for some control model runs. **B**, Responses measured in response to current injections measured in a DSGC (*bottom* panels) and in a model neuron (*top* panel). Whole cell voltage-clamp recordings of the leading edge (ON) response (*dotted lines*) measured at different holding voltages (-80 to 40 mV). The modeled currents (*solid lines*) are overlaid. For a cell with an asymmetric dendritic

morphology, a linear model of DS predicts a centrifugal preferred direction in the distal dendrites (**C**) but a centripetal preferred direction at the soma (**E**). Incorporating active Na^+ conductances in dendrites results in a centrifugal preferred direction at both dendritic terminals and the soma (**D,F**). To generate these PSPs, the light increment of the model (i.e. “contrast”) was set to generate PSPs below spike threshold. When the light level was increased to allow for action potentials, the model generated robust directionally selective spiking responses (**G**) and the cell exhibited a similar preferred direction as measured physiologically (**H**).

Chapter 3: Lag Normalization in an Electrically Coupled Neural Network

Abstract

Moving objects can cover large distances while they are processed by the eye, usually resulting in a spatially lagged retinal response (Anderson and Van Essen, 1987, Nijhawan, 1994, Berry et al., 1999, Krekelberg and Lappe, 2001, Nijhawan, 2002). Here, we identified a network of electrically-coupled motion coding neurons in mouse retina that act collectively to register the leading edges of moving objects at a nearly constant spatial location, regardless of stimulus velocity. These results demonstrate a novel neurophysiological substrate for lag normalization in the visual system.

Publication Information

This chapter has previously been published as: **Trenholm S**, Schwab DJ, Balasubramian V, Awatramani GB. Lag Normalization in an Electrically Coupled Neural Network. Nature Neuroscience. 2013, In press. All experiments were performed and analyzed by ST and were designed by ST and GBA. The computational model was developed DJS, VB and GBA. The paper was written by ST, VB and GBA.

Introduction

In the mammalian retina, there are four types of ON-OFF directionally selective ganglion cells (DSGCs), each preferentially responding to edges moving in a specific cardinal direction (Barlow et al., 1964, Vaney et al., 2012). These cells exhibit low background activity and initiate precise spiking patterns in response to movement, such that the very first spikes they generate register information about the spatial location of edges (Gollisch and Meister, 2008). In addition, their peak firing rates provide information about stimulus velocity (Barlow et al., 1964, Oyster, 1968). In the rabbit

retina, a sub-population of DSGCs is homologously coupled via gap junctions (Vaney, 1994). In the mouse retina, coupled DSGCs appear to correspond to the population of upward coding DSGCs, identified in the Hb9::eGFP (or Mnx1) transgenic line (Trenholm et al., 2011). Here, we compared the response properties of coupled and uncoupled ON-OFF DSGCs, applying two-photon assisted patch-clamp techniques in an isolated whole-mount retinal preparation.

Results

Anticipation of Moving Stimuli

We first compared the locations where DSGCs initially detected the leading edge of white bars (300x300 μm ; 96% Weber contrast) moving at 600 $\mu\text{m s}^{-1}$ in the direction that elicited a maximal response (i.e. the preferred direction). Uncoupled DSGCs began responding just as the leading edge of the moving bar entered their dendritic fields ($20 \pm 9 \mu\text{m}$ into the dendritic field; **Figure 3.1A**), consistent with their established receptive field properties (Yang and Masland, 1994). In contrast, coupled (Hb9⁺) DSGCs initiated spiking on average $106 \pm 16 \mu\text{m}$ *before* the stimulus edge reached their dendritic fields (**Figure 3.1A**; $n = 9$; $P < 0.005$). Since the different subtypes of DSGCs receive inputs from the same set of presynaptic bipolar/starburst amacrine cells (Wassle et al., 2009, Vaney et al., 2012), the early responses observed in coupled DSGCs suggest that activity in neighbouring pre-junctional cells effectively propagates through dendritic gap junctions (Vervaeke et al., 2012). Furthermore, since Hb9⁺ DSGCs possess starkly asymmetric dendritic trees (Trenholm et al., 2011; **Figure 3.1A**), it appears that lateral electrical inputs partially compensate for the lack of dendrites on the preferred side of the soma.

Lag Normalization

The most unexpected aspect of edge registration was revealed when we compared the position where spikes were initiated when bars were presented at different velocities (150-1800 $\mu\text{m s}^{-1}$). Uncoupled DSGCs detected the leading edges of moving bars at

positions that systematically shifted in space as a function of the stimulus velocity. This *spatial lag* was consistent with an apparent delay (t_d) of 99 ± 11 ms between the time when images fell on photoreceptors and the initiation of DSGC spiking responses (**Figure 3.1B,C**). For uncoupled DSGCs, at the fastest speed tested ($1800 \mu\text{m s}^{-1}$), responses initiated only after the moving edge had nearly crossed the entire dendritic field ($81 \pm 10 \mu\text{m}$ past the soma; $n = 12$). In contrast, coupled DSGCs detected edges at a nearly constant retinal location ($114 \pm 9 \mu\text{m}$ before the soma, $n = 15$) regardless of stimulus velocity (**Figure 3.1B,C**). This *lag normalization* was apparent for both positive and negative contrast stimuli (**Supplementary Figure 3.1**), suggesting that it did not require specific elements of the ON or OFF presynaptic pathways that provide inputs to DSGCs (for simplicity, we focus here on positive contrasts). Thus, gap junction coupling appears to endow DSGCs with a unique ability to compensate for processing delays that occur in the feed-forward retinal circuits.

In contrast to the initial responses to moving edges, the properties of the peak firing rates were similar in coupled and uncoupled DSGCs. In both cell types, peak responses spatially lagged the true positions of the moving edges (**Figure 3.1B,C**) and increased in amplitude as a function of velocity (**Supplementary Figure 3.2**). In coupled DSGCs, since only the initial response was lag normalized and not the peak, their response waveforms were skewed towards the leading edge (average skewness = -0.38 ± 0.02 , $n = 15$; **Figure 3.1B**; this waveform was not significantly distorted by the convolution filtering used to define instantaneous firing rates from the raw spikes – see **Supplementary Figure 3.3**). In contrast, in uncoupled DSGCs, both the initial and peak responses were equally lagged, resulting in responses that were significantly more symmetrical (average skewness = 0.07 ± 0.07 ; $n = 12$; $P = 0.029$; **Figure 3.1B**). We hypothesized that the lag uncorrected peak component arose from chemical synapses mediated by bipolar/starburst amacrine cells that stimulated coupled and uncoupled DSGCs alike, while the lag normalized response onset of coupled DSGCs arose from activity in upstream pre-junctional ganglion cells.

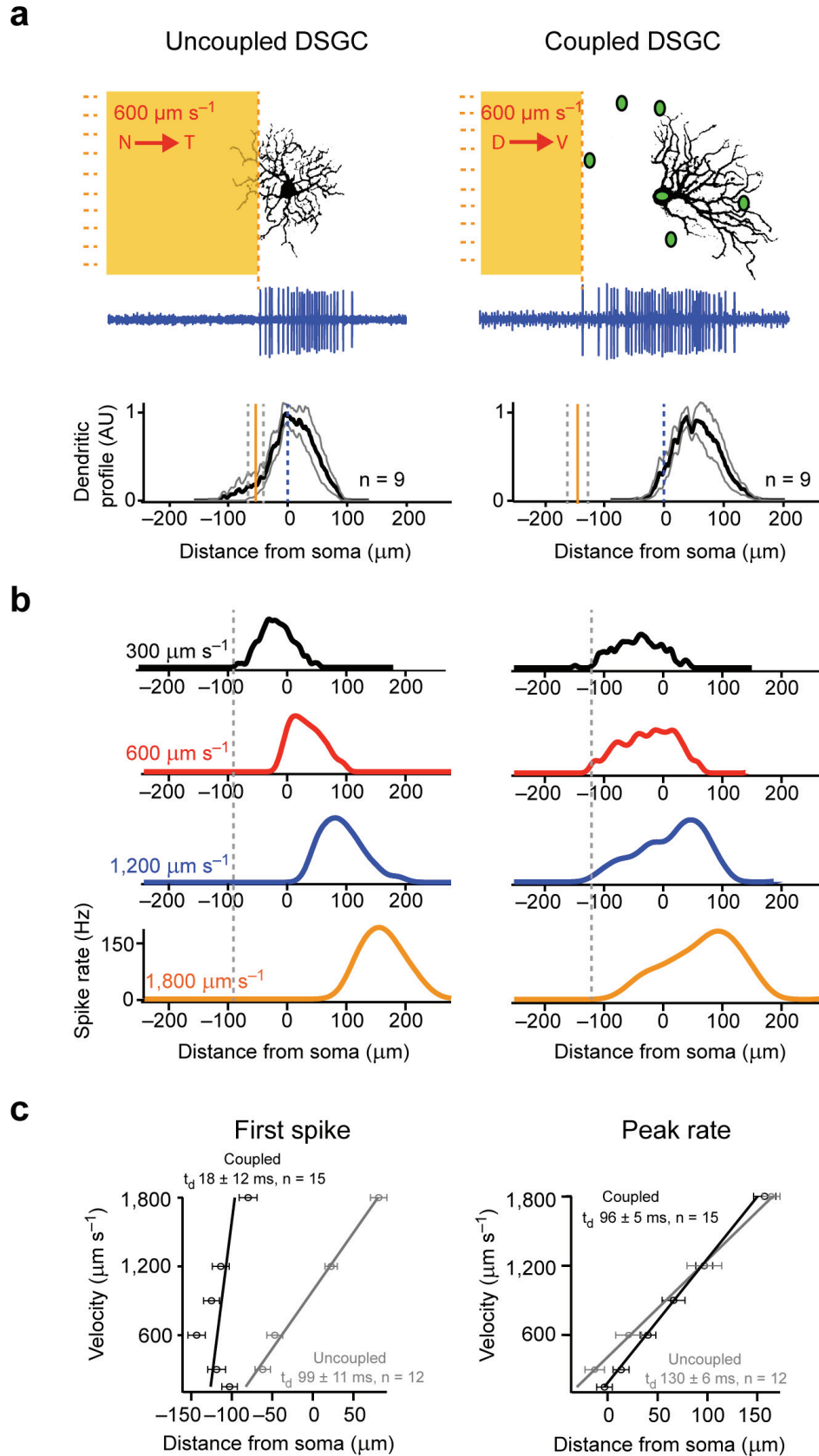


Figure 3.1. Lag normalization in the electrically-coupled population of upward coding ON-OFF DSGCs. **A**, A snapshot of moving light bars ($600 \mu\text{m s}^{-1}$) shown in relation to the dendrites of uncoupled (*left*) and coupled (*right*) DSGCs, at the positions where they triggered the first spikes. The spike train (*blue trace*) in response to the bar moving across the entire dendritic field is illustrated (note that only the leading edge ON responses and the ON dendritic fields of these bistratified ON-OFF cells have been depicted). The average start position (vertical orange line, \pm s.e.m. indicated by grey dotted lines) and dendritic profiles for 9 DSGCs are shown below (black traces, \pm s.e.m. indicated by grey traces; see Methods for details; the position of the soma is indicated by the vertical blue dotted line). Green ellipses (*top right*) represent the somata of neighbouring GFP⁺ DSGCs that are labelled in the Hb9::eGFP transgenic mouse retina. Abbreviations: D, dorsal; V, ventral; N, nasal; T, temporal. **B**, Plotting the waveform of spike activity triggered by bars moving at the indicated velocities in relation to the position of the leading edge of the stimulus, reveals spatially lagged responses in uncoupled (*left*) but not coupled (*right*) DSGC. Note, for all traces the leading edge of the stimulus is at the soma at $0 \mu\text{m}$; the grey vertical dotted lines indicate the position of the leading edge where the first spikes were generated at the slowest velocity tested. **C**, The position of the leading edge when the first spike (*left*) and the peak spiking response (*right*) were observed is plotted as a function of velocity for uncoupled and coupled DSGCs. The inverse slope of the linear fit provides an estimate of the apparent time delay (t_d ; indicated), which is proportional to the spatial lag (i.e. for perfect lag normalization, $t_d = 0$ ms delay). Error bars represent s.e.m.

Ganglion Cells Prime the Responses of Their Electrically Coupled Neighbours

To understand the nature of lateral gap junction mediated excitation, we next assessed the input contributions from a single neighbouring DSGC. To do so, we made simultaneous measurements of extracellular spiking from pre-junctional DSGCs and excitatory postsynaptic currents (EPSCs) in voltage-clamped post-junctional DSGCs (**Figure 3.2A**; $V_{\text{HOLD}} \sim -60 \text{ mV}$; 5 mM QX-314 was included in the recording pipette to block axonal and dendritic Na^+ channels (Oesch et al., 2005)). Spikes generated in pre-junctional cells were always immediately followed by low amplitude spikelets in the post-junctional cell (average amplitude $30 \pm 2 \text{ pA}$; average latency $0.37 \pm 0.3 \text{ ms}$; $n = 6$; **Figure 3.2A inset**). Thus, coupled DSGCs begin to receive excitation from a considerable distance away, when the first anticipatory spikes are generated in the *upstream* DSGC. It is important to note that since the initial coupling-mediated inputs occurred much farther from the soma than the first spikes, it suggests that coupled inputs alone do not drive spike activity in post-junctional cells. Thus, gap junction inputs are

likely to become effective when they are summed with inputs from other ganglion and/or bipolar cells. Such contextual restraints on gap junction signalling could allow for strong anticipatory signals to develop without leading to runaway excitation within the network.

Since the measured spikelet currents only represent the fast component of the gap junction-mediated priming signal, the total gap junction input is expected to be larger. Indeed, spiking responses and EPSCs of coupled DSGCs had a distinct slow rising component that was not observed in uncoupled DSGCs (**Figure 3.2B-D**; EPSC τ_{rise} 118 ± 11 ms for coupled and 66 ± 5 ms for uncoupled DSGCs; $n = 11$ for coupled, $n = 10$ for uncoupled DSGCs; $P = 0.029$). Consistent with a role for gap junctions in the early response component of coupled DSGCs, the initial phase of both EPSCs and spiking responses were selectively delayed in the presence of the gap junction antagonist 18 β -glycyrrhetic acid (25 μ M 18 β GA; **Figure 3.2B,C**; for spiking responses $\Delta = 60 \pm 8$ μ s, $n = 12$, $P < 0.001$; for EPSCs $\Delta = 125 \pm 31$ μ s, $n = 5$, $P = 0.01$), while responses of uncoupled DSGCs were not significantly affected (**Figure 3.2D**; $n = 4$; $P > 0.05$). Together, these results indicate an important role for pre-junctional DSGCs in controlling the initiation of spiking responses in their downstream neighbours, via gap junctions.

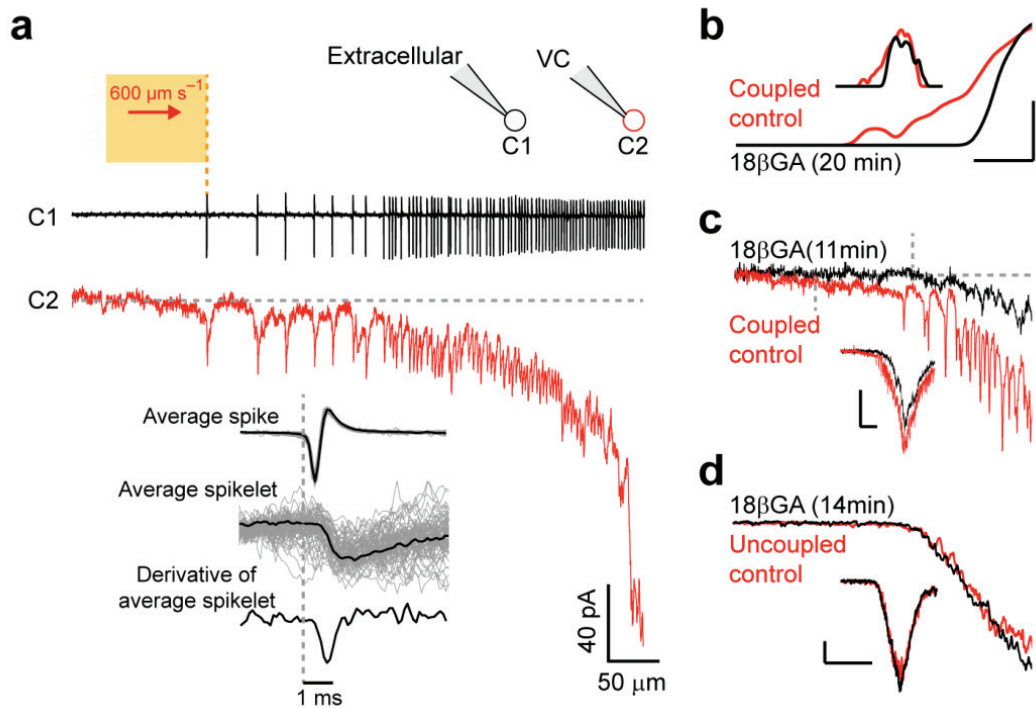


Figure 3.2. Gap junctions between upward coding DSGCs mediate lateral excitation. **A**, Responses to the leading edge of a bar moving at $600 \mu\text{m s}^{-1}$, measured simultaneously from neighbouring GFP^+ DSGCs. Spike trains in the pre-junctional DSGC (C1, *black*) were measured in cell-attached mode, while EPSCs in the post-junctional DSGC (C2, *red*) were measured in voltage-clamp ($V_{\text{HOLD}} = -60\text{mV}$; 5mM QX-314 in the patch pipette). The yellow bar indicates the position of the stimulus with respect to the positions of the somata of C1 and C2, at the position where the first spike was generated in C1. The inset illustrates the average pre-junctional spike, spike-triggered post-junctional current (average spikelet), and the derivative of the post-junctional current (*black traces*; raw data for 50 consecutive spikes/spikelets are shown in *grey*). **B,C**, Response onsets in coupled DSGCs (*red traces* in control Ringer's) are strongly attenuated in the presence of the gap junction antagonist $18\beta\text{GA}$ ($25 \mu\text{M}$; *black traces*). In the presence of $18\beta\text{GA}$, the position where the first spikes initiated shifted by $60 \pm 8 \mu\text{m}$ (**B**, $n = 12$, $P < 0.001$), and where EPSCs initiated shifted by $125 \pm 31 \mu\text{m}$ (**C**, $n = 5$, $P = 0.01$; EPSC initiation was measured when the current deviated 2 standard deviations above baseline noise). In contrast, the peak amplitudes (see *insets*) of the responses were only weakly affected. **D**, Responses of uncoupled DSGCs were not affected by application of $18\beta\text{GA}$ (average shift $38 \pm 12 \mu\text{m}$, $n = 4$, $P > 0.05$). Note, fast inward currents (spikelets) were always present in recordings from coupled DSGCs, and were abolished by the gap junction blocker (**C**). Vertical dotted lines in (**C**) indicate the start of EPSCs in control and drug conditions. Vertical/horizontal scale bar for (**B**) $50 \mu\text{m}/40 \text{Hz}$, and $250 \mu\text{m}/100 \text{Hz}$ for inset; for (**C**) $12 \mu\text{m}/25 \text{pA}$, and $100 \mu\text{m}/100 \text{pA}$ for inset; for (**D**) $50 \mu\text{m}/50 \text{pA}$, and $75 \mu\text{m}/250 \text{pA}$ for inset.

Lag Normalization Requires Gap Junctions Between DSGCs

Next, we sought to understand how converging electrical and chemical synaptic inputs result in lag normalization within the network. To compensate for spatial response lags that increase linearly with velocity, the strength of the lateral priming must increase in parallel. Indeed, signals mediated through gap junctions are expected to get larger with stimulus velocity because the peak firing rate of DSGCs increases with velocity (**Supplementary Figure 3.2**). Moreover, as gap junctions cause the responses of coupled ganglion cell to be shifted, these shifted responses in turn provide an even earlier priming signal to their downstream neighbours. Thus priming signals will compound over the network. To test that these effects suffice to produce lag normalization, we modeled an array of N coupled ganglion cells (**Figure 3.3A,B**) stimulated by experimentally measured velocity-dependent bipolar cell inputs (Methods). The coupling strength between GCs was taken as the only tuneable variable in the model. The first cell in the array (*GCI*) did not have any upstream coupled neighbours and did not exhibit lag normalization (**Figure 3.3B, left**). However, the ability to normalize spatial lag built up in subsequent DSGCs, and reached a steady state by the 6th cell (**Figure 3.3B, right**). Thus, a minimal model with a single tuneable parameter (the effective electrical coupling strength between DSGCs) captures the most salient response features of coupled DSGCs and suggests that lag normalization is a cooperative effect requiring serial gap junction interactions between several DSGCs.

To experimentally test the insights from our model, we first confirmed the role of gap junctions in lag normalization using pharmacology and found that lag normalization was significantly impaired in the presence of 25 μM 18 β GA (**Figure 3.3C**; $n = 4$; $P = 0.017$). Next, to examine how signals compounded over the network, we limited the area of retina being stimulated by presenting moving stimuli through an aperture of variable size (**Figure 3.3D**; the aperture diameter was set between 600-150 μm , and was centred over the soma). When the light stimulus was restricted over the dendritic field (150 μm aperture), peak spiking responses were left intact but lag normalization was greatly diminished (**Figure 3.3D**; $n = 5$; $P < 0.03$). However, as the aperture was made larger and upstream DSGCs were stimulated, lag normalization progressively increased. When stimuli approached from $> 300 \mu\text{m}$ upstream of the soma (i.e. 3-4 DSGC somata away)

lag normalization was restored to control levels (**Figure 3.3D**). These findings indicate that the effects of electrical signalling compound over extended areas, implicating a cooperative, serial interaction between multiple electrically-coupled DSGCs in the generation of lag normalization, as predicted by our model.

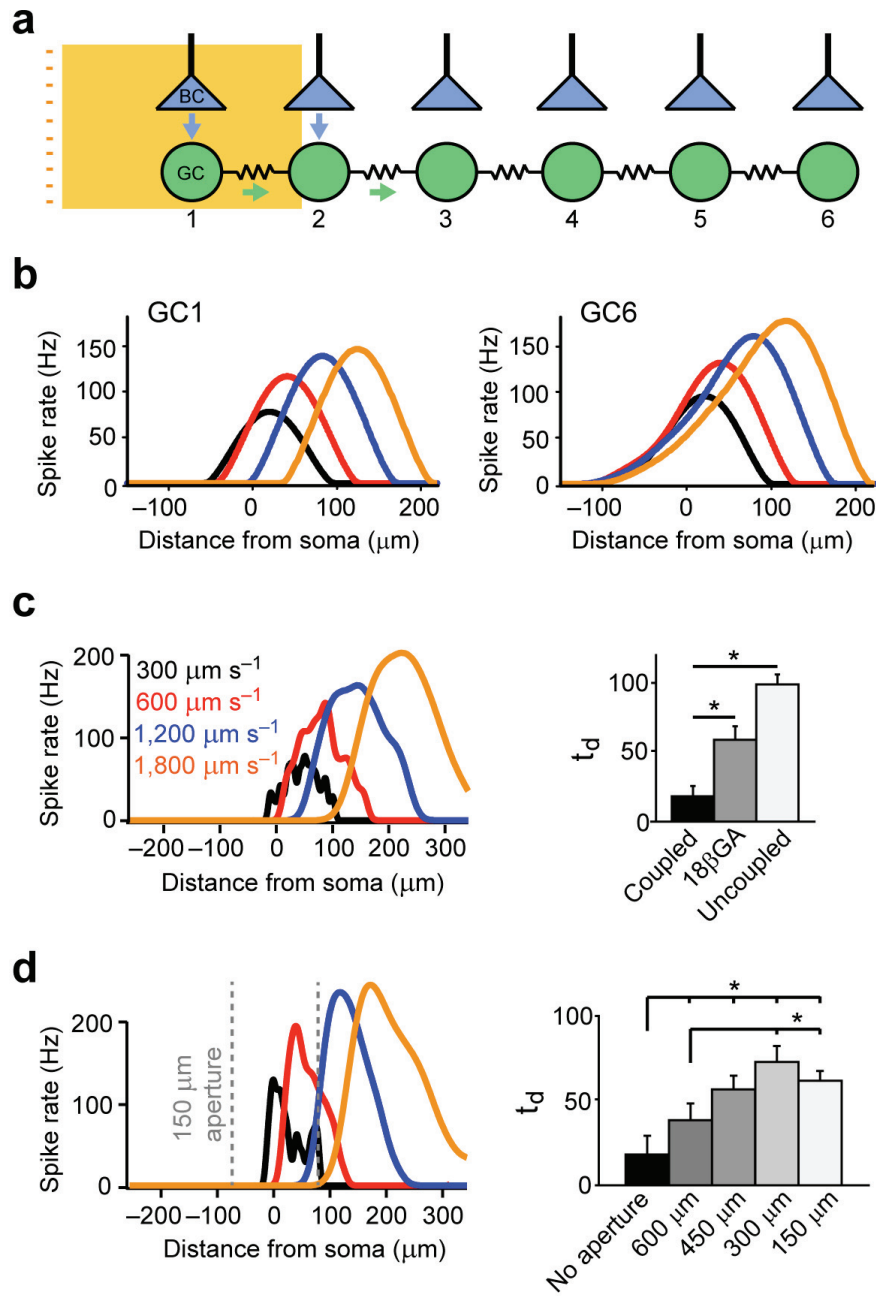


Figure 3.3. Serial interactions between multiple electrically-coupled DSGCs are required for lag normalization. **A**, Model schematic: an array of coupled ganglion cells (GC) is stimulated by feed-forward currents $J_n(t)$ from bipolar cells (BC) with experimentally measured Gaussian receptive fields, and velocity-dependent response amplitudes $g(v)$. The total current into the n th ganglion cell (I_n) is the sum of the BC input and scaled gap junction input from the preceding GC:

$$I_n(t) = J_n(t) + e^{-\beta} I_{n-1}(t) = \sum_{m=1}^n e^{-\beta(n-m)} J_m(t) \text{ with } \beta > 0$$

(the last equation is obtained by iterating the second equation). Gap junctions were made rectifying to approximate suppressive gain control and offset inhibition (Methods). Analytically, gap junction coupling causes downstream coupled cells to spike when the stimulus edge location is shifted relative to the uncoupled cell by an amount proportional to $-(1/\beta) \ln[g(v)/C]$ where C is the threshold for firing (Methods). Lag normalization in this model is thus tuned by the gap junction coupling $e^{-\beta}$ which compounds the effects of the velocity dependent response amplitude $g(v)$. **B**, Numerical model simulation with different stimulus velocities and gap junction coupling chosen to best fit the data (details in Methods). A model cell with no upstream neighbours (GC1) shows no lag normalization (*left*) while the sixth cell down the chain (GC6) shows lag normalized responses with skewed waveforms (*right*). **C**, Lag normalization measured experimentally was inhibited by application of the gap junction antagonist 18β GA (25 μ M; $P = 0.017$; $n = 4$). The average apparent delay (t_d : defined in **Figure 3.1**) is plotted in control conditions, in the presence of 18β GA and for uncoupled DSGCs ($t_d = 0$ indicates perfect lag normalization). **D**, Lag normalization, but not response amplitude, is reduced when stimuli are presented through a 150 μ m aperture to restrict movement over the dendritic field of the DSGC. The apparent delay (t_d) is plotted as a function of the diameter of the aperture (*right*). * $P < 0.05$ for the indicated pairwise comparisons. Error bars indicate s.e.m.

Discussion

Here we have described a remarkable retinal circuit that uses gap junction coupling between neighbouring upward coding DSGCs to correct for velocity-dependent spatial response lags that arise from processing delays. Lag normalization arises when each cell in a chain of electrically coupled cells primes its downstream neighbours to fire earlier, partly by exploiting and amplifying the velocity-dependence of the single cell response dynamics. This surprising new collective phenomenon could also be implemented in other specialized ganglion cells (Bloomfield and Volgyi, 2009, Volgyi et al., 2009; **Supplementary Figure 3.4**) or even in other sensory circuits that need to compensate for neural delays.

Methods

All procedures were performed in accordance with the CACR and approved by the University of Victoria's Animal Care Committee and carried out in adult wt (C57/Bl6) and Hb9::eGFP⁺ transgenic mice, similar to what we have previously described (Trenholm et al., 2011). Animals were dark adapted for 30 minutes prior to being sacrificed and retinas were dissected using IR goggles. All reagents were purchased from Sigma-Aldrich Canada Ltd. (Oakville, Ontario, Canada) unless otherwise noted.

Physiological Recordings

Extracellular spike recordings were made in cell-attached patch clamp configuration using 5-10 M Ω electrodes filled with Ringer's solution. Voltage-clamp whole-cell recordings were made using 4-7 M Ω electrodes containing (in mM): 112.5 CH₃CsO₃S, 9.7 MgSO₄, 10 EGTA, 10 HEPES, 4 ATP-Mg₂, 0.5 GTP-Na₃, 5 QX-314, 7.75 Neurobiotin (Vector Labs, Burlingame, CA) and 0.25 Alexa 594 (Invitrogen, Burlington, Ontario, Canada). The pH was adjusted to 7.4 with CsOH. The reversal potential for chloride (E_{Cl^-}) was calculated to be near -70 mV. The junction potential for the intracellular solution was ~10 mV and was left uncorrected. Recordings were made with a MultiClamp 700B amplifier (Molecular Devices, Sunnyvale, CA, USA). Signals were digitized at 10 kHz using a BNC-2090A A/D board (National Instruments, Austin, TX, USA) and acquired using custom software written in LabVIEW (Dr. David Balya, Friedrich Meischer Institute, Switzerland). GFP⁺ neurons in the Hb9::eGFP transgenic retina were visually targeted using 2-photon laser scanning microscopy (950 nm). GFP⁺ DSGCs were identified by their soma size and directionally selective response properties. Dendritic morphologies were imaged at 850 nm after individual neurons were loaded with Alexa 594. Dendritic morphologies were reconstructed and analyzed in Image J (rsbweb.nih.gov/ij/). Dendritic profiles (**Figure 3.1**) were estimated by measuring the total fluorescence after collapsing the entire image in the axis perpendicular to that of the moving stimulus.

Light Stimulus

Light stimuli were presented with a DLP projector (Hitachi Cpx1; refresh rate 75Hz) and controlled with custom software. The ambient background intensity, as measured with a calibrated spectrophotometer (USB2000; Ocean Optics, Dunedin, FL, USA) was 3×10^{12} photons $\text{s}^{-1} \text{cm}^{-2}$ (sampled at 500 nm), which is equivalent to 400 photoisomerizations $\text{cone}^{-1} \text{s}^{-1}$. Light stimuli were projected from below the specimen and were focused on the outer segments of the photoreceptors using the sub-stage condenser. The preferred direction for DSGCs was calculated after presenting stimuli in eight directions over each cell. We found that lag normalization was most robust after adapting the retinal preparation for 30 minutes with constant light (400 photoisomerizations $\text{cone}^{-1} \text{s}^{-1}$) prior to physiological recordings, which may result from increased ganglion cell coupling (Hu et al., 2010).

Analysis of Physiological Data

The spike rate was estimated by low-pass filtering the spike train via convolution with a Gaussian kernel with a fixed width, $\sigma = 25\text{ms}$. The skewed response waveform of coupled DSGCs remained largely constant as σ was varied between 5 and 50 ms, indicating that filtering methods did not introduce biases in the spike rate measurements (**Supplementary Figure 3.3**). To depict where spikes are registered in space, spike rates are plotted as a function of the position of the leading edge of the stimulus. All spiking data represent averages of 2-4 trials (unless otherwise indicated). Skewness for the ON response spike waveforms was computed as the third moment divided by the second moment raised to the $3/2$ power. Negative values correspond to leftward skew. Comparisons between groups were made with t-tests. Comparisons made in recordings from the same cell before and after applying pharmacological agents were made using paired t-tests. For data that failed normality tests, we used the Mann-Whitney Rank Sum test instead of t-tests and the Signed Rank test instead of paired t-tests. Data are presented as mean \pm s.e.m.

Model of DSGC Network

To understand how the network of coupled DSGCs collectively works to normalize spatial lag, we constructed a simplified computational model with a linear array of ganglion cells ($GC_1, GC_2 \dots GC_n \dots$) spaced $\Delta = 75 \mu\text{m}$ apart (reflecting the approximate spacing of cells (Trenholm et al., 2011)). The current input into the n th ganglion cell (I_n) was taken to be

$$I_n(t) = J_n(t) + \alpha I_{n-1}(t) \quad (1)$$

where J_n is the feedforward input from the bipolar cells, I_{n-1} is the current in the preceding ganglion cell in the array, and α is a parameter reflecting the net strength of gap junction coupling between cells $n-1$ and n . The proportionality constant $0 < \alpha < 1$ is the only free parameter and captures the effective strength of the ensemble of gap junctions that couple a pair of cells (**Figure 3.3** defines $\alpha = e^{-\beta}$). Our data (**Figure 3.1C; Supplementary Figure 3.3**) showed that coupled DSGC responses were skewed towards the side from which the stimulus was approaching, suggesting that downstream cells were not as effective in driving spikes in upstream cells, likely reflecting offset inhibition and suppressive gain control. For example, offset inhibition implies that the inhibitory input to a DSGC will overlap with excitatory gap junction input from downstream cells, suppressing the priming effect provided by the latter. We modeled this effect approximately by allowing current in cell $i-1$ to contribute to the current in cell i (weighted by the effective coupling α), while the cell $i+1$ did not influence the current in cell i (i.e., offset inhibition and suppressive gain control are taken to entirely suppress the effects of possible priming signals from downstream cells). To keep the model simple we also neglected time delays in gap junction transmission.

Iterating Eq. 1 gives an equation relating the current in cell n to the bipolar cell input channeled through the previous ganglion cells in the array:

$$I_n(t) = \sum_{m=1}^n \alpha^{n-m} J_m(t) \quad (2)$$

We estimated the spatial receptive field giving rise to the excitatory currents J_m by fitting EPSCs experimentally measured in uncoupled DSGCs as a function of bar position

(data not shown) with a Gaussian (standard deviation $\delta = 58.5 \mu\text{m}$). The velocity dependent maximum amplitude $g(v)$ of the current J_m was taken directly from measurements in uncoupled cells (data not shown). Thus, when a bar with a trajectory $x(t) = v t$ moved over our model network of DSGCs, the bipolar input to the m th ganglion cell was described by

$$J_m(t) = g(v) \exp\left[-\frac{(x(t-\tau) - m\Delta)^2}{2\delta^2}\right] \quad (3)$$

where $g(v)$ is the measured velocity dependent response amplitude, $x(t) = v t$ is the stimulus edge trajectory, $\tau \sim 70 \text{ ms}$ is a fixed transmission delay between the retinal input and the ganglion cells (reflecting a typical effective delay in uncoupled cells), $\Delta = 75 \mu\text{m}$ is the spacing between neighboring ganglion cells, and $\delta = 58.5 \mu\text{m}$ is the measured standard deviation of the receptive field.

The sum in Eq. 2 can be evaluated numerically and passed through a spike generator (see details below and **Figure 3.3**), but it is insightful to first carry out an approximate analytic calculation to determine the qualitative features of the model. To do so, we observe that since Eq. 2 is a sum of Gaussians multiplied by a decaying exponential it will be dominated by the largest term in the sum, provided that the standard deviation δ and the coupling α are relatively small. We can find the largest term by differentiating the summands $\alpha^{n-m} J_m$ with respect to m and requiring the derivative to equal zero. This determines the index of the largest summand to be

$$m^* = \frac{\beta\delta^2}{\Delta^2} + \frac{x(t-\tau)}{\Delta} \quad (4)$$

where we have defined the logarithm of the coupling $\beta = -\ln \alpha$. More precisely, the index of the largest summand is the integer closest to m^* . This treatment applies when the coupling α is large enough; otherwise $m^* = n$. Note also that $\beta > 0$ since $0 < \alpha < 1$. Thus, in this approximation we write

$$I_n(t) \approx \alpha^{n-m^*} J_{m^*}(t) \quad (5)$$

To find the position of the stimulus when the n th ganglion cell begins spiking we then set $I_n(t) = C$ where C is the current threshold for spiking. Solving the equation $I_n(t) = C$ within our approximation determines that the n th DSGC in our model array starts spiking when the stimulus edge is at a location x^* determined by

$$x^* - n\Delta = v\tau - \frac{\Delta}{\beta} \ln\left(\frac{g(v)}{C}\right) - \frac{\beta\delta^2}{2\Delta} \quad (6)$$

The left hand side of Eq. 6 gives the position of the stimulus relative to the receptive field center of the n th ganglion cell. The first term on the right hand side (RHS), $v\tau$, is a velocity dependent spatial lag that arises from the fixed time delay τ due to slow signal transduction. The third term on the RHS, $K = \beta\delta^2/2\Delta$, gives a velocity-independent shift. The second term on the RHS provides a velocity-dependent shift, and is manifestly negative since $\beta > 0$ and $g(v) > C$ given the existence of a spiking response. Thus, within a range of velocities for which $g(v) \sim \exp(\gamma v)$ the gap junction coupling $\beta = -\ln \alpha$ can be tuned to cancel the term $v\tau$ and thus achieve perfect lag normalization. Of course, in detail $g(v)$ cannot be exponential and saturates at high velocities. We observed from **Figure 3.1** that the spatial lag is almost perfectly normalized for the first and third of the tested velocities (300 $\mu\text{m/s}$ and 1200 $\mu\text{m/s}$). If we consider the $g(v)$ for these two velocities as being fit by an exponential, our model predicts *over*-compensation of the lag at intermediate velocities (because of the super-exponential values of $g(v)$) and *under*-compensation at high velocities (due to sub-exponential growth of $g(v)$). Precisely this pattern is seen in our data.

To more fully capture lag normalization in our model, and to correctly reproduce any constant shifts in the location of the stimulus which first evokes responses, we numerically summed Eq. 2 to determine the input current into the n th cell in the array. Spike rates were calculated by passing the input current through a threshold linear rectifier. That is, when input current was below the threshold $C=100\text{pA}$, the spike rate was zero. Above threshold, the spike rate was taken to increase linearly with input current with a proportionality coefficient of 0.7. The spike rate parameters were set to best reproduce the response amplitudes of uncoupled ganglion cells in our data for a

range of stimulus velocities. This simple model captures the essential features of lag normalization as seen in our data.

To further refine our model we added dynamic gain control $g(t)$ to the gap junction synapses in the model network. Gap junction signals were exponentially filtered and then passed through a sigmoidal nonlinearity to arrive at a multiplicative gain factor, which was applied to subsequent gap junction input. Briefly, the dynamics was described by the equation (Shapley and Victor, 1978, Berry et al., 1999)

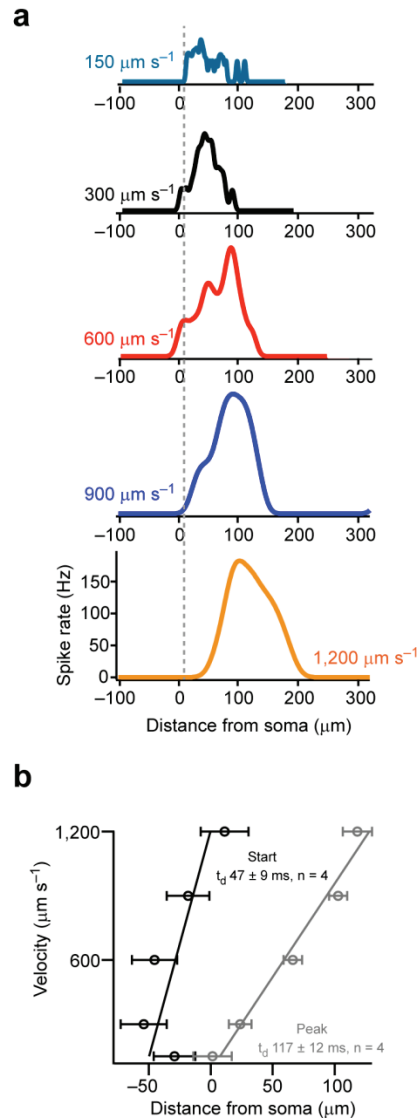
$$\frac{dg_n(t)}{dt} = -\frac{1}{\tau_g} g_n(t) + \lambda I_n(t) \quad (7)$$

where the constants $\tau_g = 17\text{ms}$, $\lambda = 0.0002$ were selected to obtain best fit the experimentally observed peak firing rates of coupled DSGCs, and the subscript n refers to the n th cell. The sigmoidal non-linearity is described by replacing the static coupling α by

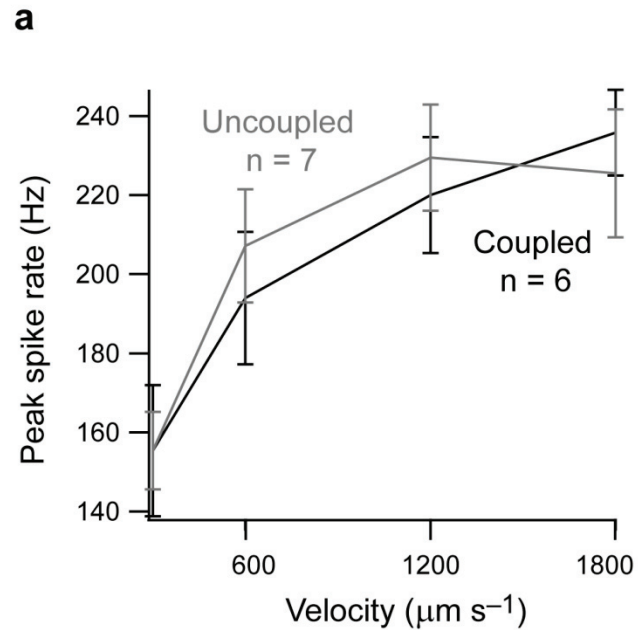
$$\alpha^*(t) = \alpha \frac{K^4}{K^4 + g_n(t)^4} \quad (8)$$

with $K = 3.5$. The coupling strength $\alpha = 0.63$ was fit to best reproduce the experimental spike onset locations, x^* , of coupled cells. The model required an array of ~ 5 cells to establish a stable response profile, similar to what was observed in our masking experiments (**Figure 3.3**). In addition to reproducing lag normalization, the model with gain control also correctly predicted the spatial offset (i.e. skewness) in the response and is included in the text (**Figure 3.3**).

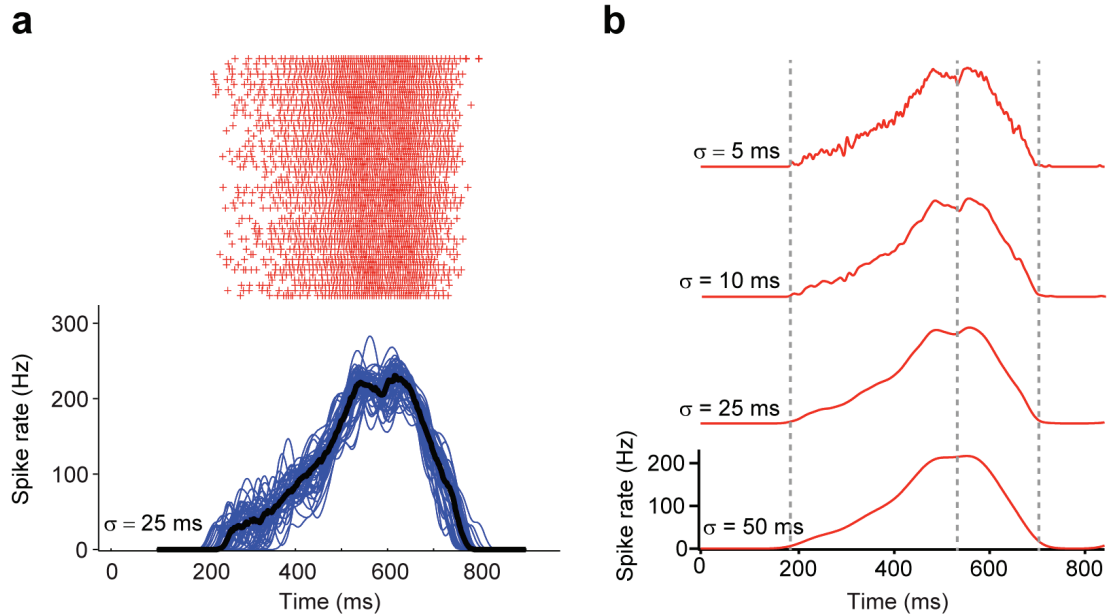
Supplementary Material



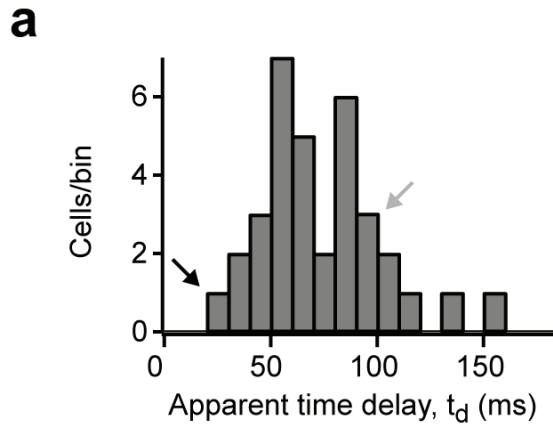
Supplementary Figure 3.1. Responses to negative contrast stimuli are lag normalized. **A**, Spike rate in a coupled DSGC plotted as a function of bar position for negative contrast stimuli (96% Weber contrast black bars on a white background) moving in the preferred direction at the indicated velocities. Only the leading edge (OFF) responses have been illustrated. **B**, The position of the stimulus edge at the time the first spike (*black*) and peak spiking response (*grey*) are plotted as a function of stimulus velocity. The inverse slope provides an estimate of the apparent time delay (t_d), which largely accounts for the spatial lag of the peak responses.



Supplementary Figure 3.2. Coupled and uncoupled ON-OFF DSGCs show similar velocity tuning. A, The average peak spike rate, evoked by preferred direction moving stimuli in uncoupled (*grey*) and coupled (*black*) ON-OFF DSGCs, increases as a function of velocity. Error bars indicate s.e.m.



Supplementary Figure 3.3. Spiking responses in a coupled DSGC are consistent over many trials and are not biased by filtering. **A** (*top*), Raster plot of spike trains showing responses to 50 consecutive trials of a moving stimulus (a $300 \times 300 \mu\text{m}$ bar moving in the preferred direction at $600 \mu\text{m/s}$). **A** (*bottom*), The temporal waveform of the response estimated by low-pass filtering the spike train through convolution with a Gaussian kernel with a fixed width ($\sigma = 25$ ms) for each of the 50 trials (*blue*) and the average response (*black*). **B**, The shape of the response waveform is not significantly affected when the standard deviation of the Gaussian kernel is varied over a 10-fold range ($\sigma = 5$ - 50 ms).



Supplementary Figure 3.4. Lag normalization in non-DS retinal ganglion cells. **A**, A histogram showing the spread of apparent time delays (i.e. the time from light falling on photoreceptors until the initiation of ganglion cells spiking, as measured from the inverse slope of the velocity/distance curves (see **Figure 3.1** for details)) for 35 non-DS ganglion cells. The black and grey arrows indicate where the apparent time delays for coupled and uncoupled ON-OFF DSGCs, respectively, would appear on the histogram. It should be noted that while our main experimental results only show lag normalization in a population of DSGCs that exhibit exclusively *homologous* gap junction coupling (i.e. coupling that occurs between the same type of DSGC and not with amacrine cells), amongst the non-DS ganglion cells, very few ganglion cell types exhibit only homologous coupling. Most ganglion cells also tend to be coupled to amacrine cells (others are exclusively coupled to amacrine cells). Thus, we do not necessarily expect lag normalization of the sort that we report to be a widespread phenomenon. Nevertheless, the results above show that the average apparent time delay (t_d ; see main text for definition) for these cells to be 77 ± 6 ms, with the shortest (most lag normalized) delay being 23 ms and the longest delay being 152 ms. The t_d of 18ms observed in coupled ON-OFF DSGCs falls in the low range of these values and the t_d of 99 ms for uncoupled ON-OFF DSGCs fall closer to the higher values. These results indicate that coupled DSGCs are among the best retinal ganglion cells at lag normalizing and most other ganglion cells cannot perform this task. One of the non-DS ganglion cells that appeared to have lag normalizing response (t_d of 23ms) was a sustained ON ganglion cell that had a large soma ($20.8 \mu\text{m}$ diameter) and dendritic field ($287 \mu\text{m}$). All ON ganglion cells with similar morphological characteristics have been shown to exhibit electrical coupling to other ganglion and/or amacrine cells. However, further studies using a targeted approach will reveal whether similar mechanisms underlie lag normalization in non-DS ganglion cells.

Chapter 4: Dynamic Modulation of Gap Junction-Mediated Anticipatory Signals in a Network of Directionally Selective Retinal Neurons

Abstract

Recently, we found that superior-coding ON-OFF directionally selective ganglion cells (DSGCs), labelled in the Hb9::eGFP transgenic mouse retina, anticipate moving stimuli. Here, we demonstrate that this DSGC population exhibits weak gap junction coupling that provides a substrate for extensive subthreshold excitatory receptive fields. However, in response to moving stimuli, sequential activation of electrical and chemical synapses effectively recruit these subthreshold regions, allowing coupled cells to anticipate moving stimuli. Surprisingly, these lateral excitatory signals appeared to functionally rectify (i.e. upstream DSGCs primed downstream cells, but not vice versa), producing skewed responses. This was not due to voltage-dependent inactivation of the gap junction conductance itself, but instead arose from activity-dependent postsynaptic depression that rendered downstream gap junction signals ineffective. Thus, dynamic interactions between electrical and chemical synapses and intrinsic membrane properties allow the network of DSGCs to propagate anticipatory responses along their preferred direction without promoting runaway excitation.

Publication Information

This chapter is from a recently submitted, unpublished manuscript: **Trenholm S** and **Awatramani GB**. Dynamic modulation of gap junction-mediated anticipatory signals in a network of directionally selective retinal neurons. Submitted to *Neuron*, December 2012. All experiments were performed and analyzed by ST and were designed by ST and GBA. The paper was written by ST and GBA.

Introduction

Neural signals mediated by chemical and electrical synapses are intimately linked (Vervaeke et al., 2012), but their interactions during natural patterns of activity have rarely been investigated. Similar to chemical synapses, electrical signals mediated by gap junctions are subject to various forms of activity-dependent regulation and plasticity (reviewed by Pereda et al., 2012) that may control signal spread through neural networks. Activity can modify either the properties of the gap junctions themselves (Zsiros and Maccaferri, 2008, Kothmann et al., 2012) or modulate the efficacy of electrical signalling indirectly, through changes in membrane properties (Llinas et al., 1974, Mann-Metzer and Yarom, 1999, Curti et al., 2012, Trenholm et al., 2012). However, to date most gap junction studies have used *in-vitro* preparations where natural patterns of activity are not preserved. Thus, the dynamics of hybrid chemical-electrical signalling in specific neural computations have not been fully explored.

To this end, here we put forward retinal ON-OFF directionally selective ganglion cells (DSGCs) as a model system for studying interactions between electrical and chemical synapses. ON-OFF DSGCs consist of four subtypes, each of which preferentially responds to stimuli moving in a particular cardinal direction (Oyster and Barlow, 1967). Preferred direction stimuli trigger glutamatergic excitation followed by GABAergic inhibition from arrays of bipolar and spatially offset starburst amacrine cells, respectively (Fried et al., 2002, Vaney and Taylor, 2002, Lee et al., 2010, Wei et al., 2011, Yonehara et al., 2011). Stimuli moving in the opposite, or null direction evoke inhibition that precedes excitation, vetoing spiking responses (Borst and Euler, 2011, Vaney et al., 2012). In addition, a subset of ON-OFF DSGCs are electrically coupled (Vaney, 1994, Weng et al., 2005), and the recent identification of genetic markers labelling distinct populations of ON-OFF DSGCs (Huberman et al., 2009, Kay et al., 2011, Trenholm et al., 2011) allows for a targeted approach towards studying their function. By comparing activity in coupled and uncoupled cells possessing similar and clearly defined spatiotemporal patterns of chemical synaptic inputs, a clear assessment of gap junction function during specific neural computations, such as directional coding, can be undertaken.

Recently, we reported that superior coding ON-OFF DSGCs, identified in the Hb9::eGFP transgenic retina, use a combination of chemical and electrical synapses to normalize spatial lags arising from transmission delays (i.e. they can detect moving edges at a constant retinal location regardless of stimulus velocity; Trenholm et al., in press). This remarkable computation requires strong gap junction-mediated priming signals from upstream ganglion cells. However, exactly how gap junctions can provide powerful lateral excitation, and what impact these signals have on receptive field structure remain unclear. In other coupled ganglion cells, some studies have reported that gap junction inputs are strong enough to drive synchronous spike activity in coupled neighbours (Mastrorade, 1983, Brivanlou et al., 1998, Hu and Bloomfield, 2003), while other studies suggest that gap junction signals are weak compared to chemical synaptic inputs and contribute little to spike synchrony (Trong and Rieke, 2008). One possibility is that specific interactions with chemical synapses are required for effective gap junction communication, and as such, roles for gap junctions might only be revealed under specific stimulus conditions.

A second unusual property of coupled DSGCs that we recently described was that their anticipatory priming signals appear to dynamically rectify during responses to moving stimuli, such that upstream ganglion cells primed responses of downstream DSGCs, but not the other way around. Indeed, models incorporating rectification provide a reasonable description of lag normalization (Trenholm et al., in press). Without rectification, excitation can be continually passed through re-entrant loops resulting in network oscillations (Manor et al., 1997, Trenholm et al., 2012). Interestingly, gap junctions between DSGCs are thought to express connexin 45 (Schubert et al., 2005, Pan et al., 2010), which are known to exhibit a strong voltage dependence in expression systems (Moreno et al., 1995, Barrio et al., 1997). This raises the possibility that the gap junction conductance is dynamically modulated as stimuli move across the receptive fields of coupled DSGCs. However, to date, the properties of connexin 45-containing electrical synapses have not been probed under physiological conditions, and it is unclear whether they would exhibit strong voltage dependence in intact neurons. Alternatively, postsynaptic mechanisms including GABAergic inhibition or postsynaptic gain control mechanisms could also serve to control the effectiveness of gap junction signalling.

To understand how gap junction signals are dynamically regulated during response to moving stimuli, we first characterized the properties of gap junctions in superior coding DSGCs (which we demonstrate to be the only coupled population of ON-OFF DSGC). We find that coupling gives rise to extensive excitatory subthreshold receptive fields (when probed with spot stimuli) that can be effectively converted to suprathreshold regions by moving stimuli. The effectiveness of gap junction signalling is sensitive to activity-dependent postsynaptic gain control mechanisms, which promotes the unidirectional spread of lateral signals through the electrically coupled network. Together, these results demonstrate how interactions between electrical synapses, chemical synapses and intrinsic adaptation mechanisms contribute to the anticipatory responses of DSGCs.

Results

Reciprocal Gap Junction Coupling in Superior Coding DSGCs

In the rabbit retina, ~40% of ON-OFF DSGCs are homologously tracer coupled (Vaney, 1994). However, since tracer coupling methods have never been combined with functional analysis, it remains unclear whether coupling occurs within single or multiple populations of DSGCs. Here, we use a combination of tracer coupling methods, mouse genetics and physiological recordings to demonstrate that superior coding DSGCs are the only strongly electrically coupled population of ON-OFF DSGC in the mouse retina.

Loading individual GFP⁺ DSGCs (**Figure 4.1A, left**) in the Hb9::eGFP transgenic retina (Trenholm et al., 2011), with the gap junction permeable tracer Neurobiotin not only revealed the dendritic arborisations of the injected ganglion cell, but also lead to robust labeling of somata of neighbouring ganglion cells (**Figure 4.1A, middle**). Tracer coupling was only present in other GFP⁺ cells (**Figure 4.1A, right**), demonstrating that superior coding DSGCs were homologously tracer coupled. On average, GFP⁺ DSGCs were tracer coupled to 7.4 ± 0.7 neighbouring DSGCs (n = 5/5). We saw no evidence of heterologous tracer coupling to amacrine cells or other ganglion cell types. Both the morphological and coupling patterns of GFP⁺ DSGCs bore similarities to the coupled

putative ON-OFF DSGCs from Schubert et al. (2005). In contrast, Neurobiotin labeling of GFP⁻ DSGCs showed no significant coupling to neighbouring ganglion or amacrine cells (7/7; **Figure 4.1B**).

While Neurobiotin labeling confirms the presence of gap junction coupling between superior coding DSGCs, the absence of tracer coupling in other populations does not conclusively demonstrate that these cells were not coupled. As an alternate method, we assessed coupling in the live retinal preparation by testing the ability of DSGCs to drive reciprocal feedback spikelets. When superior coding DSGCs were voltage-clamped at depolarized potentials (+40 mV), fast inward currents which had an average peak amplitude of 21 ± 2 pA ($n = 6$) were observed (**Figure 4.1C-H**). These depolarization-induced spikelets were also apparent in superior coding ON-OFF DSGCs in the non-transgenic retina, indicating that they are not an artifact of transgenic GFP expression ($n = 4$; **Supplementary Figure 4.1**). Below, we present several lines of evidence demonstrating that spikelets arise from spike activity in neighbouring coupled cells, triggered as the command voltage spreads through gap junctions.

First, spikelets exhibited a clear threshold ~ 0 mV (i.e. a 60 mV depolarization), indicating that only a small fraction of the depolarizing current spread into neighbouring Hb9⁺ ganglion cells. The frequency of spikelets increased proportionally with the level of depolarization of the voltage-clamped cell (**Figure 4.1C,F**; $n = 6$). Second, consistent with a gap junction origin, spikelets did not exhibit a reversal potential and remained inward even at a holding potential of +40 mV, a potential where excitatory chemical synaptic currents are expected to be reversed (**Figure 4.1C**; **Supplementary Figure 4.2**). Third, blocking action potentials with the voltage-gated Na⁺ channel blocker TTX (1 μ M) completely abolished spikelets (**Figure 4.1D**; $n = 4$). The actions of TTX were likely mediated through blocking action potentials of neighbouring coupled DSGCs, since a Na⁺ channel blocker (QX-314; 5mM) was included in the intracellular recording solution. Fourth, application of the gap junction blocker 18 β -glycyrrhetic acid (18 β GA, 25 μ M) also abolished depolarization induced spikelets (**Figure 4.1E**; $n = 5$), while it did not block light driven spiking responses in neighbouring coupled cells (see **Figure 4.5C**).

To directly demonstrate that spikelets arise from action potentials in neighbouring coupled DSGCs, we made paired recordings from adjacent Hb9⁺ DSGCs and examined the temporal relationship between spikes and spikelets. In these experiments, capacitive spikes were measured in one cell in cell-attached mode, and currents were measured in a neighbouring cell in voltage-clamp mode (**Figure 4.1G**). When a GFP⁺ DSGC was voltage-clamped near -60 mV, its coupled neighbour was quiescent. However, when depolarized to +40 mV, a train of spikes was evoked in the neighbouring DSCG (**Figure 4.1G**; n = 10 pairs). In turn, every action potential in the train was followed by an inward spikelet in the voltage-clamped cell (**Figure 4.1G,H**; n = 10 pairs). Spike-triggered events, representing the average spikelet, exhibited a uniform waveform (**Figure 4.1I**). Moreover, the derivative of the average spikelet current allowed for a direct comparison of the spikelet waveform to the capacitive spike waveform (**Figure 4.1I**) and revealed that spikelets peaked 0.44 ± 0.04 ms (n = 10) after the action potential in the pre-junctional cell, consistent with notion that spikelets arise from action potentials in neighbouring cells. However, every spikelet in the voltage-clamped cell was not preceded by an action potential in the neighbouring cell we were recording from (**Figure 4.1H**), suggesting that spikelets arise from multiple surrounding coupled ganglion cells.

In summary, we have shown that depolarization induced feedback spikelets arise from reciprocal coupling and provide a convenient way to determine whether DSGCs are electrically coupled in the live preparation. Interestingly, while depolarization-induced feedback spikelets were observed in every GFP⁺ DSGC tested (n = 20/20), they were never observed in GFP⁻ DSGCs (**Figure 4.1C**; n = 0/17 comprising 4 dorsal coding, 2 nasal coding and 11 temporal coding ON-OFF DSGCs). These findings provide further evidence that superior coding DSGCs are the only strongly coupled population of ON-OFF DSGC in the adult mouse retina.

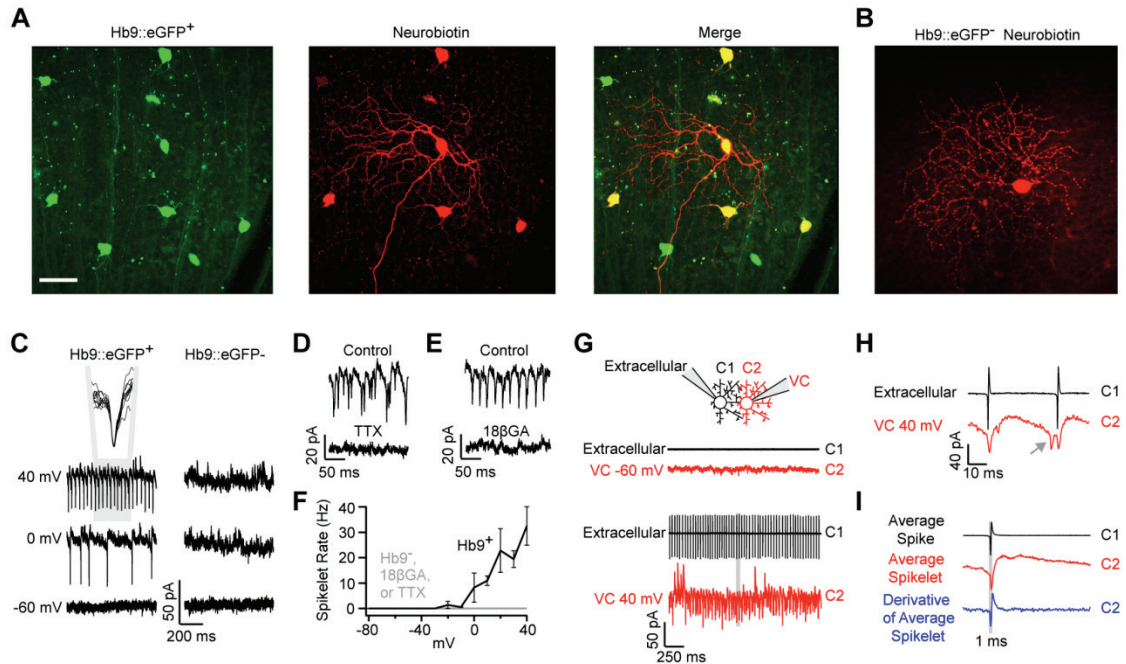


Figure 4.1. Superior coding Hb9::eGFP directionally selective ganglion cells are homologously tracer coupled and exhibit coupled spikelets. **A**, Injection of the gap junction permeable tracer Neurobiotin into a single GFP⁺ DSGC labelled in the Hb9::eGFP mouse retina (*green channel, left*) revealed the dendritic tree of the injected cell and also labelled several neighbouring somata (*red channel, middle*). Overlaying the red and green channels (*right*) revealed that Hb9⁺ DSGCs were exclusively coupled to other GFP⁺ DSGCs, indicating that coupling is homologous. On average, Hb9⁺ DSGCs were coupled to 7.4 ± 0.7 neighbouring DSGCs, but no other ganglion cells or amacrine cells ($n = 5/5$). **B**, Neurobiotin injection into an Hb9⁻ DSGC revealed the dendritic tree of the injected cell but did not label any neighbouring cells ($n = 7/7$). Scale bar = 50 μm . **C**, Fast inward currents (spikelets) are generated upon depolarizing Hb9⁺ (*left*), but not Hb9⁻ (*right*) ON-OFF DSGCs in voltage-clamp mode. The inset in (**C**) shows the overlay of 10 consecutive spikelets, indicating that spikelets exhibit a uniform size and waveform. Depolarization induced spikelets are blocked by application of the voltage gated Na⁺ channel blocker TTX (**D**; 1 μM) and by application of the gap junction blocker 18 β GA (**E**; 25 μM ; application > 10 minutes). **F**, Spikelet frequency increases as a function of depolarization. **G**, An example of a paired recording where activity in cell 1 (C1) was measured using the extracellular cell-attached technique while whole-cell voltage-clamping its neighbour (C2) near -60 mV (*top*) or +40 mV (*bottom*). **H**, A high-resolution view of the area highlighted in grey in (**G**), showing that spikelets (*red*) immediately follow action potentials (*black*). The grey arrow points to a spikelet that do not correspond to an action potential in C1, which likely arose from an action potential in another DSGC that is coupled to C2. **I**, The average spike in C1 (*black*), and spike triggered average current in C2 (*red*, $V_{\text{HOLD}} \sim 0$ mV) are plotted for the pair of cells shown in (**G**). The average prejunctional spike, postjunctional current and the derivative spikelet (*blue*) is illustrated.

Coupling is Weak and Symmetrical Along the Preferred-Null Axis

In line with previous studies in the retina (Mastrorarde, 1983, Hu and Bloomfield, 2003) the experiments outlined above clearly demonstrate that depolarizing a single coupled ganglion cell can effectively drive spiking activity in its neighbours. However, this required a relatively strong depolarization ($V_{\text{HOLD}} > 0$ mV) of the Cs⁺-filled DSGC, making it questionable whether gap junction signals from individual DSGCs could drive suprathreshold activity in neighbouring cells under physiological conditions. To directly test the extent to which responses in one cell drive neighbouring cells under more physiological conditions, we made whole-cell current-clamp recordings (with K⁺-gluconate in the pipette) from pairs of coupled DSGCs and examined how modulating the membrane potential of a single cell (the donor) affected the membrane potential of its neighbour (the acceptor). Furthermore, we selected cells that were aligned along the preferred-null (dorsal-ventral) axis to investigate potential directional asymmetries in gap junction signalling.

First, we measured the coupling strength of DSGCs by measuring responses to mild hyperpolarizing steps (-80 pA) so as to avoid the activation of non-linear conductances. Hyperpolarizing the donor resulted in a hyperpolarization of smaller amplitude in the acceptor (**Figure 4.2A**). The strength of coupling was measured by calculating a coupling coefficient (CC), defined as the fraction of the voltage deflection in the acceptor compared to that observed in the donor cell ($\Delta V_{\text{acceptor}}/\Delta V_{\text{donor}}$). Regardless of whether the donor was on the preferred or null side, the CC was similar (Preferred-Null CC = 0.14 ± 0.01 ; Null-Preferred CC = 0.13 ± 0.01 ; $P > 0.05$; $n = 11$ pairs). Plotting the CC measured in the preferred versus the null direction for each pair resulted in values that were fit by a line with a slope of 0.94 ± 0.07 , indicating that gap junction coupling was symmetrical (**Figure 4.2B**; $n = 11$ pairs).

Next, we tested whether spiking activity in an individual coupled neuron could drive suprathreshold activity in its coupled neighbours. Injecting large currents (up to 200 pA; to mimic bipolar cell input), triggered a train of action potentials (84 ± 4 Hz) riding a 13 ± 1 mV plateau depolarization in the donor cell, but never resulted in the generation of action potentials in the acceptor cell ($n = 12$ cells from 6 pairs; **Figure 4.2A**). Instead,

each action potential was highly attenuated and manifest as a spikelet in the soma of the neighbouring cell. Coupled spikelets appeared as low-pass filtered versions of the action potential, suggesting that gap junctions do not trigger non-linear conductances in the dendrites of DSGCs (Oesch et al., 2005). Together, these results indicate the coupling between DSGCs is symmetrical along the preferred-null axis, and that spike activity in one coupled cell results in subthreshold activity in its coupled neighbours.

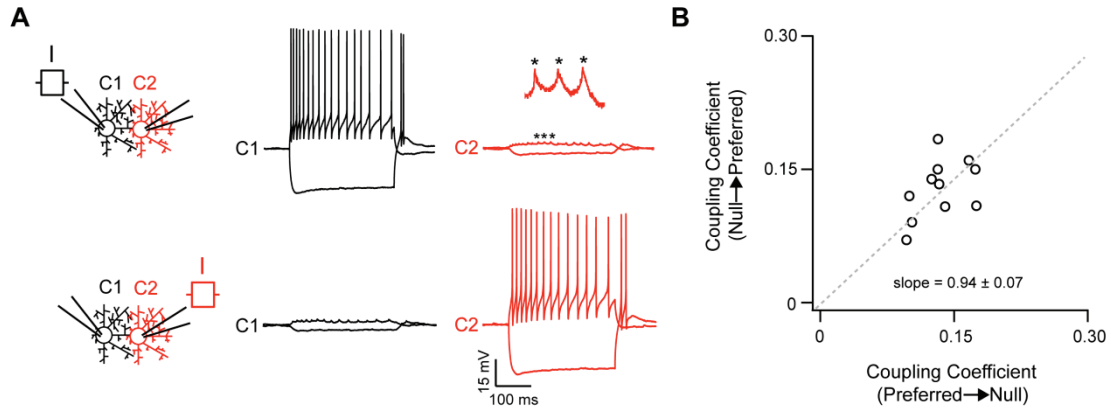


Figure 4.2. Reciprocal coupling between ON-OFF DSGCs is symmetrical and weak. **A**, Modulating the membrane potential by direct current injections into C1 (-200pA , $+120\text{pA}$, respectively) also drives weak voltage deflections in its coupled neighbour C2 (*top*). Similar results are obtained when current is injected into C2, indicating that coupling is reciprocal (*bottom*). The inset shows a magnified view of coupled spikelets (indicated by *) which closely follow action potentials in the prejunctional cell. **B**, A plot of the coupling coefficient (see text for definition) for preferred vs null directions for 11 coupled pairs. The grey dotted line represents the line of best fit, with a slope = 0.94 ± 0.07 , indicating that coupling is symmetrical along the preferred-null axis.

Consistent with the finding that gap junctions provide a conduit for current to spread to coupled DSGCs, we found that the input resistance for coupled DSGCs ($169 \pm 11\text{ M}\Omega$, $n = 11$) was significantly lower than for uncoupled DSGCs ($353 \pm 29\text{ M}\Omega$; $n = 14$; $P < 0.001$). Further evidence that this difference in input resistance was due to gap junctions came from the finding that application of $18\beta\text{GA}$ ($25\text{ }\mu\text{M}$) significantly increased the input resistance in coupled DSGCs by $100 \pm 36\text{ M}\Omega$ (**Supplementary Figure 4.3**; $n = 5$; $P < 0.05$) while it had no significant effect on the input resistance of uncoupled DSGCs (**Supplementary Figure 4.3**; $n = 4$; $P = 0.3$). It should be noted that

changes in input resistance occurred over several minutes (**Supplementary Figure 4.3**), consistent with the slow actions of gap junction blockers (Veruki and Hartveit, 2009, Trenholm et al., 2012).

Excitatory Subthreshold Receptive Fields of Coupled DSGCs

We next examined the impact of gap junctions on the spatial receptive fields of DSCGs. To do so, we first compared the size of classical receptive fields (cRF) of coupled and uncoupled DSCGs in relation to their dendritic arborizations, as previously described (Yang and Masland, 1994). cRFs were defined as the area over which a small spot stimuli (40 μm diameter, 96% Weber contrast) evoked spike activity. Dendritic arborizations were imaged immediately after the recordings using two-photon microscopy techniques (**Figure 4.3A**). We observed that the average ratio of the cRF to dendritic field was similar for both coupled and uncoupled DSCGs (Hb9⁺ RF:DF = 1.38 ± 0.09 for ON and 1.34 ± 0.07 for OFF, $n = 9$; Hb9⁻ RF:DF = 1.20 ± 0.08 for ON and 1.13 ± 0.05 for OFF, $n = 11$; $P > 0.05$). These results indicate that coupling does not significantly expand the cRF, consistent with previous studies on the OFF α -ganglion cells (Hu et al., 2010).

While the size of the cRFs of coupled DSCGs did not appear expanded, stimulating flanking regions (i.e. the surround) revealed the presence of excitatory subthreshold responses (**Figure 4.3C**). These subthreshold responses were small in amplitude (~ 0.25 -10 mV) and exhibited many spikelets, indicating that they were driven, at least partly, by gap junction inputs from neighbouring cells. Indeed, simultaneous measurements from pairs of coupled cells revealed that subthreshold spikelets were aligned with the spiking response in neighbouring cells (**Figure 4.3A,B**; $n = 7$ pairs). In addition, mildly depolarizing the membrane above $E_{\text{Cl-}}$ did not significantly affect excitatory subthreshold responses in the surround, indicating that these responses were not mediated by inhibition (**Supplementary Figure 4.4**). The average size of the excitatory subthreshold receptive field in GFP⁺ DSCGs was $36183 \pm 3350 \mu\text{m}^2$ ($n = 6$; **Figure 4.3C**), which corresponds to a region extending roughly 100 μm around the

periphery of the cRF (cRF diameter $\approx 200 \mu\text{m}$), consistent with the average spacing of Hb9^+ DSGCs ($\sim 100 \mu\text{m}$ apart; Trenholm et al., 2011), indicating that subthreshold receptive fields are the result of nearest neighbour interactions. In contrast, uncoupled GFP^- DSGCs exhibited significantly smaller subthreshold receptive fields compared to their GFP^+ counterparts (**Figure 4.3D**; $17986 \pm 2,594 \mu\text{m}^2$, $n = 5$; $P = 0.002$). Together, these results demonstrate that under physiological conditions, activity in individual DSGCs does not appear to be strong enough to drive suprathreshold activity in its coupled neighbours, but instead endows coupled DSGCs with large, silent *excitatory* surrounds.

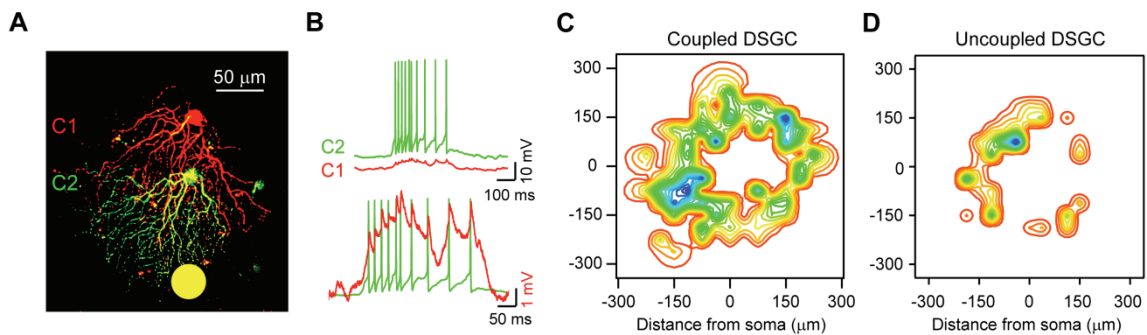


Figure 4.3. Coupled DSGCs have extensive excitatory subthreshold receptive fields. **A**, A 2-photon reconstruction showing two neighbouring Hb9^+ DSGCs loaded with Alexa 594 (red) and Alexa 488 (green). The location of the light flash ($40 \mu\text{m}$, 96% positive Weber contrast) whose responses are shown in **(B)** is indicated with the yellow spot. **B top**, The light responses of C1 and C2 are shown, to the light flash indicated in **(A)** that preferentially stimulated C2. **B bottom**, The responses of C1 and C2 are normalized to show that every spike in C2 drives a coupled spikelet in C1. **C**, A contour plot of the subthreshold receptive field (RF) of a coupled DSGC. **D**, Plots of the subthreshold RF for an uncoupled DSGC. For the subthreshold RFs, each concentric circle represents an increase of 0.5 mV , with the outermost circle representing 0.25 mV .

Gap Junction-Mediated Priming of DSGC Responses

While gap junction inputs on their own appeared to be ineffective in driving spike activity in neighbouring cells, we next investigated whether they could prime DSGCs by sensitizing weak bipolar cell inputs. To test this, we made paired current-clamp

recordings from adjacent coupled DSGCs (C1 and C2) and either 1) stimulated subthreshold bipolar cell inputs to C2 using low contrast light flashes (**Figure 4.4A, left**), 2) stimulated purely gap junction-mediated responses in C2 by directly injecting current pulses to C1 (100-150 ms pulse; 200-700 pA; **Figure 4.4A, middle**) or 3) triggered gap junction and bipolar cell inputs in quick succession (50 ms apart), to mimic sequential activity of DSGCs evoked by moving stimuli (**Figure 4.4A, right**). When presented alone, light-driven inputs and electrical inputs gave rise to subthreshold responses in C2 (**Figure 4.4A, left and middle**). However, when light-driven responses were preceded by gap junction inputs, they were effectively primed (**Figure 4.4A, right**). On average, gap junction input decreased the contrast required to generate a spike by $21 \pm 10 \%$ (**Figure 4.4B**; $n = 6$; $P = 0.031$). It is important to note that when the contrast of the spot was increased, the effect of priming by electrical synaptic input was less pronounced. These results suggest that activity in a single coupled ganglion cell can significantly affect responses in its neighbour when the neighbour is near spike threshold.

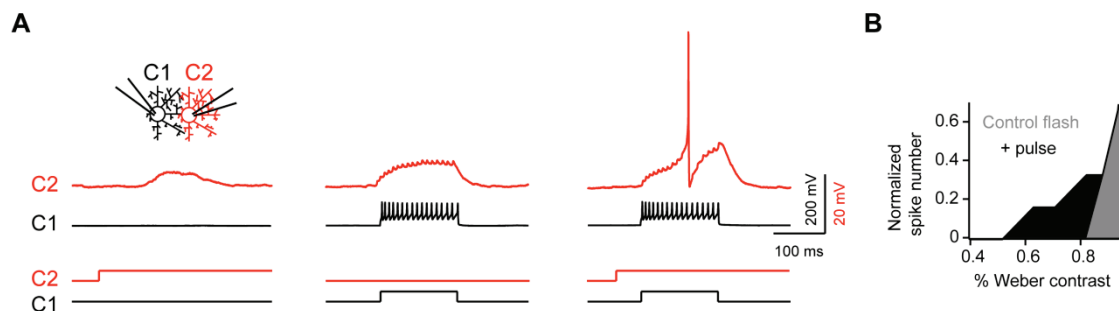


Figure 4.4. Lateral electrical signals boost weak light-evoked responses. A, A paired current-clamp recording from coupled neighbouring DSGCs (C1 & C2) illustrating responses to a low contrast light flash delivered to C2 (*left*), 400 pA current injection to C1 (*middle*) or to the same light flash and current injection delivered in quick succession. The timing of the current pulse to C1 was delayed ~ 50 ms from the onset of the flash, such that it preceded the light-evoked EPSP in C2 by ~ 50 ms (shown in the bottom panel: light stimuli red; current pulse in black). **B,** Priming by gap junction input was found to decrease the contrast required to drive spike activity by $21 \pm 10 \%$ (Weber contrast; $n = 6$; $P = 0.031$).

Next, to demonstrate that electrical priming was important during motion coding, we measured the spatial location where moving stimuli evoked spikes in relation to the cRF (as previously described). cRFs were mapped using static stimuli, and approximated along the preferred-null axis using a one dimensional Gaussian (**Figure 4.5A**; Rodieck, 1965). To estimate the region of retina that was associated with particular spikes stimulated during motion, we shifted responses to moving stimuli by the distance the stimulus travelled during the estimated transmission delay (see Methods). We found that for uncoupled DSCGs, the initial spikes to moving stimuli were generated at the edge of the cRF ($10 \pm 5 \mu\text{m}$ inside the cRF; $n = 7$; **Figure 4.5A**). In contrast, coupled DSGCs responded $100 \pm 25 \mu\text{m}$ outside of their cRFs (**Figure 4.5B**; $n = 6$), in a region that was defined as subthreshold when mapped with stationary spot stimuli (see **Figure 4.3**). It should also be noted that moving stimuli generate more sustained responses than static stimuli (**Supplementary Figure 4.5**), and thus electrical inputs to their neighbours are also likely to be stronger under this regime.

As further evidence that the initial responses arose from priming by lateral electrical signals, blocking gap junctions with $18\beta\text{GA}$ significantly delayed the onset of spiking by $97 \pm 10 \mu\text{m}$ ($n = 7$; **Figure 4.5C**), while only mildly reducing the peak firing rate ($21 \pm 7 \%$; $n = 7$). Thus, the sequential activation of electrical and chemical synapses by moving objects that stimulate the chain of coupled DSGCs appears to drive regions of the subthreshold receptive field past spike threshold.

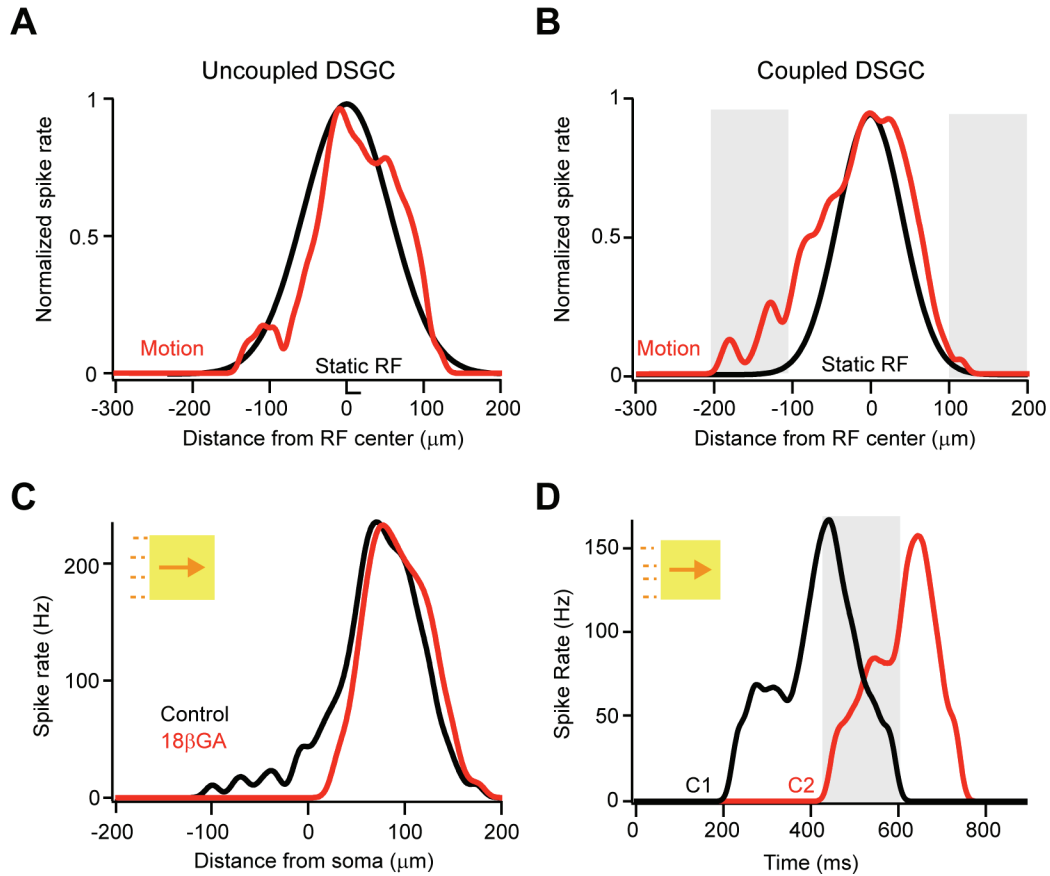


Figure 4.5. Moving stimuli evoke responses outside of the classical receptive field of coupled DSGCs. **A,B,** A Gaussian approximation of the classical receptive fields (mapped with a 40 μm spot) for an uncoupled (**A**) and coupled DSGC (**B**; black traces). The spiking response to a bar (300x300 μm bar; 96% Weber contrast) moving at 600 $\mu\text{m/s}$ in the preferred direction is plotted in relation to the edge of the stimulus (the leading edge of the stimulus is at the soma at 0 μm ; red traces). The response waveform of moving stimuli were shifted $\sim 36 \mu\text{m}$ to account for the distance the edge travelled during the $\sim 60 \text{ ms}$ processing delay time (see Methods). The approximate extent of the subthreshold receptive field is shaded in grey. **C,** Application of the gap junction blocker 18 βGA selectively affects the rising phase of the response of coupled DSGCs to moving stimuli. **D,** A paired extracellular recording from neighbouring coupled DSGCs reveals the window of coincident activity during moving stimuli, and shows how responses are skewed towards the leading edge of the moving stimulus.

Lateral Priming Signals Rectify During Responses to Moving Stimuli

Unlike the rising phase of the response to moving stimuli, the falling phase closely matched the shape of the cRF for both coupled and uncoupled types (**Figure**

4.5A,B; for both coupled and uncoupled, responses to moving stimuli terminated near the end of the cRF; $P = 0.7$; $n = 6$ coupled and 7 uncoupled DSGCs). This likely occurs due to a combination of factors including the transient nature of the DSGC's impulse response, as well as additional gain control mechanisms (Berry et al., 1999). Furthermore, since the initial rising but not the falling phase of responses in coupled DSCS were primed, the overall responses to moving stimuli were significantly skewed towards the leading edge of the stimulus. In contrast, responses for uncoupled DSCGs and were relatively symmetrical. The average skew index (SI; where a value of 1 indicates a symmetrical response, and values > 1 or < 1 indicate skew towards or away from the leading edge of the response, respectively; see Methods) for responses to bars moving at $600 \mu\text{m/s}$ in the preferred direction was 1.6 ± 0.1 for coupled DSGCs (**Figure 4.5D**; $n = 23$) and 1.1 ± 0.1 for uncoupled DSGCs (data not shown; $n = 8$; $P = 0.009$). Consistent with the hypothesis that electrical inputs only mildly contributed to the falling phase of the response, $18\beta\text{GA}$ had no significant effect on the spatial location where responses terminated ($2 \pm 5 \mu\text{m}$; **Figure 4.5C**; $P = 0.66$; $n = 7$). Since $18\beta\text{GA}$ blocked priming responses, the overall effect of blocking gap junctions was to significantly reduce response asymmetry (**Figure 4.5C**; control SI = 1.6 ± 0.1 ; $18\beta\text{GA}$ SI = 0.7 ± 0.1 ; $n = 7$; $P = 0.001$). Together, these results indicate that moving stimuli effectively promote gap junction mediated priming of threshold responses of coupled DSGCs, resulting in anticipatory responses. In contrast, gap junctions do not appear to boost the falling phase of the response to moving stimuli.

Why do gap junctions boost the leading but not falling phase of the response to moving stimuli? This suggested that upstream DSGCs effectively boost the leading edge of the response, but that downstream DSGCs fail to boost the response of the falling phase (note that upstream and downstream coupled cells are strongly active during the rising and falling phases of the response of a given DSGCs, respectively; **Figure 4.5D**). This finding is unexpected given the measured symmetry of the gap junction conductance between coupled DSGCs (see **Figure 4.2**). However, since ON-OFF DSGCs are putatively coupled with connexin 45 (Schubert et al., 2005, Pan et al., 2010) which are known to exhibit strong voltage-dependent properties in culture systems (Moreno et al., 1995, Barrio et al., 1997), we wondered whether the rectification of lateral signals arose

from activity-dependent inactivation of the gap junction conductance. To directly test this hypothesis, we made voltage-clamp recordings from pairs of coupled DSGCs and measured the voltage-dependence of the gap junction conductance (in the presence of TTX to block reciprocal feedback spikelet activity).

Applying brief voltage pulses in a DSGC cell (-120 mV to 0 mV, 0.2 to 1 s) from a holding potential of -60 mV, led to robust gap junction-mediated currents in its coupled neighbour (**Figure 4.6A,C**). As in the previous experiments, coupling was reciprocal (**Figure 4.6B**). However, in contrast to the expected behaviour of Cx45 gap junction based on previous studies (Moreno et al., 1995, Barrio et al., 1997), coupling currents in DSGCs scaled linearly over a wide range of voltages (± 60 mV; **Figure 4.6D**; $n = 4$). In addition, gap junction currents did not show any signs of inactivation during long periods of strong hyperpolarization or depolarization (1 s; **Figure 4.6C**). The gap junction conductance was measured to be 871 ± 31 pS ($n = 4$). Thus, these findings suggest that a voltage-dependent inactivation of the gap junction conductance is unlikely to play a significant role in dynamically shaping response waveforms. Thus the contextual rectification of priming signals that occurs during the response to moving stimuli must occur downstream of gap junctions.

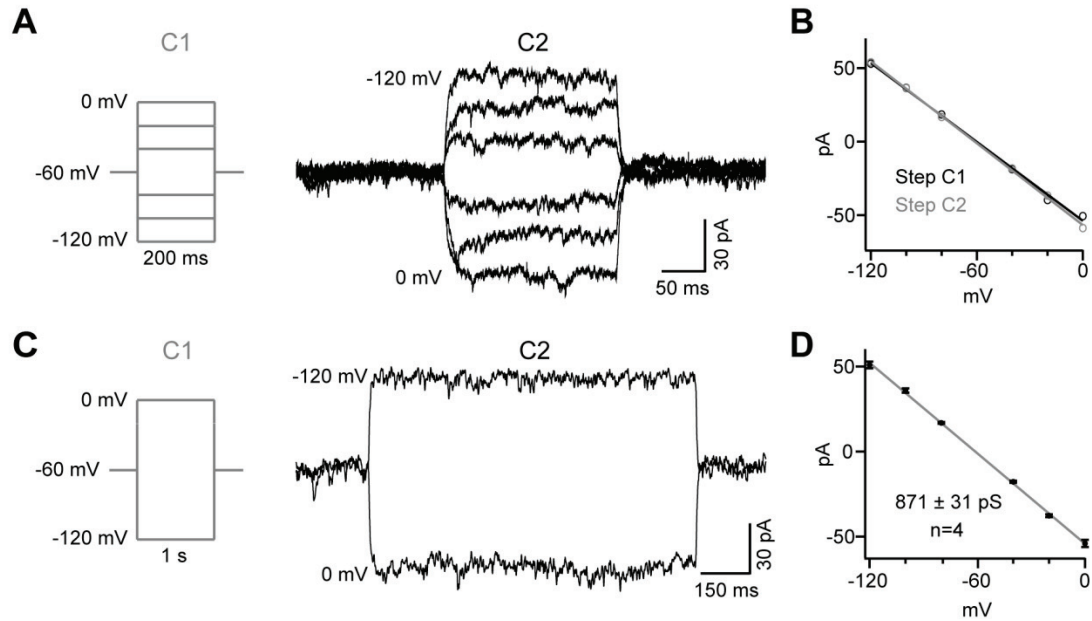


Figure 4.6. Gap junctions between ON-OFF DSGCs do not exhibit voltage-dependent inactivation. **A**, Paired voltage-clamp recording from neighbouring ganglion cells in which a series of voltage pulses are applied to C1 (*left, grey*) while activity in C2 is passively measured (*right, black*). **B**, Plotting the average current during the pulse in C2 as a function of the command voltage in C1 reveals a linear relationship (*black trace*), indicating gap junctions do not exhibit any voltage-dependent rectification. A similar curve is obtained when voltage pulses are applied to C2 and gap junction current is measured in C1 (*grey trace*). **C**, Longer voltage steps (1 s) show no signs of voltage-dependent inactivation. **D**, The average gap junction conductance (measured as slope of the I-V curve) was 871 ± 31 pS ($n = 4$).

Postsynaptic Gain Control Underlies Rectification

DSGCs are known to receive spatially offset postsynaptic inhibition from starburst amacrine cells (Fried et al., 2002, Vaney and Taylor, 2002, Lee et al., 2010, Wei et al., 2011, Yonehara et al., 2011). Indeed, inhibitory receptive fields of coupled DSGCs (**Supplementary Figure 4.6**; inhibitory currents were measured in cells voltage-clamped at ~ 0 mV) were offset from excitatory receptive fields (**Supplementary Figure 4.6**; measured at ~ -60 mV) by 52 ± 9 μm (**Supplementary Figure 4.6**; $n = 5$; $P = 0.008$) towards the null side of the receptive field (**Supplementary Figure 4.6**). Thus, it might

be expected that delayed inhibition could selectively shunt gap junction signals in the falling phase of the response to moving stimuli and prevent them from being effectively converted into spikes. To test this possibility, we next measured responses in the presence of the GABA_A receptor blocker picrotoxin. As expected, blocking GABA_A receptors significantly increased the peak spike rate (**Figure 4.7A**; 198 ± 14 Hz for control; 244 ± 18 Hz in picrotoxin; $n = 6$; $P = 0.03$), but responses remained skewed towards the leading edge (SI in control = 1.6 ± 0.2 , SI in picrotoxin = 2.3 ± 0.3 ; $n = 6$; $P = 0.031$). Under inhibitory receptor blockade, spiking responses initiated on average 70 ± 23 μm earlier than under control conditions (**Figure 4.7A**; $n = 6$; $P = 0.028$), but terminated at nearly the same spatial location (**Figure 4.7A**; $n = 6$; 15 ± 11 μm ; $P = 0.245$). Thus, inhibition does not appear to be responsible for the lack of gap junction priming on the falling phase of the response of DSGCs to moving stimuli.

Consistent with previous studies (Caldwell et al., 1978), null responses were greatly augmented in the presence of picrotoxin. The peak spike rate of null direction responses increased from 27 ± 12 Hz in control to 202 ± 14 Hz in picrotoxin (**Figure 4.7B**; $n = 4$; $P < 0.001$). Under these conditions, we observed that the downstream ventrally located DSGCs, which were unable to effectively prime responses during preferred direction motion, could prime responses to stimuli moving in the opposite direction. Thus, regardless of the direction of the stimulus, responses were always skewed towards the leading edge of the stimulus (**Figure 4.7B**; SI for null direction responses = 3.1 ± 0.5), suggesting that an activity-dependent gain control mechanism, that does not rely on GABAergic inhibition, shapes ganglion cell responses.

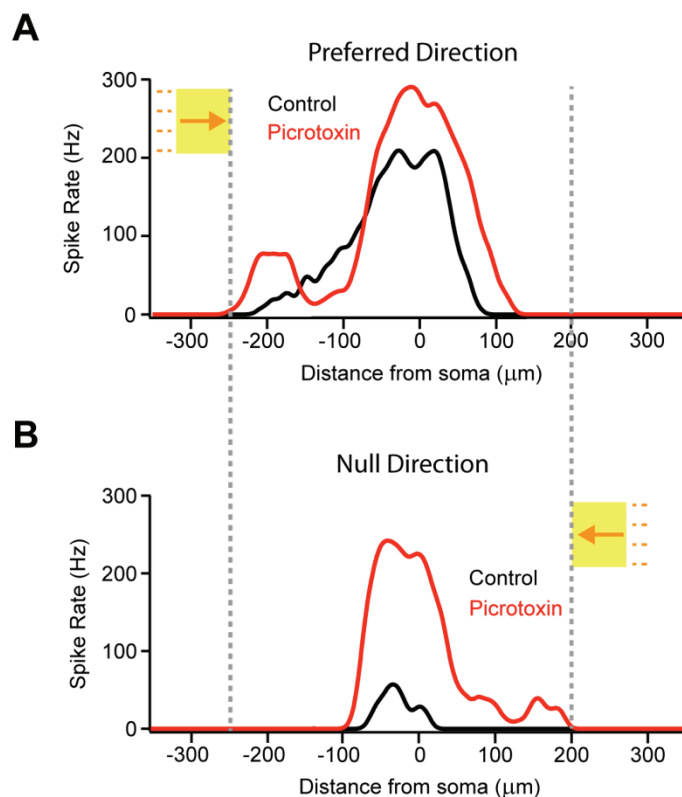


Figure 4.7. Offset inhibition does not drive skewed responses. The preferred (A) and null (B) ON spike rates of a coupled DSGC is shown in control conditions and during application of the GABA_A receptor blocker picROTOXIN (50 μM).

Previous studies have suggested that an inactivation of Na⁺ channels (Kim and Rieke, 2003) and/or an activation of Ca²⁺-dependent K⁺ channels (Wang et al., 1998, Benison et al., 2001) may render ganglion cells less excitable after strong bouts of activity. To examine if activity-dependent adaptation during responses might cause DSGCs to be less responsive to gap junction inputs during the falling phase of their responses, we compared DSGC spiking responses and synaptic currents, recorded sequentially from the same cells (**Figure 4.8A**). Examination of the current/spike-rate relationship revealed that current in the rising phase of the response was more effectively translated into spikes than current in the falling phase of the response (**Figure 4.8A,B**; current at half-maximum response during rising phase 88 ± 22 pA, versus 193 ± 36 pA in

the falling phase; $n = 7$, $P = 0.029$). Moreover, the apparent spike threshold (i.e. the current amplitude associated with spikes) in the beginning of the spike train was significantly lower compared to that observed at the end of the response (**Figure 4.8C**; $n = 7$; $P = 0.003$). Thus, a dynamic, activity-dependent increase in apparent spike threshold appears to underlie the ability of upstream but not downstream coupled DSGCs to boost synaptic signals generated by moving stimuli.

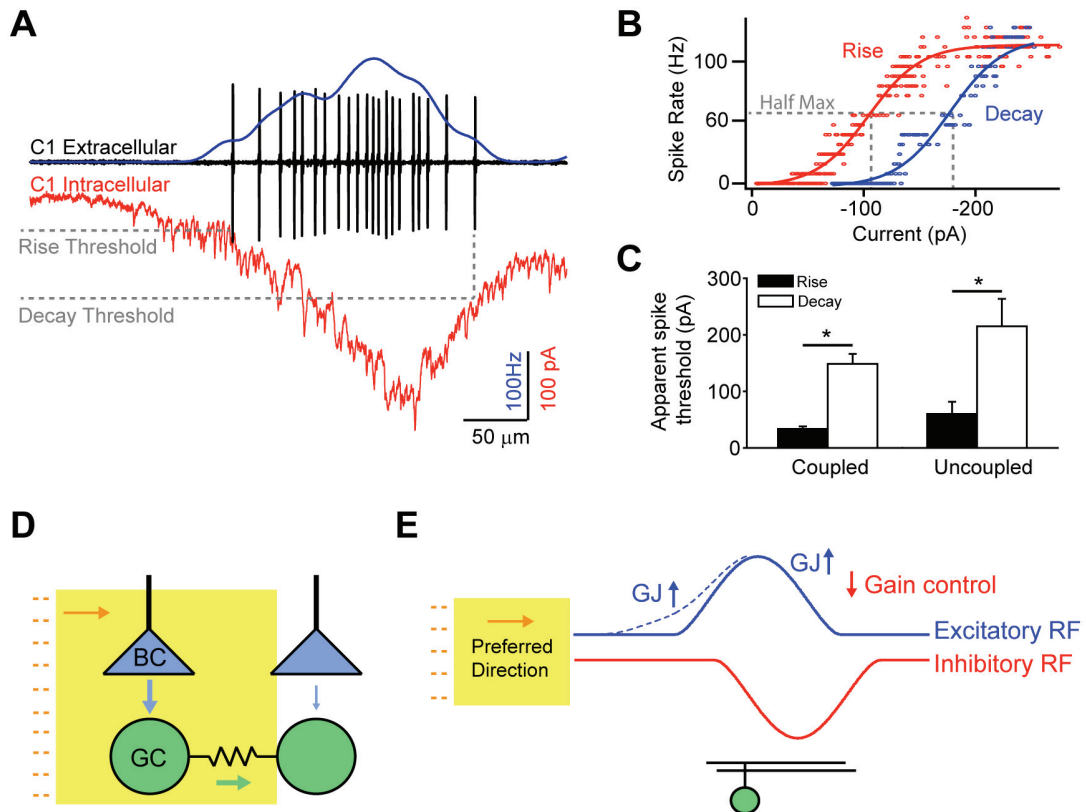


Figure 4.8. Post-synaptic gain control is important for terminating responses. **A**, The spiking ON waveform measured in a coupled DSGC (*blue*; raw spike traces are shown in *black*) is compared to its excitatory synaptic inputs (*red*; $V_{\text{HOLD}} \sim -60$ mV; these recordings were made in succession from the same DSGC). **B**, A plot of the spike rate versus the current for the rising (*red*) and decaying (*blue*) phases of the responses shown in (**A**) reveal a dynamic change in the spike/current relationship during the light response (the current at half-maximum response during rising phase was 88 ± 22 pA, compared to 193 ± 36 pA during the falling phase; $n = 7$, $P = 0.029$) **C**, The average apparent spike threshold (i.e. the amplitude of the synaptic EPSC at the point of the first and last spikes in the spike train) is plotted for the rising and decaying response phases of ON responses for both coupled ($n = 7$) and uncoupled ($n = 6$) DSGCs responding to a $300 \times 300 \mu\text{m}$ bar

(96% Weber contrast) moving at 600 $\mu\text{m/s}$ in the preferred direction. * = $P < 0.05$. **D**, A diagram illustrating priming by gap junction-mediated lateral excitation. A moving stimuli (*yellow bar*), that has fully activated the bipolar cell (BC) and the ganglion cell (GC) on the left (*thick blue arrow*), which primes downstream GC (green arrow) and sensitizes it to the approaching stimulus. **E**, A schematic illustrating that gap junctions boost the rising phase of the responses to moving stimuli. During the falling phase, gain control and offset GABAergic inhibition work together to curb gap junction signalling.

Discussion

Dendrodendritic Electrical Coupling in Superior Coding ON-OFF DSGCs

Here we present multiple lines of evidence to indicate the superior coding DSGCs are the only strongly coupled population of ON-OFF DSGC in the mouse retina. First, superior coding DSGCs exhibited tracer coupling and depolarization-induced feedback spikelets, while other types of DSGCs did not. Second, superior coding DSGCs had much larger subthreshold receptive fields compared to the other types. Third, Hb9⁺ cells appear to be the only DSGC population with the ability to lag normalize (Trenholm et al., in press).

While anatomical work in mouse retina indicates that there maybe two types of coupled ON-OFF DSGCs (type 2 and 3 bistratified ganglion cells in Schubert et al., 2005, G16 and 17 in Pan et al., 2010) , both these cells bear strong morphological similarities with superior coding DSGCs. Both cells have highly asymmetric dendritic trees, and their dendritic arbour sizes fall within the range described for genetically identified superior coding DSGCs (BD cells in Kay et al., 2011, Hb9 cells in Trenholm et al., 2011), suggesting that both cells likely belong to this class of DSGC. The finding that only a single type of ON-OFF DSGCs is labelled in the retina also appears to be the case in the rabbit retina, in which labelling is restricted to neighbouring DSGCs with non-overlapping dendritic fields (Vaney, 1994).

Ganglion cells could be coupled at their axons and/or dendrites (Hidaka et al., 2004) and both tracer coupling methods and/or examination of reciprocal feedback

spikelets could not definitively distinguish between these possibilities. However, we found that in some cases, DSGCs remained well coupled even after an axon was unintentionally severed (**Supplementary Figure 4.7**), indicating that coupling must occur in the dendrites. These recordings confirm that spikelets reflect spikes originating in neighbouring ganglion cells that are strongly attenuated by the resistance of the gap junction in combination with the dendritic resistance and capacitance. Together these results establish the Hb9::eGFP retina as an ideal model system for studying the role of dendrodendritic gap junctions in neural computations.

Composite Receptive Field Structure of Coupled DSGCs

Classic work (Barlow, 1953, Kuffler, 1953) showed that receptive fields of retinal ganglion cells, mapped with small spots of light, typically consist of an excitatory centre and a concentric antagonistic surround, often modelled as a difference of Gaussians (Rodieck, 1965). These components are formed by combing excitatory inputs from bipolar cells with inhibitory inputs from horizontal/amacrine cells. In addition, many ganglion cells in the mammalian retina are homologously coupled to other ganglion and/or inhibitory amacrine cells (Volgyi et al., 2009), though the impact of such coupling on receptive field structure has remained elusive (Hu et al., 2010). Our recordings reveal that in the context of small spots, the cRF remains well matched to the dendritic field of coupled DSGCs (see also; Hu et al., 2010), because under these conditions the electrical inputs are weak compared to the chemical inputs. However, homologous gap junction coupling in superior coding ON-OFF DSGCs gives rise to an extensive subthreshold receptive field that surrounds the cRF. Since most studies have utilized spike measurements to map receptive fields of ganglion cells, it appears that subthreshold components arising from coupling have been previously overlooked.

Small spots effectively activated individual ganglion cells, thus permitting the integration of *excitation* from the ring of surrounding neighbouring coupled ganglion cells. Since, signals passing through electrical synapses are strongly attenuated, gap junction-mediated excitation is subthreshold (~1-5 mV in peak amplitude). Moreover, as

the somata of coupled DSGCs are spaced ~ 100 μm apart and the average strength of coupling is similar in all directions, the subthreshold receptive field forms a fairly uniform doughnut shape, extending well beyond the cRF. Although the subthreshold receptive field is weak when probed with small spots, it becomes important in the context of large moving stimuli. Such recruitment of subthreshold receptive fields during motion stimuli has also been observed in higher centres of the visual system (Grinvald et al., 1994, Hirsch et al., 1998, Bringuier et al., 1999, Jancke et al., 2004a), where long range horizontal connections spread waves of subthreshold activity and prime neurons responding to approaching stimuli.

Priming by Gap Junction-Mediated Lateral Excitation

Our results suggest that activation of individual DSGCs during physiological levels of activity rarely, if ever, directly triggers spiking in coupled neighbours. Direct current injection or spot stimuli that robustly stimulated individual DSCGs only produced subthreshold depolarizations in their neighbours. Furthermore, during moving stimuli, the initial coupling-mediated inputs occurred much farther from the soma than the first spikes, also suggesting that coupled inputs alone do not drive spike activity in post-junctional cells (Trenholm et al., in press). Thus, gap junction inputs need to act collectively with inputs from other ganglion and/or bipolar cells in order to become effective (i.e. trigger spikes). Here, by independently stimulating electrical and chemical inputs, we directly demonstrated that subthreshold gap junction-mediated inputs boosted subsequent light-driven inputs. However, boosting by gap junctions occurs most effectively under conditions whereby the conductance of chemical synaptic activity is low (i.e. during the rising phase of the response). Under these conditions, the input resistance is high and the relatively weak gap junction inputs can effectively prime the cell.

Priming arises from two main factors. First, activity in upstream coupled ganglion cells provides an additional source of excitatory current, bringing the downstream cell closer to spike threshold. Second, when neighbouring coupled cells are

coincidentally active, currents from chemical synaptic inputs no longer leak into their active neighbours (if neighbours are not simultaneously active they contribute to a substantial sink). This prevention of current leak through gap junctions raises the local membrane resistance between the coincidentally active neighbours, thus enhancing their excitability (Curti et al., 2012). However, the latter effect is expected to become negligible as the chemical synaptic conductance gets larger.

Controlling the timing of the initial spikes in a spike train is especially important since this may provide the brain information about the appearance of a novel stimuli (Gollisch and Meister, 2008). The sequential activation of closely spaced DSGCs (~80 cells/mm²; Trenholm et al., 2011) allows for a long window of coincident activation of upstream and downstream coupled neighbouring cells during motion, resulting in effective gap junction priming. Interestingly, while the coincident window gets briefer with increasing velocity, the excitatory drive increases and causes priming signals to get stronger with velocity, remarkably allowing these cells to remove spatial lag associated with transmission delays (Trenholm et al., in press).

Rectification of Lateral Excitatory Signals in Coupled DSGCs

To date, rectification of electrical synapses has been observed in several invertebrate species including crayfish (Furshpan and Potter, 1959), leech (Baylor and Nicholls, 1969, Nicholls and Purves, 1970) and lobster (Johnson et al., 1993). Interestingly, Cx45 mediated gap junctions that are expressed by ON-OFF DSGCs (Schubert et al., 2005, Pan et al., 2010) are amongst the most voltage-dependent gap junctions, at least when examined in expression systems (Moreno et al., 1995, Barrio et al., 1997). However, our voltage-clamp measurements from pairs of DSGCs revealed no inactivation or rectification of the gap junction conductance, even when the membrane of the DSGC was strongly depolarized or hyperpolarized for long periods. One possible explanation for the lack of voltage-dependence of gap junctions in coupled DSGCs is that in these cells, Cx45 could form heterologous gap junctions with other types of connexions that may be expressed in these cells, including Cx30.2 (Muller et al., 2010).

Regardless of the mechanisms, the lack of voltage-dependence suggests that direct modulation of these channels during physiological responses is unlikely. Instead, here we present evidence that activity-dependent changes in the intrinsic membrane properties effectively gate the efficacy of gap junctions, thus creating a *functional* rectification of electrical signals, allowing upstream, but not downstream DSGCs to provide effective priming signals to their neighbours.

In the presence of GABA_A receptor antagonist, which reduces directional selectivity, such rectification can be observed in response to stimuli moving in all directions, suggesting that it arises from an activity-dependent mechanism rather than from postsynaptic inhibition and/or heterogeneities in cell distributions or gap junction conductances. This appears to arise from a dynamic increase in the apparent spike threshold during the spike train. Indeed Na⁺ channel inactivation (Kim and Rieke, 2003), and/or a build-up of Ca²⁺-dependent K⁺ conductances (Wang et al., 1998, Benison et al., 2001) as have previously described for retinal ganglion cells, could explain such a phenomenon. It is important to note that such gain control mechanisms also operate on uncoupled ganglion cells (Berry et al., 1999). However, coupled DSGCs receive prolonged weak inputs as stimuli traverse their subthreshold receptive fields, and changes in threshold have more dramatic effects on where their spikes initiate in space.

Conclusion

Neural networks formed by coupled DSGCs are faced with the challenge of providing strong lateral excitatory signals without causing a large expansion of receptive fields (which may decrease visual resolution) or promoting runaway excitation. Here we demonstrate two important features that permit this to occur. First, we posit that the effective spread of lateral gap junction mediated excitation requires chemical synaptic inputs. As such, lateral excitation can only spread in a limited fashion, enabling superior coding ON-OFF DSGCs to detect moving stimuli far from their dendritic fields. Furthermore, we show that activity-dependent mechanisms gate the functional efficacy of gap junction signalling (**Figure 4.8D,E**). Such refractoriness prevents electrical signals

from back-propagating through the network and promotes the spread of priming signals along the preferred axis.

Gap junction mediated signals allow ganglion cells to anticipate moving stimuli, implying a possible role for these cells in reflexive behaviour. Indeed superior coding DSGCs also send their projections to the accessory optic nuclei, which control reflexive eye movements (Kay et al., 2011). However, why only superior-coding DSGCs are electrically coupled is still a mystery.

Methods

Wholemout Retinal Preparation

All procedures were performed in accordance with the CACR and approved by the University of Victoria's Animal Care Committees. Experiments were carried out in adult wt (C57/B16) or Hb9::eGFP transgenic mice (Arber et al., 1999, Wilson et al., 2005, Trenholm et al., 2011) of either sex that were maintained on a 12 hr light/dark cycle. In brief, mice were dark adapted for 30 minutes prior to being anaesthetised and decapitated. During the removal of the eyes, the dorsal side of the retina was marked to keep track of orientation. After removal of the eyes, the retina was dissected in Ringer's solution under infrared (IR) light, and mounted on a 0.22 mm membrane filter (Millipore, Bedford, MA, USA) with a pre-cut window through which light was able to reach the retina, enabling the preparation to be viewed under IR illumination using a Spot RT3 CCD camera (Diagnostic Instruments, Sterling Heights, MI, USA) attached to an upright Olympus BX51 WI fluorescent microscope equipped with a 40X water-immersion lens (Olympus Canada, Markham, Ontario, Canada). The retinal preparation was continually perfused with 35-37°C Ringer's solution containing (in mM): 110 NaCl, 2.5 KCl, 1 CaCl₂, 1.6 MgCl₂, 10 dextrose, and 22 NaHCO₃ that was bubbled with carbogen (95% O₂: 5% CO₂ [pH 7.4]). All reagents were purchased from Sigma-Aldrich Canada Ltd. (Oakville, Ontario, Canada) unless otherwise noted.

Physiological Recordings

Extracellular recordings were made in loose cell-attached patch clamp mode using 5-10 M Ω electrodes filled with Ringer's solution. Voltage-clamp whole-cell recordings were made using 4-7 M Ω electrodes containing (in mM): 112.5 CH₃CsO₃S, 1 MgSO₄, 1.5 EGTA, 10 HEPES, 4 ATP-Mg₂, 0.5 GTP-Na₃, 5 QX-314, 0.25 Alexa 594 (Invitrogen, Burlington, Ontario, Canada) and 7.75 Neurobiotin (Vector Laboratories Inc, Burlingame, CA). The reversal potential for chloride (ECl) was calculated to be \sim -70 mV. The pH was adjusted to 7.4 with CsOH. For current-clamp experiments electrodes contained (in mM): 115 K⁺ gluconate, 5 KCl, 1 MgCl₂, 1 EGTA, 10 HEPES, 4 ATP Mg²⁺, 0.5 GTP Na³⁺, 0.025 Alexa 594 and 7.75 Neurobiotin. The pH was adjusted to 7.4 with KOH. Recordings were made with a MultiClamp 700B amplifier (Molecular Devices, Sunnyvale, CA, USA). Signals were digitized at 10 kHz using a BNC-2090A A/D board (National Instruments, Austin, TX, USA) and acquired using custom software written in LabVIEW (Dr. David Balya, Friedrich Meischer Institute, Switzerland). GFP positive ganglion cells were visually targeted for recordings using 2-photon laser scanning microscopy techniques with the wavelength at 950 nm to minimize photoreceptor bleaching. GFP⁻ DSGCs were identified by their soma size and directionally selective response properties.

Light Stimulus

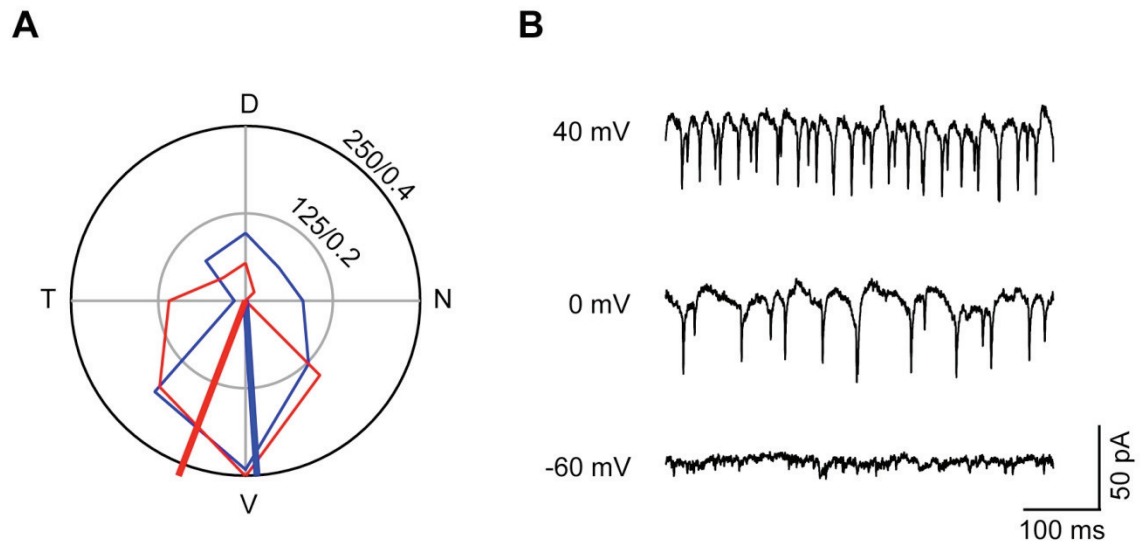
Light stimuli were generated with a digital projector (Hitachi Cpx1; refresh rate 75Hz) and controlled with custom software. The ambient background intensity, as measured with a calibrated spectrophotometer (USB2000; Ocean Optics, Dunedin, FL, USA) was 3×10^{12} photons s⁻¹ cm⁻² (sampled at 500 nm), which is equivalent to 400 photoisomerizations cone⁻¹ s⁻¹. Retinas were light adapted for 30 minutes after dissection prior to recordings in attempt to increase ganglion cell coupling (Hu et al., 2010). Light stimuli were projected from below the preparation and focused on the photoreceptor outer segments using the sub-stage condenser. The preferred direction for DSGCs was

calculated by computing a vector sum of the peak spike rates after presenting a 300x300 μm (96% positive Weber contrast) stimuli moving at 600 $\mu\text{m/s}$ in eight directions over each cell.

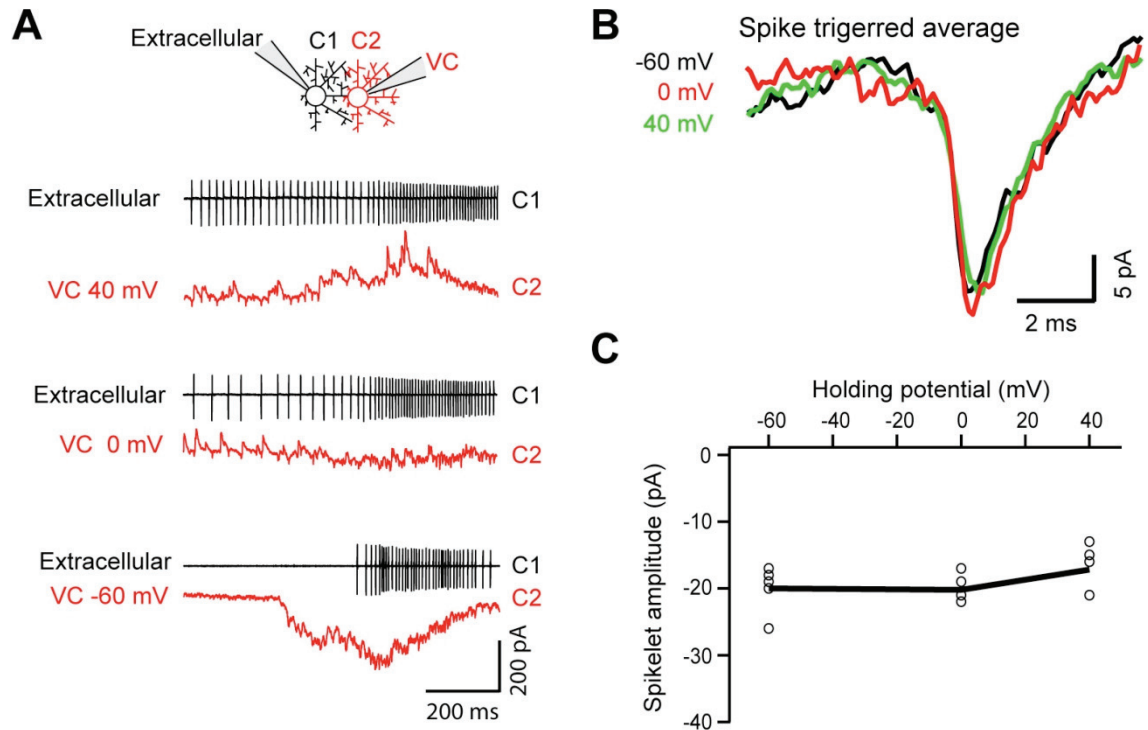
Data Analysis

Receptive field size was calculated by measuring the area of the X-Y contour plot of the data obtained by flashing a 40 μm spot pseudorandomly above the cell of interest. Dendritic field size was calculated by first loading neurons with Alexa 594, then imaging neuronal morphologies with 2-photon laser scanning microscopy techniques with the laser at 850 nm. Dendritic morphologies were then reconstructed using Image J (rsbweb.nih.gov/ij/). Dendritic area was calculated by making a convex polygon obtained by linking the peripheral dendritic tips. Spike rates were estimated by low-pass filtering spike trains through convolution with a Gaussian kernel with a fixed width, $\sigma = 25\text{ms}$. Spike rates were then plotted as a function of the stimulus edge distance from the soma. To compare classical receptive fields to responses generated by moving stimuli, we corrected for the expected spatial lag that occurs from fixed transmission delays during which the stimuli covers a certain distance. In our experiments, transmission delays were estimated by flashing a 300x300 μm , which resulted in a ~ 60 ms delay from light onset until ganglion cell spiking. Since stimuli moved at 600 $\mu\text{m/s}$, we shifted the response waveform by 36 μm . A skew index (SI) was used to quantify the response asymmetry and was computed as the ratio of the distance from start-to-peak/peak-to-end of the spiking response. SI values > 1 indicate skew towards the start of the response; a value of 1 indicates a symmetrical response; values < 1 indicate skew towards the trailing edge of the response. Comparisons between groups were made with t-tests. Comparisons made between recordings from the same cell before and after applying pharmacological agents were made using paired t-tests. For data that failed normality tests, we used the Mann-Whitney Rank Sum test instead of t-tests and we used the Signed Rank test instead of paired t-tests. Data are presented as mean \pm s.e.m.

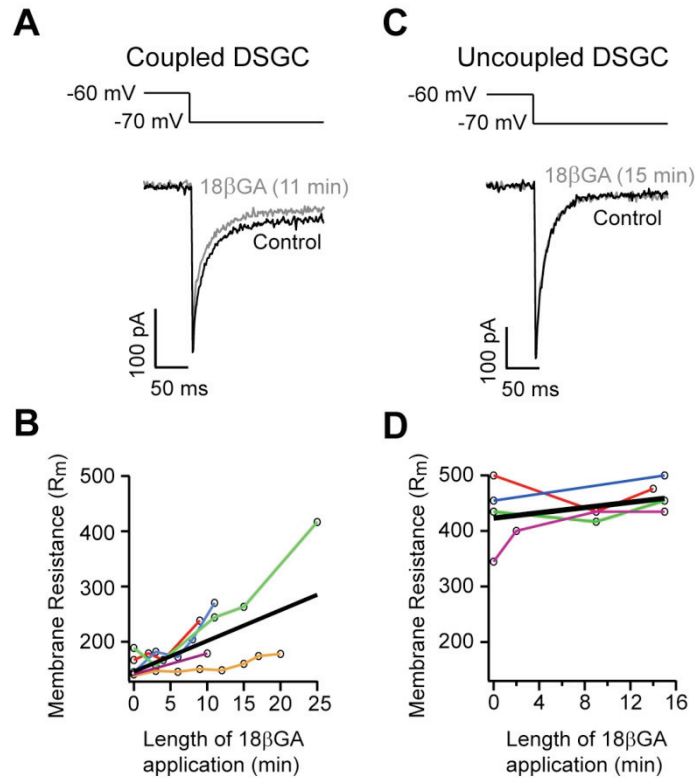
Supplementary Material



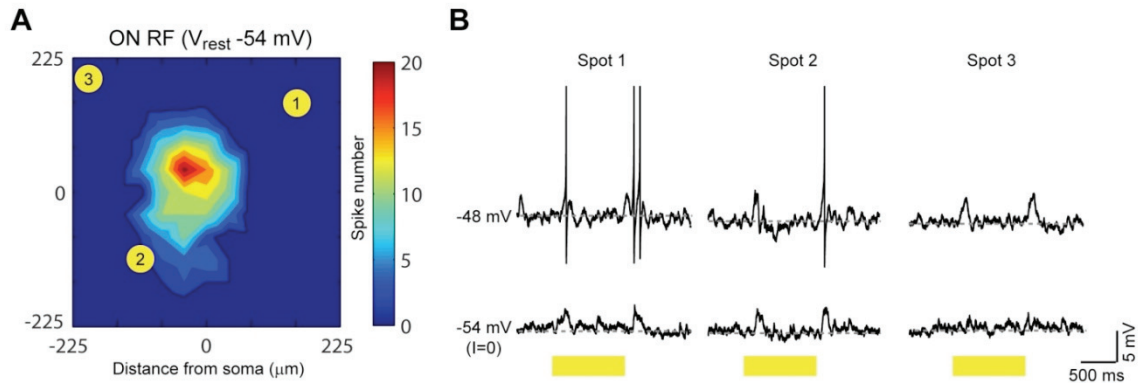
Supplementary Figure 4.1. Superior coding DSGCs exhibit depolarization induced feedback spikelets in wt retina. **A**, A polar plot indicating the ON and OFF spike rates generated to 8 by a 300x300 μm bar (96% Weber contrast) moving at 600 $\mu\text{m}/\text{s}$ in 8 directions. ON and OFF responses are shown in blue and red, respectively. Scale bar: Hz/DSI. The directional selectivity index (DSI) was calculated as Preferred-Null/Preferred+Null, and is indicated by the thick blue (ON DSI) and red (OFF DSI) lines, which also indicates the preferred direction calculated as the vector sum of the polar plot. **B**, A voltage-clamp recording from a superior coding ON-OFF DSGC in wt retina shows the presence of depolarization induced feedback spikelets. These results indicate that electrical coupling is not a transgenic artifact in the Hb9::eGFP retina.



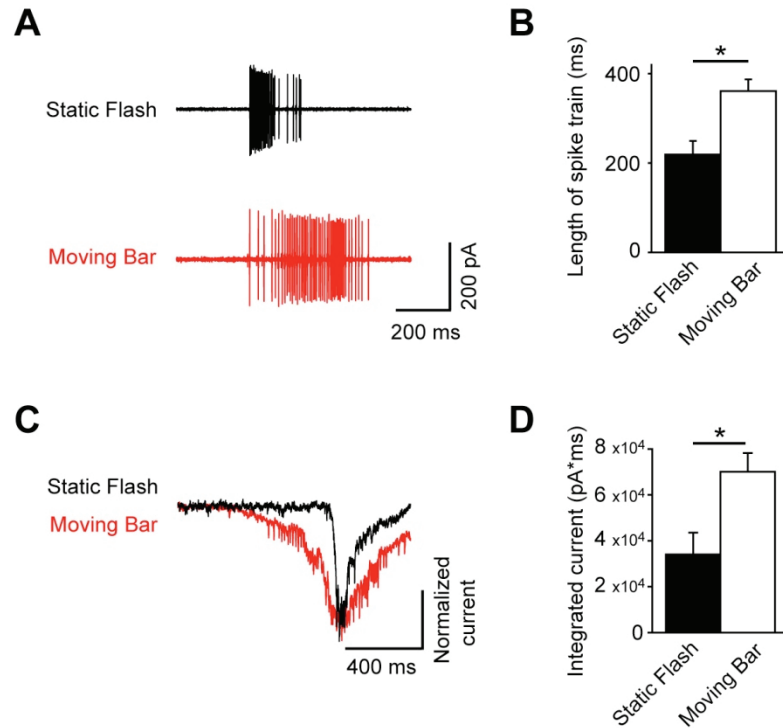
Supplementary Figure 4.2. Depolarization induced feedback spikelets do not exhibit a reversal potential. **A**, An example of a paired recording where activity in cell 1 (C1) is passively measured using the extracellular cell-attached technique and the activity in cell 2 (C2) is controlled in voltage-clamp mode (similar to **Figure 4.1**). The example traces show the light driven (and depolarization driven) spiking activity in C1 (black) when the membrane potential of C2 (red) was held near -60, 0 or 40 mV. **B**, Spikes in C1 were used to make spike triggered averages in C2 to measured size of the average spikelet. **C**, Spikelets measured at -60, 0 or 40 mV had similar amplitudes ($n = 5$; $P > 0.05$).



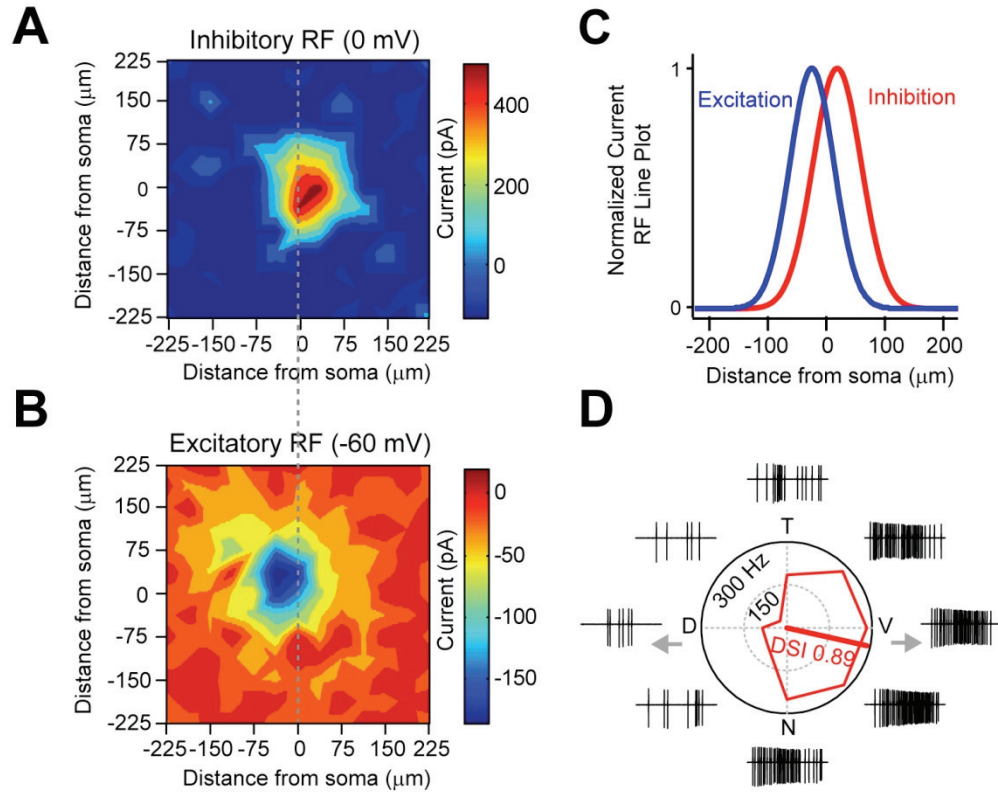
Supplementary Figure 4.3. Gap junctions lower input resistance. **A**, A voltage step from -60 mV to -70 mV in voltage-clamp mode is used to measure the input resistance of a coupled DSGC. Blocking gap junctions with application of 25 μ M 18 β GA lead to an increase in input resistance for coupled (Hb9⁺) DSGCs of 100 ± 36 M Ω ($n = 5$; $P < 0.05$), that took several minutes to take effect (**B**). The different colours in (**B,D**) represent different cells. **C,D**, The input resistance of uncoupled DSGCs (353 ± 29 M Ω ; $n = 14$; $P < 0.001$) was significantly higher than for coupled DSGCs (169 ± 11 M Ω , $n = 11$). Also, the input resistance of uncoupled DSGCs was not significantly affected by application of 18 β GA ($n = 4$; $P = 0.3$). For all these recordings, cells were only included when the series resistance changed by less than 10% throughout the length of the recording.



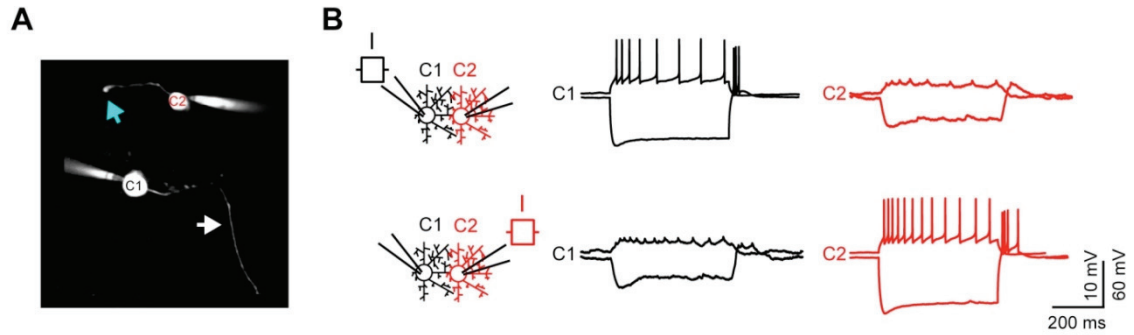
Supplementary Figure 4.4. Subthreshold receptive fields are excitatory. To ensure that subthreshold depolarizations measured in regions flanking the classical (suprathreshold) receptive field (**A**) were not depolarizing as a result of the neuron being held below E_{Cl} , we tested the effect of slightly depolarizing the membrane on these subthreshold response. **A**, Shows a classical receptive field of a coupled DSGC, mapped with a $40\ \mu\text{m}$ spot flashed pseudorandomly above the cell. The three yellow spots (1,2,3) indicate the location of small ($40\ \mu\text{m}$) spots whose responses are shown in (**B**). **B**, The bottom traces show the subthreshold light responses measured to spots 1-3 at $I = 0$, which for this cell meant a resting membrane potential of $-54\ \text{mV}$. Injecting $25\ \text{pA}$ of depolarizing current changed the resting membrane potential to $-48\ \text{mV}$, but this did not eliminate the subthreshold events seen at $-54\ \text{mV}$. These results indicate that subthreshold depolarizing events measured near $I = 0$ are mediated by excitation, not inhibition. It should be noted that spikes are truncated to emphasize the subthreshold PSPs.



Supplementary Figure 4.5. Responses to moving stimuli are more sustained than to static stimuli. **A**, The spiking response of a coupled DSGC to a 300x300 μm bar either flashed (*black*) or moved (at 600 $\mu\text{m}/\text{s}$ in the preferred direction; *red*) over the cell. **B**, On average, stimuli moving at 600 $\mu\text{m}/\text{s}$ drive more sustained spike trains than static stimuli ($n = 7$). **C**, A plot of the EPSCs evoked by static (*black*) and moving (*red*) stimuli (same stimulus as in **A**). **D**, On average, responses to moving stimuli carry more charge ($n = 5$).



Supplementary Figure 4.6. Spatially offset inhibition. Inhibitory (**A**) and excitatory (**B**) receptive fields for the ON responses of a coupled DSGC (measured in voltage-clamp at 0 and -60 mV, respectively). **C**, Gaussian fits of the inhibitory and excitatory receptive fields measured in (**A,B**), measured along the preferred-null axis indicate that the peaks of the excitatory and inhibitory RFs are offset by $52 \pm 9 \mu\text{m}$ ($n = 5$). **D**, Peak spike rates of responses to stimuli moving in 8 directions are presented in a polar plot, confirming that inhibition was offset in the null direction.



Supplementary Figure 4.7. Coupling between ON-OFF DSGCs appears to be dendrodendritic. **A**, A 2-photon reconstruction of an Alexa 594 labelled pair of neighbouring coupled DSGCs. The recording electrodes are shown touching the somata of C1 (bottom) and C2 (top). The white arrow points to the axon of C1 that is streaming away from C2. The blue arrow points to the torn axon of C2, that does not contact C1. **B**, A paired current-clamp recording showing that hyperpolarizing (-400 pA) and depolarizing (80 pA) current injection to either C1 or C2 result in attenuated coupling mediated voltage deflections in the neighbouring cell, indicating that DSGCs remain reciprocally coupled despite having non-contacting axons. As such, coupling must be mediated via dendrodendritic gap junctions.

Chapter 5: Discussion

Motion Coding Strategies in the Retina

Together, the results from this thesis expand upon the current understanding of how moving objects are detected and encoded by the retina. For the last 50 years, great strides have been made in understanding how motion is processed by the retina. Here, I will put my findings into the broader context of motion coding strategies in the retina.

Classical Directional Selectivity

The initial discovery of directionally selective responses in the retina contradicted the idea at the time that the retina simply relayed signals about light intensity to higher visual centers for processing. Nonetheless, upon the initial discovery of retinal DS, visual scientists already had enough insight into the mechanistic underpinnings of DS to make a mostly correct hypothesis about its origins. It would take roughly 40 years before this initial hypothesis was proven true. On the mechanism of retinal DS, Barlow and Levick postulated that it arose from offset inhibition, which shunted excitatory responses during null direction motion (1965). The evidence for this hypothesis first started to solidify with early pharmacological tests that found blocking GABAergic inhibition could eliminate DS responses (Wyatt and Day, 1976, Caldwell, 1978). Finally, direct evidence of asymmetric inhibitory inputs were shown by Taylor et al. (2000) who made the first whole-cell voltage clamp recordings from DSGCs and showed that IPSCs were significantly larger for null direction stimuli than for preferred direction stimuli. Subsequently, paired recordings revealed that the source of this asymmetric lateral inhibition was starburst amacrine cells (SACs; Fried et al., 2002, Fried et al., 2005, Lee et al., 2010, Wei et al., 2011, Yonehara et al., 2011). These radially symmetrical cells appeared to respond preferentially to stimuli moving in the centrifugal direction (i.e. away from the soma; Euler et al., 2002). Furthermore, SACs were subsequently found to make exquisitely refined synaptic connections with DSGCs, such that each SAC provides effective DS signals to the 4 different directions of ON-OFF DSGCs (Briggman et al., 2011).

In the retina, there are three types of DSGCs: ON, OFF and ON-OFF. Both ON and ON-OFF DSGCs tend to stratify near the cholinergic bands in the retina, which label the dendritic layers of the starburst amacrine cells (Borst and Euler, 2011, Vaney et al., 2012). As such, the classical mechanisms for driving DS (i.e. asymmetric lateral inhibition) appear to be conserved for both of ON and ON-OFF DSGCs. In contrast, while OFF DSGCs also appear to receive offset lateral inhibition (Kim et al., 2008), though they do not stratify in cholinergic bands, making it less likely that their directional responses are mediated by inhibition from starburst amacrine cells.

ON DSGCs project to non-vision forming centers including accessory optic system (Oyster et al., 1980) and respond to much slower moving stimuli than ON-OFF DSGCs. As such, they appear to be important for reflexes driven by moving visual scenes, such as the optokinetic responses (Oyster et al., 1972). The function of ON-OFF DSGCs and OFF DSGCs in higher visual signalling remains poorly understood. Recent work has shown that ON-OFF DSGCs project to subcortical visual centers (Huberman et al., 2009, Kay et al., 2011), though their role in cortical DS signals remains up for debate. Nonetheless, recent work has shown a putative role for ON-OFF DSGCs in driving DS responses in LGN (Marshel et al., 2012), indicating that ON-OFF DSGCs likely promote DS responses in cortex. OFF DSGCs, which only appear to code superior motion and project mostly to superior colliculus (Kim et al., 2008), putatively drive the superior coding SC neurons described by Drager and Hubel (1975), therefore providing a possible pathway for OFF DSGC signals to drive cortex.

Despite these recent advances, many questions remain unresolved with regards to classical DS mechanisms in the retina. First, if starburst amacrine cells are the main drivers for classical DS, how can ON and ON-OFF DSGCs have such significantly different velocity tuning profiles (ON DSGCs stop responding at much slower speeds than ON-OFF DSGCs)? Is it possible that there are different types of starburst amacrine cells that differentially synapses with ON vs. ON-OFF DSGCs, or is there a specific amacrine cell that synapses with ON but not ON-OFF DSGCs and that preferentially inhibits ON DS cells at faster velocities? Second, while the behavioural roles for ON DSGCs have been largely identified, the roles for ON-OFF and OFF DSGCs remain to be explored. Third, while starburst amacrine cells are both GABAergic and cholinergic, and

much work has been undertaken to show the role for GABAergic transmission, very little is known about the role of acetylcholine in forming DS responses.

Non-Classical DS

Chapter 2 of this thesis presents some of the first strong evidence for a non-classical form of DS in ON-OFF DSGCs that functions under physiological conditions. While it had previously been found that 1) blocking GABA receptors did not always block DS in ON-OFF DSGCs (Smith et al., 1996, Grzywacz et al., 1997) and that some ON-OFF DSGCs exhibited stark dendritic asymmetries (Amthor et al., 1989, Oyster et al., 1993, Yang and Masland, 1994), the lack of genetic markers did not allow for a systematic assessment of the contribution of morphology to DS. The results of this thesis, utilizing a mouse line that exclusively labels superior coding ON-OFF DSGCs with GFP, indicate that certain populations of ON-OFF DSGCs use dendritic asymmetries to confer directional selectivity. This non-classical form of DS appeared to arise due to the stark asymmetry of dendrites that possessed non-linear processing capabilities, resulting in an intrinsic soma-to-dendrite preferred direction. Functionally, this second, parallel (to classical inhibition-dependent DS) form of DS likely strengthens the directional selectivity of these cells. Furthermore, as these cells have no dendrites on the preferred side of their soma (i.e. the side from which preferred direction stimuli approach), a region of the cell described as the non-discriminatory zone in more symmetrical DSGCs (Barlow and Levick, 1965, He et al., 1999, Trenholm et al., 2011), asymmetric DSGCs appear to have rid themselves of their non-DS subunits. This systematic dendritic asymmetry is similar to that found for superior coding OFF DSGCs (Kim et al., 2008), though it has yet to been shown whether OFF DSGCs possess DS responses in the absence of inhibitory inputs, or whether they possess active dendrites.

Other forms of non-classical DS – mainly involving reversal of DS – have also been described for ON-OFF DSGCs. Upon blocking GABA receptors, Smith et al. (1996) and Grzywacz et al. (1997) found that DS responses in some ON-OFF DSGCs reversed direction. The mechanism for this reversal of DS is unknown, but could possibly be related to a similar finding in ON DSGCs, where it was found that blocking GABA receptors revealed an OFF response that was DS with the opposite directional preference

to the ON response under control conditions (Ackert et al., 2009). The directional selectivity of this unmasked OFF response relied on gap junctions and cholinergic transmission (Ackert et al., 2009). Recently, a GABA receptor dependent form of DS reversal was described by Rivlin-Etzion et al. (2012), using drifting gratings moving in the null direction for > 30 s. This reversal of the preferred direction was found to last for lengths of > 20 min, indicating a form of medium-long term plasticity in the DS circuitry. The mechanism for this reversal appeared to involve switching the direction of motion that invoked greater inhibition, though how this happens is unclear since starburst amacrine cells have been shown to make only very weak contacts with DSGCs in the preferred direction (Fried et al., 2002, Lee et al., 2010, Briggman et al., 2011, Wei et al., 2011, Yonehara et al., 2011). Also, it remains unclear whether this form of plasticity would ever occur during naturalistic situations, or whether certain stimuli could reset the system to its original preferred direction.

Anticipation

Chapters 3 and 4 of this thesis describe how superior coding ON-OFF DSGCs utilize gap junction signalling to anticipate moving stimuli by responding far from their dendritic trees. Furthermore, gap junction signalling allows these cells to normalize for lags inherent in retinal signal processing, such that these cells initiate responses at the same spatial location, regardless of the velocity of the moving stimulus (Chapter 3). Functionally, this could be important in driving a reflex, since responses from these cells would arrive sooner at upstream targets than response from non-coupled neighbouring cells, though such a reflex restricted to superior moving stimuli remains to be described. Additionally, a mechanism similar to that described in Chapters 3 and 4 could be responsible for the finding in visual cortex that moving stimuli are processed with a shorter delay than static stimuli (Jancke et al., 2004b).

The discovery of anticipatory responses in superior coding DSGCs contrasts with previous findings of anticipation in the retina by Berry et al (1999). While superior coding DSGCs respond to moving stimuli far from their dendritic fields, Berry et al. (1999) found that most ganglion cells respond to moving stimuli within their classically defined (Gaussian fit, measured with static flashes) receptive fields, but that a gain

control mechanism truncates responses to moving stimuli such that the peak spike rate occurs earlier than would be expected based on the Gaussian receptive field. This finding is similar to the gain control effects described here in Chapter 4. While the findings of Berry et al. (1999) appear to hold for many types of ganglion cells, their effect is much more subtle than that found for superior coding DSGCs.

Other than providing an early signal, anticipation appears to be linked to a warning system, whereby the retina generates an alarm signal when its prediction is incorrect. Schwartz et al. (2007) found that when the direction of a smoothly moving stimulus was abruptly reversed, a population of ganglion cells fired a burst of highly correlated spikes. As such, ganglion cells appear to not only anticipate moving stimuli, they appear to robustly respond when their prediction is violated.

Conclusion

Together, the results of this thesis show how asymmetric dendritic morphology and gap junctions can provide unique and diverse strategies for coding moving stimuli. These mechanisms could be utilized for diverse purposes elsewhere in the CNS, where polarized dendritic morphologies and gap junctions abound, and where sensory processing lags need to be corrected.

Appendix: Copyright Permissions

Elsevier Licence Terms and Condition

Jan 08, 2013

This is a License Agreement between Stuart Trenholm ("You") and Elsevier ("Elsevier") provided by Copyright Clearance Center ("CCC").

Supplier: Elsevier Limited, The Boulevard, Langford Lane, Kidlington, Oxford, OX5 1GB, UK

Registered Company Number: 1982084

Customer name: Stuart Trenholm

Customer address: #10 550 Quadra St, Victoria BC, V8V 3S3

Licensed content publisher: Elsevier

Licensed content publication: Neuron

Licensed content title: Parallel Mechanisms Encode Direction in the Retina

Licensed content author: Stuart Trenholm, Kyle Johnson, Xiao Li, Robert G. Smith, Gautam B. Awatramani

Licensed content date: 25 August, 2011

Licensed content volume number: 71

Licensed content issue number: 4

Number of pages: 12 (683-694)

Type of Use: reuse in a thesis/dissertation

Portion: full article

Format: both print and electronic

Are you the author of this Elsevier article: Yes


Will you be translating: No

Title of your thesis/dissertation: Motion Coding Strategies in the Retina

Expected completion date: Feb 2013

Estimated size (number of pages): 125

Elsevier VAT number: GB 494 6272 12

- **Permission Status:**  **Granted, Nature Neuroscience article**
- **Permission type:** Republish or display content
- **Type of use:** Republish in a thesis/dissertation

Requestor type	Author of requested content
Format	Print, Electronic
Portion	chapter/article
Title or numeric reference of the portion(s)	"Lag normalization in an electrically coupled neural network"
Editor of portion(s)	n/a
Author of portion(s)	Stuart Trenholm
Volume of serial or monograph	16
Issue, if republishing an article from a serial	2
Page range of portion	
Publication date of portion	2013
Rights for	Main product
Duration of use	Life of current edition
Creation of copies for the disabled	No
With minor editing privileges	No
For distribution to	Canada
In the following language(s)	Original language of publication
With incidental promotional use	No
Lifetime unit quantity of new product	0 to 499
Made available in the following markets	Educational and professional

The requesting person/organization	Stuart Trenholm
Order reference number	CAO2710
Author/Editor	Stuart Trenholm
The standard identifier	n/a
The proposed price	n/a
Title	MOTION CODING STRATEGIES IN THE RETINA
Publisher	Dalhousie University, Halifax, Canada
Expected publication date	Feb 2013
Estimated size (pages)	130

References

- Ackert JM, Farajian R, Volgyi B, Bloomfield SA (2009) GABA blockade unmasks an OFF response in ON direction selective ganglion cells in the mammalian retina. *J Physiol* 587:4481-4495.
- Amthor FR, Takahashi ES, Oyster CW (1989) Morphologies of rabbit retinal ganglion cells with complex receptive fields. *J Comp Neurol* 280:97-121.
- Anderson CH, Van Essen DC (1987) Shifter circuits: a computational strategy for dynamic aspects of visual processing. *Proc Natl Acad Sci U S A* 84:6297-6301.
- Arber S, Han B, Mendelsohn M, Smith M, Jessell TM, Sockanathan S (1999) Requirement for the homeobox gene Hb9 in the consolidation of motor neuron identity. *Neuron* 23:659-674.
- Auferkorte ON, Baden T, Kaushalya SK, Zabouri N, Rudolph U, Haverkamp S, Euler T (2012) GABA(A) receptors containing the alpha2 subunit are critical for direction-selective inhibition in the retina. *PLoS One* 7:e35109.
- Barlow HB (1953) Summation and inhibition in the frog's retina. *J Physiol* 119:69-88.
- Barlow HB, Hill RM (1963) Selective sensitivity to direction of movement in ganglion cells of the rabbit retina. *Science* 139:412-414.
- Barlow HB, Hill RM, Levick WR (1964) Retinal Ganglion Cells Responding Selectively to Direction and Speed of Image Motion in the Rabbit. *J Physiol* 173:377-407.
- Barlow HB, Levick WR (1965) The mechanism of directionally selective units in rabbit's retina. *J Physiol* 178:477-504.
- Barrio LC, Capel J, Jarillo JA, Castro C, Revilla A (1997) Species-specific voltage-gating properties of connexin-45 junctions expressed in *Xenopus* oocytes. *Biophys J* 73:757-769.
- Baylor DA, Nicholls JG (1969) Chemical and electrical synaptic connexions between cutaneous mechanoreceptor neurones in the central nervous system of the leech. *J Physiol* 203:591-609.
- Benison G, Keizer J, Chalupa LM, Robinson DW (2001) Modeling temporal behavior of postnatal cat retinal ganglion cells. *J Theor Biol* 210:187-199.

- Bennett MV, Zukin RS (2004) Electrical coupling and neuronal synchronization in the Mammalian brain. *Neuron* 41:495-511.
- Berry MJ, 2nd, Brivanlou IH, Jordan TA, Meister M (1999) Anticipation of moving stimuli by the retina. *Nature* 398:334-338.
- Bloomfield SA, Volgyi B (2009) The diverse functional roles and regulation of neuronal gap junctions in the retina. *Nat Rev Neurosci* 10:495-506.
- Borst A, Egelhaaf M (1989) Principles of visual motion detection. *Trends Neurosci* 12:297-306.
- Borst A, Euler T (2011) Seeing things in motion: models, circuits, and mechanisms. *Neuron* 71:974-994.
- Branco T, Clark BA, Hausser M (2010) Dendritic discrimination of temporal input sequences in cortical neurons. *Science* 329:1671-1675.
- Briggman KL, Helmstaedter M, Denk W (2011) Wiring specificity in the direction-selectivity circuit of the retina. *Nature* 471:183-188.
- Bringuier V, Chavane F, Glaeser L, Fregnac Y (1999) Horizontal propagation of visual activity in the synaptic integration field of area 17 neurons. *Science* 283:695-699.
- Brivanlou IH, Warland DK, Meister M (1998) Mechanisms of concerted firing among retinal ganglion cells. *Neuron* 20:527-539.
- Bulthoff H, Bulthoff I (1987) GABA-antagonist inverts movement and object detection in flies. *Brain Res* 407:152-158.
- Caldwell JH, Daw NW, Wyatt HJ (1978) Effects of picrotoxin and strychnine on rabbit retinal ganglion cells: lateral interactions for cells with more complex receptive fields. *J Physiol* 276:277-298.
- Connors BW, Long MA (2004) Electrical synapses in the mammalian brain. *Annu Rev Neurosci* 27:393-418.
- Coombs J, van der List D, Wang GY, Chalupa LM (2006) Morphological properties of mouse retinal ganglion cells. *Neuroscience* 140:123-136.
- Curti S, Hoge G, Nagy JI, Pereda AE (2012) Synergy between electrical coupling and membrane properties promotes strong synchronization of neurons of the mesencephalic trigeminal nucleus. *J Neurosci* 32:4341-4359.

- Demb JB (2007) Cellular mechanisms for direction selectivity in the retina. *Neuron* 55:179-186.
- Drager UC, Hubel DH (1975) Responses to visual stimulation and relationship between visual, auditory, and somatosensory inputs in mouse superior colliculus. *J Neurophysiol* 38:690-713.
- Euler T, Detwiler PB, Denk W (2002) Directionally selective calcium signals in dendrites of starburst amacrine cells. *Nature* 418:845-852.
- Fried SI, Munch TA, Werblin FS (2002) Mechanisms and circuitry underlying directional selectivity in the retina. *Nature* 420:411-414.
- Fried SI, Munch TA, Werblin FS (2005) Directional selectivity is formed at multiple levels by laterally offset inhibition in the rabbit retina. *Neuron* 46:117-127.
- Furshpan EJ, Potter DD (1957) Mechanism of nerve-impulse transmission at a crayfish synapse. *Nature* 180:342-343.
- Furshpan EJ, Potter DD (1959) Transmission at the giant motor synapses of the crayfish. *J Physiol* 145:289-325.
- Gollisch T, Meister M (2008) Rapid neural coding in the retina with relative spike latencies. *Science* 319:1108-1111.
- Grinvald A, Lieke EE, Frostig RD, Hildesheim R (1994) Cortical point-spread function and long-range lateral interactions revealed by real-time optical imaging of macaque monkey primary visual cortex. *J Neurosci* 14:2545-2568.
- Grzywacz NM, Tootle JS, Amthor FR (1997) Is the input to a GABAergic or cholinergic synapse the sole asymmetry in rabbit's retinal directional selectivity? *Vis Neurosci* 14:39-54.
- Hausselt SE, Euler T, Detwiler PB, Denk W (2007) A dendrite-autonomous mechanism for direction selectivity in retinal starburst amacrine cells. *PLoS Biol* 5:e185.
- He S, Jin ZF, Masland RH (1999) The nondiscriminating zone of directionally selective retinal ganglion cells: comparison with dendritic structure and implications for mechanism. *J Neurosci* 19:8049-8056.
- Hidaka S, Akahori Y, Kurosawa Y (2004) Dendrodendritic electrical synapses between mammalian retinal ganglion cells. *J Neurosci* 24:10553-10567.

- Hirsch JA, Alonso JM, Reid RC, Martinez LM (1998) Synaptic integration in striate cortical simple cells. *J Neurosci* 18:9517-9528.
- Hu EH, Bloomfield SA (2003) Gap junctional coupling underlies the short-latency spike synchrony of retinal alpha ganglion cells. *J Neurosci* 23:6768-6777.
- Hu EH, Pan F, Volgyi B, Bloomfield SA (2010) Light increases the gap junctional coupling of retinal ganglion cells. *J Physiol* 588:4145-4163.
- Hubel DH, Wiesel TN (1959) Receptive fields of single neurones in the cat's striate cortex. *J Physiol* 148:574-591.
- Huberman AD, Wei W, Elstrott J, Stafford BK, Feller MB, Barres BA (2009) Genetic identification of an On-Off direction-selective retinal ganglion cell subtype reveals a layer-specific subcortical map of posterior motion. *Neuron* 62:327-334.
- Jancke D, Chavane F, Naaman S, Grinvald A (2004a) Imaging cortical correlates of illusion in early visual cortex. *Nature* 428:423-426.
- Jancke D, Erlhagen W, Schonher G, Dinse HR (2004b) Shorter latencies for motion trajectories than for flashes in population responses of cat primary visual cortex. *J Physiol* 556:971-982.
- Johnson BR, Peck JH, Harris-Warrick RM (1993) Amine modulation of electrical coupling in the pyloric network of the lobster stomatogastric ganglion. *J Comp Physiol A* 172:715-732.
- Kay JN, De la Huerta I, Kim IJ, Zhang Y, Yamagata M, Chu MW, Meister M, Sanes JR (2011) Retinal ganglion cells with distinct directional preferences differ in molecular identity, structure, and central projections. *J Neurosci* 31:7753-7762.
- Kim IJ, Zhang Y, Yamagata M, Meister M, Sanes JR (2008) Molecular identification of a retinal cell type that responds to upward motion. *Nature* 452:478-482.
- Kim KJ, Rieke F (2003) Slow Na⁺ inactivation and variance adaptation in salamander retinal ganglion cells. *J Neurosci* 23:1506-1516.
- Kothmann WW, Trexler EB, Whitaker CM, Li W, Massey SC, O'Brien J (2012) Nonsynaptic NMDA receptors mediate activity-dependent plasticity of gap junctional coupling in the AII amacrine cell network. *J Neurosci* 32:6747-6759.
- Krekelberg B, Lappe M (2001) Neuronal latencies and the position of moving objects. *Trends Neurosci* 24:335-339.

- Kuffler SW (1953) Discharge patterns and functional organization of mammalian retina. *J Neurophysiol* 16:37-68.
- Lee S, Kim K, Zhou ZJ (2010) Role of ACh-GABA cotransmission in detecting image motion and motion direction. *Neuron* 68:1159-1172.
- Livingstone MS (1998) Mechanisms of direction selectivity in macaque V1. *Neuron* 20:509-526.
- Llinas R, Baker R, Sotelo C (1974) Electrotonic coupling between neurons in cat inferior olive. *J Neurophysiol* 37:560-571.
- London M, Hausser M (2005) Dendritic computation. *Annu Rev Neurosci* 28:503-532.
- Mann-Metzer P, Yarom Y (1999) Electrotonic coupling interacts with intrinsic properties to generate synchronized activity in cerebellar networks of inhibitory interneurons. *J Neurosci* 19:3298-3306.
- Manor Y, Rinzel J, Segev I, Yarom Y (1997) Low-amplitude oscillations in the inferior olive: a model based on electrical coupling of neurons with heterogeneous channel densities. *J Neurophysiol* 77:2736-2752.
- Marshall JH, Kaye AP, Nauhaus I, Callaway EM (2012) Anterior-posterior direction opponency in the superficial mouse lateral geniculate nucleus. *Neuron* 76:713-720.
- Mastrorade DN (1983) Interactions between ganglion cells in cat retina. *J Neurophysiol* 49:350-365.
- Moreno AP, Laing JG, Beyer EC, Spray DC (1995) Properties of gap junction channels formed of connexin 45 endogenously expressed in human hepatoma (SKHep1) cells. *Am J Physiol* 268:C356-365.
- Muller LP, Dedek K, Janssen-Bienhold U, Meyer A, Kreuzberg MM, Lorenz S, Willecke K, Weiler R (2010) Expression and modulation of connexin 30.2, a novel gap junction protein in the mouse retina. *Vis Neurosci* 27:91-101.
- Nicholls JG, Purves D (1970) Monosynaptic chemical and electrical connexions between sensory and motor cells in the central nervous system of the leech. *J Physiol* 209:647-667.
- Nijhawan R (1994) Motion extrapolation in catching. *Nature* 370:256-257.

- Nijhawan R (2002) Neural delays, visual motion and the flash-lag effect. *Trends Cogn Sci* 6:387.
- Oesch N, Euler T, Taylor WR (2005) Direction-selective dendritic action potentials in rabbit retina. *Neuron* 47:739-750.
- Ogmen H (1991) On the Mechanisms Underlying Directional Selectivity. *Neural Computation* 3:333-349.
- Oyster CW (1968) The analysis of image motion by the rabbit retina. *J Physiol* 199:613-635.
- Oyster CW, Amthor FR, Takahashi ES (1993) Dendritic architecture of ON-OFF direction-selective ganglion cells in the rabbit retina. *Vision Res* 33:579-608.
- Oyster CW, Barlow HB (1967) Direction-selective units in rabbit retina: distribution of preferred directions. *Science* 155:841-842.
- Oyster CW, Simpson JI, Takahashi ES, Soodak RE (1980) Retinal ganglion cells projecting to the rabbit accessory optic system. *J Comp Neurol* 190:49-61.
- Oyster CW, Takahashi E, Collewijn H (1972) Direction-selective retinal ganglion cells and control of optokinetic nystagmus in the rabbit. *Vision Res* 12:183-193.
- Pan F, Paul DL, Bloomfield SA, Volgyi B (2010) Connexin36 is required for gap junctional coupling of most ganglion cell subtypes in the mouse retina. *J Comp Neurol* 518:911-927.
- Pereda AE, Curti S, Hoge G, Cachope R, Flores CE, Rash JE (2012) Gap junction-mediated electrical transmission: Regulatory mechanisms and plasticity. *Biochim Biophys Acta*.
- Rall W (1964) Theoretical significance of dendritic trees for neuronal input-output relations. In: *The Theoretical Foundation of Dendritic Function*(Segev, I., ed), pp 117-146: M.I.T. Press.
- Rivlin-Etzion M, Wei W, Feller MB (2012) Visual stimulation reverses the directional preference of direction-selective retinal ganglion cells. *Neuron* 76:518-525.
- Rodieck RW (1965) Quantitative analysis of cat retinal ganglion cell response to visual stimuli. *Vision Res* 5:583-601.

- Schachter MJ, Oesch N, Smith RG, Taylor WR (2010) Dendritic spikes amplify the synaptic signal to enhance detection of motion in a simulation of the direction-selective ganglion cell. *PLoS Comput Biol* 6.
- Schubert T, Maxeiner S, Kruger O, Willecke K, Weiler R (2005) Connexin45 mediates gap junctional coupling of bistratified ganglion cells in the mouse retina. *J Comp Neurol* 490:29-39.
- Schwartz G, Taylor S, Fisher C, Harris R, Berry MJ, 2nd (2007) Synchronized firing among retinal ganglion cells signals motion reversal. *Neuron* 55:958-969.
- Shapley RM, Victor JD (1978) The effect of contrast on the transfer properties of cat retinal ganglion cells. *J Physiol* 285:275-298.
- Smith RD, Grzywacz NM, Borg-Graham LJ (1996) Is the input to a GABAergic synapse the sole asymmetry in turtle's retinal directional selectivity? *Vis Neurosci* 13:423-439.
- Sun W, Li N, He S (2002) Large-scale morphological survey of mouse retinal ganglion cells. *J Comp Neurol* 451:115-126.
- Taylor WR, He S, Levick WR, Vaney DI (2000) Dendritic computation of direction selectivity by retinal ganglion cells. *Science* 289:2347-2350.
- Taylor WR, Vaney DI (2002) Diverse synaptic mechanisms generate direction selectivity in the rabbit retina. *J Neurosci* 22:7712-7720.
- Taylor WR, Vaney DI (2003) New directions in retinal research. *Trends Neurosci* 26:379-385.
- Trenholm S, Borowska J, Zhang J, Hoggarth A, Johnson K, Barnes S, Lewis TJ, Awatramani GB (2012) Intrinsic oscillatory activity arising within the electrically coupled AII amacrine-ON cone bipolar cell network is driven by voltage-gated Na⁺ channels. *J Physiol* 590:2501-2517.
- Trenholm S, Johnson K, Li X, Smith RG, Awatramani GB (2011) Parallel mechanisms encode direction in the retina. *Neuron* 71:683-694.
- Trong PK, Rieke F (2008) Origin of correlated activity between parasol retinal ganglion cells. *Nat Neurosci* 11:1343-1351.
- Tukker JJ, Taylor WR, Smith RG (2004) Direction selectivity in a model of the starburst amacrine cell. *Vis Neurosci* 21:611-625.

- Vaney DI (1994) Territorial organization of direction-selective ganglion cells in rabbit retina. *J Neurosci* 14:6301-6316.
- Vaney DI, Sivyer B, Taylor WR (2012) Direction selectivity in the retina: symmetry and asymmetry in structure and function. *Nat Rev Neurosci* 13:194-208.
- Vaney DI, Taylor WR (2002) Direction selectivity in the retina. *Curr Opin Neurobiol* 12:405-410.
- Veruki ML, Hartveit E (2009) Meclofenamic acid blocks electrical synapses of retinal AII amacrine and on-cone bipolar cells. *J Neurophysiol* 101:2339-2347.
- Vervaeke K, Lorincz A, Nusser Z, Silver RA (2012) Gap junctions compensate for sublinear dendritic integration in an inhibitory network. *Science* 335:1624-1628.
- Volgyi B, Chheda S, Bloomfield SA (2009) Tracer coupling patterns of the ganglion cell subtypes in the mouse retina. *J Comp Neurol* 512:664-687.
- Wang GY, Robinson DW, Chalupa LM (1998) Calcium-activated potassium conductances in retinal ganglion cells of the ferret. *J Neurophysiol* 79:151-158.
- Wassle H, Puller C, Muller F, Haverkamp S (2009) Cone contacts, mosaics, and territories of bipolar cells in the mouse retina. *J Neurosci* 29:106-117.
- Wei W, Hamby AM, Zhou K, Feller MB (2011) Development of asymmetric inhibition underlying direction selectivity in the retina. *Nature* 469:402-406.
- Weng S, Sun W, He S (2005) Identification of ON-OFF direction-selective ganglion cells in the mouse retina. *J Physiol* 562:915-923.
- Wilson JM, Hartley R, Maxwell DJ, Todd AJ, Lieberam I, Kaltschmidt JA, Yoshida Y, Jessell TM, Brownstone RM (2005) Conditional rhythmicity of ventral spinal interneurons defined by expression of the Hb9 homeodomain protein. *J Neurosci* 25:5710-5719.
- Wyatt HJ, Day NW (1976) Specific effects of neurotransmitter antagonists on ganglion cells in rabbit retina. *Science* 191:204-205.
- Yang G, Masland RH (1994) Receptive fields and dendritic structure of directionally selective retinal ganglion cells. *J Neurosci* 14:5267-5280.

Yonehara K, Balint K, Noda M, Nagel G, Bamberg E, Roska B (2011) Spatially asymmetric reorganization of inhibition establishes a motion-sensitive circuit. *Nature* 469:407-410.

Yoshida K, Watanabe D, Ishikane H, Tachibana M, Pastan I, Nakanishi S (2001) A key role of starburst amacrine cells in originating retinal directional selectivity and optokinetic eye movement. *Neuron* 30:771-780.

Zsiros V, Maccaferri G (2008) Noradrenergic modulation of electrical coupling in GABAergic networks of the hippocampus. *J Neurosci* 28:1804-1815.